AD_____

Award Number: W81XWH-10-1-0838

TITLE: Alteration of Motor Network Function Following Injury

PRINCIPAL INVESTIGATOR: David J. Schulz

CONTRACTING ORGANIZATION: University of Missouri
Columbia, MO 65211-3020

REPORT DATE: October 2012

TYPE OF REPORT: Annual

PREPARED FOR: U.S. Army Medical Research and Materiel Command
Fort Detrick, Maryland 21702-5012

DISTRIBUTION STATEMENT: Approved for Public Release;
Distribution Unlimited

The views, opinions and/or findings contained in this report are those of the author(s) and should not be construed as an official Department of the Army position, policy or decision unless so designated by other documentation.

REPORT DOCUMENTATION PAGE

Form Approved
OMB No. 0704-0188

1. REPORT DATE	2. REPORT TYPE	3. DATES COVERED
27-Oct-2012	Annual	30Sep2011 – 29Sep2012

4. TITLE AND SUBTITLE

Alteration of Motor Network Function Following Injury

5a. CONTRACT NUMBER

5b. GRANT NUMBER W81XWH-10-1-0838

5c. PROGRAM ELEMENT NUMBER

6. AUTHOR(S)

David J. Schulz

E-Mail: schulzd@missouri.edu

5d. PROJECT NUMBER

5e. TASK NUMBER

5f. WORK UNIT NUMBER

7. PERFORMING ORGANIZATION NAME(S) AND ADDRESS(ES)
University of Missouri
Columbia, MO 65211-3020

8. PERFORMING ORGANIZATION REPORT NUMBER

9. SPONSORING / MONITORING AGENCY NAME(S) AND ADDRESS(ES)
U.S. Army Medical Research and Materiel Command
Fort Detrick, Maryland 21702-5012

10. SPONSOR/MONITOR'S ACRONYM(S)

11. SPONSOR/MONITOR'S REPORT NUMBER(S)

12. DISTRIBUTION / AVAILABILITY STATEMENT
Approved for Public Release; Distribution Unlimited

13. SUPPLEMENTARY NOTES

14. ABSTRACT
We have made substantial progress over the past year with this proposal. Our primary goal is the understanding of functional impacts of removal of descending inputs to the motor network. We determined that transient blockade of descending inputs causes changes in this system whereby subsequent restored input is unable to re-establish normal functional motor output. However, we also determined that a partial blockade results in an over-sensitivity of the motor network to restored (full) connectivity. We have generated a mechanistic understanding of the causes of both change in sensitivity to modulation, as well as the effects of this injury on underlying molecular and physiological processes crucial to motor network output. In addition, we have uncovered compensatory changes and their underlying mechanisms responsible for homeostatic plasticity responsible for changing the physiology of neurons in an attempt to maintain their excitability. All of these shed substantial light on underlying mechanisms that may be involved in changes in motor networks as a result of injury that removes descending control input.

15. SUBJECT TERMS
Spinal Cord Injury, Decentralization, Ion channels, Ionic conductance, Network output

16. SECURITY CLASSIFICATION OF:			17. LIMITATION OF ABSTRACT	18. NUMBER OF PAGES	19a. NAME OF RESPONSIBLE PERSON USAMRMC
a. REPORT	**b. ABSTRACT**	**c. THIS PAGE**			**19b. TELEPHONE NUMBER** *(include area code)*
U	U	U	UU		

Table of Contents

INTRODUCTION

Much research has examined the potential for axon regeneration across an injury site to re-establish functional connectivity between higher motor centers and spinal networks[1,2]. Functional recovery may remain elusive, however, should the networks that carry out movement be so altered after injury that they no longer respond to a newly reconnected source of input. The overall goal of this project was to address an understudied aspect of regeneration -- how does removal of descending neural input alter motor network activity below the site of injury, and what are its consequences should we become able to reconnect higher motor centers to motor networks? The study objective was to begin to understand the extent and mechanisms by which neural networks change after removing descending input, and to characterize activity that results from re-establishing connectivity. Our over-arching hypothesis was that neural networks are fundamentally altered when descending inputs are removed, therefore making the effects of reconnecting these networks unpredictable. Ultimately the goal is to understand the full suite of medical intervention that may be necessary to allow for spinal cord injury recovery, including preventing or rectifying changes in neural networks below the injury site.

BODY

From the point of view of the nervous system, the cure for spinal cord injury must progress on at least two complementary fronts: re-establishing connectivity between the brain and spinal networks (regeneration)[2], and understanding how to safeguard or recover functional viability of isolated spinal networks in order to receive input from regenerated tracts[3-5]. Our work is aimed at elucidating the biological basis by which isolated spinal networks may remain functionally viable, which is the foundation for developments that aim to increase function and recovery among those who have suffered a spinal cord injury. This basic research approach to uncover mechanism of how networks are altered by denervation (disrupting nerve input) is a critical first step towards this goal, as simply describing these phenomena will fail to add insight into possible future therapeutic approaches. Only by understanding what is changing, as opposed to simply understanding that networks change, will we progress towards viable treatment options.

The CDMRP was willing to "think out of the box" on this work, and fund basic research in neural networks in an unlikely system for spinal cord injury: namely crustacean motor networks such as the stomatogastric ganglion (STG)[6]. While the STG is an invertebrate preparation, it provides many parallels to the organization of motor networks in mammalian systems, yet offers a substantial level of manipulation that is currently unachievable in mammalian systems. Our overall model system for this proposal was the transient removal and restoration of descending command inputs to motor networks, and the effects that this "decentralization" has on subsequent function with restored inputs. In addition, we focus on the underlying cellular mechanisms involved in these kinds of changes, including those responsible for "homeostatic plasticity" which attempts to restore normal function to cellular output after a substantial disruption in that activity. Our hypothesis is that the onset of these homeostatic mechanisms is actually detrimental to the restoration of activity through restored connectivity of descending inputs.

We have made substantial progress over the past year with this proposal. Here we summarize our progress in understanding the functional impacts of removal of descending inputs to motor networks. For clarity and succinctness, I will report these results from the past 12 months in a bulleted list format. All of the following descriptions of results from this proposal can be supported by data in the attached publications found in the Appendices.

THE FOLLOWING SUMMARY (OVERLAPPING WITH THE PREVIOUS ANNUAL REPORT) OF RESEARCH IS NOW PUBLISHED AND FOUND IN THE FOLLOWING ARTICLE ATTACHED IN THE APPENDICES:
Nahar J, Lett KM, Schulz DJ (2012) Restoration of descending inputs fails to rescue activity following deafferentation of a motor network. *Journal of Neurophysiology* 108: 871-881.

- Removal of modulatory, descending projections (stomatogastric nerve – STN) to the motor network (the STG) causes an immediate and complete loss of the motor output. This "decentralization" is achieved by a simple removable block of isotonic sucrose that blocks all descending neural activity without injuring the axons of the blockade. The block is completely reversible and under control of the experimenter at all times, so we can decentralize for any time period we like and then reconnect the descending control centers to the network at will.
- Over the first ~12 hours of blockade, subsequent restoration of descending inputs is able to re-establish full functional motor output. Subsequent periods of 48h, 72h, and 96h of blockade lead to an inability to restore full functionality in the motor network, with the effect becoming more pronounced over longer blockade schemes. We performed multiple experiments to ensure the health of the blocked axons in these experiments, and determined that sucrose blockade is not damaging these fibers. This effect seems to be some physiological change in the system that alters the ability of the descending projections and motor network to communicate effectively after extended blockade.
- The effects above are seemingly not due to a loss of the descending projections to release neuromodulator. After 3 days of blockade, we can electrically stimulate the descending nerve both above (with the block removed) and below the block (with the block intact) and see an increase in motor activity of equal magnitude. But neither of these stimulation regimes is able to restore full functionality to the motor network.
- There is a significant decrease in the *activity* of the descending projections over the course of the blockade that is highly correlated to the decrease in the ability of restored projections to drive appropriate motor output. This was perhaps our least expected result. We had initiated these experiments to look at changes in the motor network itself as a result of it losing inputs, but apparently altering feedback interactions between higher centers and the motor network alter activity of the descending projections themselves.
- There is a significant change in the sensitivity of the STG to exogenously applied neuromodulation following 3 days of blockade. However, this is not across all modulators. A neuropeptide (proctolin) causes enhanced responses in blocked preparations, but responses to a biogenic amine analog of noradrenaline (octopamine) show no differences between blocked and unblocked preparations.

THE FOLLOWING SUMMARY OF RESEARCH IS NOW PUBLISHED AND FOUND IN THE FOLLOWING ARTICLE ATTACHED IN THE APPENDICES:

Ransdell JL, Nair SS, Schulz DJ (2012) Rapid homeostatic plasticity of intrinsic excitability in a central pattern generator network stabilizes functional neural network output. *Journal of Neuroscience* 32: 9649-9658.

- We determined that mRNA levels in single identified motor neurons for the channels which encode I_A and I_{KCa} are positively correlated, yet the ionic currents themselves are negatively correlated, across a population of motor neurons. We then determined that these currents are functionally coupled; decreasing levels of either current within a neuron causes a rapid increase in the other. These results suggest that compensatory interactions may exist that are utilized in times of perturbation to cell output that could ultimately be initiated by, and influence recovery from, injury.

- This functional interdependence results in homeostatic stabilization of both the individual neuronal and the network output. Perturbations that alter ionic currents and disrupt motor network activity cause an initial drastic change in the motor network's ability to create behaviorally appropriate output. However, after a relatively short time (within one hour) there is stabilizing compensation that occurs to help restore normal network activity. This restoration causes a significant change in the underlying physiology of the neuron, resulting in a compensatory increase in I_A when I_{KCa} is blocked, and vice versa.

- These compensatory increases are mechanistically independent (proceeding by distinct intracellular signaling mechanisms), suggesting robustness in the maintenance of neural network output that is critical for survival. Taken together, we generate a complete model for homeostatic plasticity from mRNA to network output where rapid post-translational compensatory mechanisms acting on a reservoir of channels proteins regulated at the level of gene expression provide homeostatic stabilization of both cellular and network activity. We feel these compensatory mechanisms, while initially beneficial, may ultimately impact long-term recovery from perturbation or cause tradeoffs in the network's ability to further respond to other extrinsic input.

THE FOLLOWING SUMMARY OF RESEARCH IS NOT YET PUBLISHED BUT IS IN PREPARATION FOR SUBMISSION WITHIN THE NEXT 3 MONTHS. FIGURES PROVIDED AS SUPPORTING DATA AND INCLUDED IN THE BODY OF THIS REPORT:

- Neurons that undergo loss of modulatory inputs do not show gross overall changes in expression level for ion channels (Fig 1). However, this does not indicate that gene expression for these critical components is not changing (see next point).

- Neurons that undergo a loss of connectivity show changes in their underlying ion channel gene expression patterns. For example, under control conditions, levels of mRNA levels for ion channels show correlated patterns of expression (Fig 2). In other words, there are correlations in mRNA copy number between channel genes for voltage-gated channels such as *shal* ($K_v4.1$), *shab* ($K_v2.1$), *Ca(v)1* ($Ca_v1.1$), *Ca(v)2* ($Ca_v1.2$), and

Ca(v)3 (Ca$_v$3.1).   Following decentralization, these correlated patters of conductance and channel expression are completely disrupted (Fig 2).

- This loss of correlated channel expression is in part due to the loss of neurochemical modulation directly, and not just the activity that elicited by them. If we disrupt activity, but artificially replace neuromodulators, we can "rescue" the loss of some of the correlated patterns of channel expression (Fig 3).

Taken together, our work has set the stage for an improved understanding and investigation of the underlying mechanisms of the changes in motor networks that are deprived of their descending inputs. Overall, the changes are widespread, seemingly affecting cells both above and below the injury/block site. Also quite striking is the fact that, over the first set of time scales we examined, that the effect was not reversible simply by restoring the connections.

KEY RESEARCH ACCOMPLISHMENTS

- We have established that motor networks do not respond appropriately to reconnected descending inputs within 24 hours of the initial injury or blockade

- Descending projections are still capable of releasing neurotransmitters/neuromodulators, suggesting that transient block does not cause a loss of ability to release chemical transmitters.

- Targets (motor neurons) of descending projections have altered sensitivity to neuromodulatory compounds.

- Targets (motor neurons) undergo changes to their intrinsic properties and gene expression, including loss of coordinated expression of ionic conductances and mRNA levels for the channels underlying those conductances.

- The activity of descending inputs is also seemingly altered by this blockade, presumably as a result of loss of feedback interactions with the motor network itself.

- Restoring inputs fails to restore both activity and the underlying physiology over a time course of multiple days. That is, the effects listed above are not ameliorated by reconnecting the inputs, at least over the time scale we have investigated.

- Functional interdependence of ionic currents results in homeostatic stabilization of both the individual neuronal and the network output. Perturbations that alter ionic currents and disrupt motor network activity cause an initial drastic change in the motor network's ability to create behaviorally appropriate output.

- After a relatively short time (within one hour) there is stabilizing compensation that occurs to help restore normal network activity. This restoration causes a significant change in the underlying physiology of the neuron, resulting in a compensatory increase in I_A when I_{KCa} is blocked, and vice versa.

- Neurons that lose descending modulatory input show altered patterns of gene expression that correlate with disrupted activity. However, these patterns are only seen by a more thorough analysis of <u>relationships </u>among gene products, as mean amounts are not seen to significantly change across individuals.

- These changes in gene expression patterns can in part be prevented by exogenous application of neuromodulators that mimic that actions of endogenous neuromodulatory compounds.

REPORTABLE OUTCOMES

The work funded by CDMRP has resulted in 3 publications thus far:

1. Temporal, S., et al., (2012) Neuromodulation independently determines correlated channel expression and conductance levels in motor neurons of the stomatogastric ganglion. *J Neurophysiology* 107" 718-727. See Appendix 1.
2. Ransdell JL, Nair SS, Schulz DJ (2012) Rapid homeostatic plasticity of intrinsic excitability in a central pattern generator network stabilizes functional neural network output. *Journal of Neuroscience* 32: 9649-9658. [Featured in "This Week in The Journal"]. See Appendix 2.
3. Nahar J, Lett KM, Schulz DJ (2012) Restoration of descending inputs fails to rescue activity following deafferentation of a motor network. *Journal of Neurophysiology* 108: 871-881. See Appendix 3.

In addition, we have presented this work as a total of 7 contributed or invited presentations:

1. Temporal S, Lett KM, Schulz DJ (2011) Recovery of rhythmic activity in decentralized cells of the stomatogastric ganglion is independent of correlated levels of channel expression. Society for Neuroscience Annual Meeting 2011, Washington DC.
2. Lett KM, Nahar J, Lane B, Schulz DJ (2011) Decentralization alters neuromodulator sensitivity in the pyloric network of the stomatogastric ganglion. Society for Neuroscience Annual Meeting 2011, Washington DC.
3. Schulz DJ (2011) Invited talk in the symposium titled "Adaptive Significance of Individual and Species Variation in Neuroendocrine Mechanisms" at the 15th annual Society for Behavioral Endocrinology meeting, Queretaro, Mexico.

4. Lett KM, Nahar J, Schulz DJ (2012) Isolated pattern generating network fails to respond to restored modulatory input. Society for Neuroscience Annual Meeting 2012, New Orleans, LA.
5. Temporal S, Schulz DJ (2012) Neuromodulation maintains channel mRNA correlations in neurons of the stomatogastric ganglion. Society for Neuroscience Annual Meeting 2012, New Orleans, LA.
6. Ransdell J, Nair SS, Schulz DJ (2012) Rapid homeostatic plasticity of intrinsic excitability and electrical synapse strength in a central pattern generator network stabilizes neuron and network output. Society for Neuroscience Annual Meeting 2012, New Orleans, LA.
7. Lane B, Lett K, Schulz DJ (2012) The Effect of Neuromodulation on the Synchronization of Motor Neurons in the Cardiac Ganglion of C. borealis. Satellite Meeting - Society for Neuroscience Annual Meeting 2012, New Orleans, LA.

The data generated by this research has allowed me to apply for other sources of funding to continue this work, as well as transition the hypotheses being developed into higher mammalian systems. While a subsequent DoD CDMRP proposal based on these findings was declined for further support, the Missouri Spinal Cord Injuries Research Program has funded new mammalian work in my laboratory that builds off of some of the hypotheses generated by the research in this report.

CONCLUSION

Taken together, our work has set the stage for an improved understanding and investigation of the underlying mechanisms of the changes in motor networks that are deprived of their descending inputs. Overall, the changes are widespread, seemingly affecting cells both above and below the injury/block site. Also quite striking is the fact that, over the first set of time scales we examined, that the effect was not reversible simply by restoring the connections. Our work will continue to characterize the nature of changes both above and below block/injury sites, as well as determine the time course over which these changes occur. We will attempt to determine whether the effect is reversible with restored connectivity over time, and also determine whether intervention can occur during the blockade time to prevent the changes that are causing loss of motor function. Ultimately the goal is to determine whether these results can be applied to spinal cord injury to begin to inform the full suite of therapeutic intervention necessary to carry out regeneration of injured fibers (not in the scope of this proposal), but also to ensure that reconnected networks appropriately communicate.

REFERENCES

1.   Bolsover, S., J. Fabes, and P.N. Anderson, Axonal guidance molecules and the failure of axonal regeneration in the adult mammalian spinal cord. Restor Neurol Neurosci, 2008. 26(2-3): p. 117-30.

2.   Lee, J.K. and B. Zheng, Axon regeneration after spinal cord injury: insight from genetically modified mouse models. Restor Neurol Neurosci, 2008. 26(2-3): p. 175-82.

3.   Dunlop, S.A., Activity-dependent plasticity: implications for recovery after spinal cord injury. Trends Neurosci, 2008. 31(8): p. 410-8.

4.   Rossignol, S., et al., Spinal cord injury: time to move? J Neurosci, 2007. 27(44): p. 11782-92.

5.   Frigon, A. and S. Rossignol, Functional plasticity following spinal cord lesions. Prog Brain Res, 2006. 157: p. 231-260.

6.   Marder E, Bucher D. Understanding circuit dynamics using the stomatogastric nervous system of lobsters and crabs. Annu Rev Physiol. 2007;69: p. 291-316.

FIGURES CITED IN THE BODY OF THIS REPORT
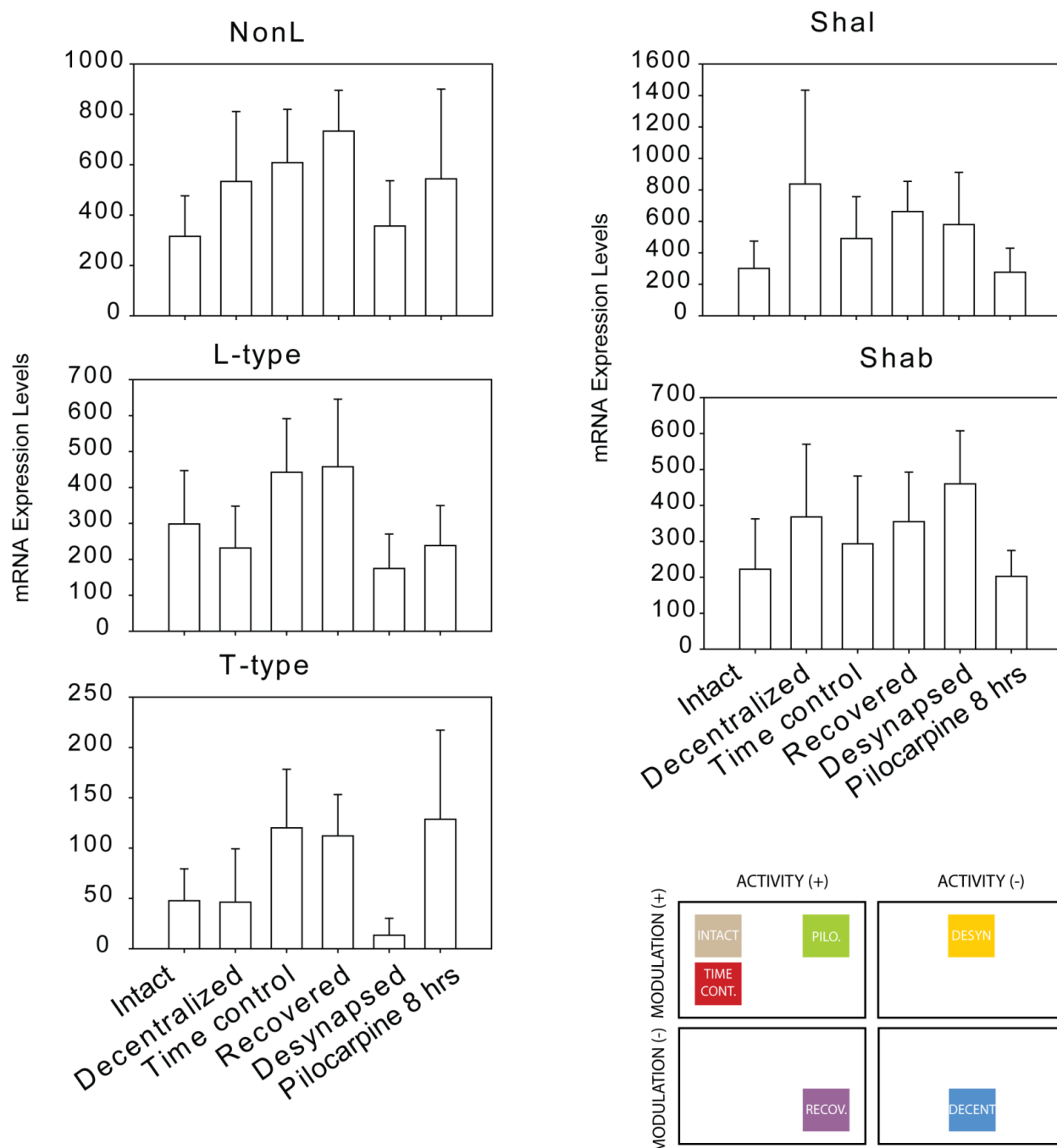
Figure 1. Comparison of mean mRNA (+/- SD) expression levels for different channels of the STG-pacemaker cell, PD under various network conditions that had either neuromodulation, activity, neither or both inputs removed.
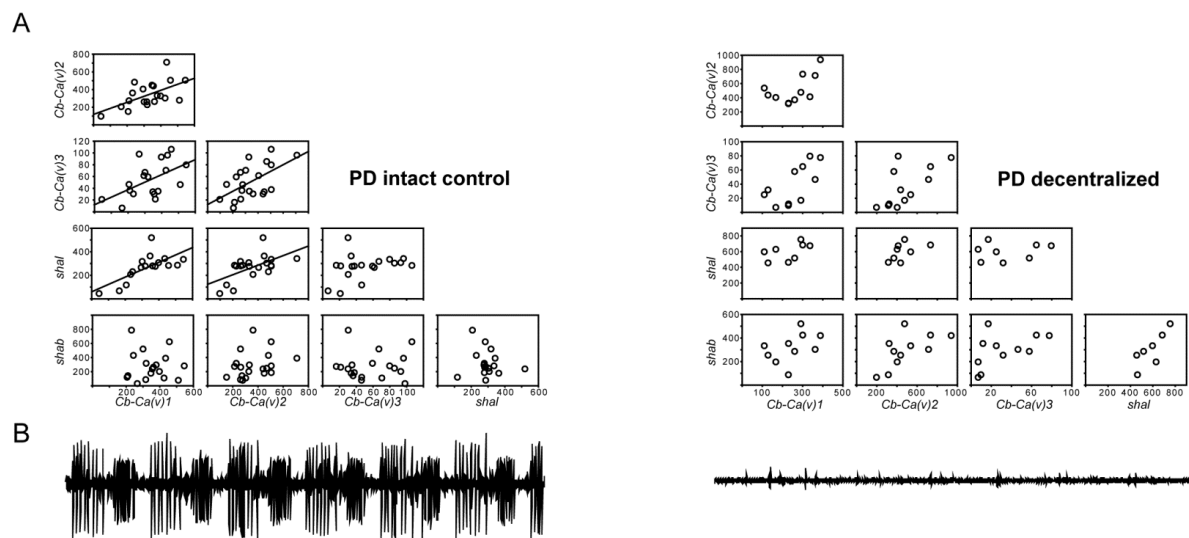
A

B

Figure 2. A Correlations among ion channel expression level from intact control and decentralized conditions for PD, the STG pacemaker cell. Open circles represent the mRNA levels of an individual cell. Regression lines are shown for significant correlations (Pearson's test P<0.05). B Representative lvn extracellular recording to show typical pyloric rhythm prior to pulling individual cell.
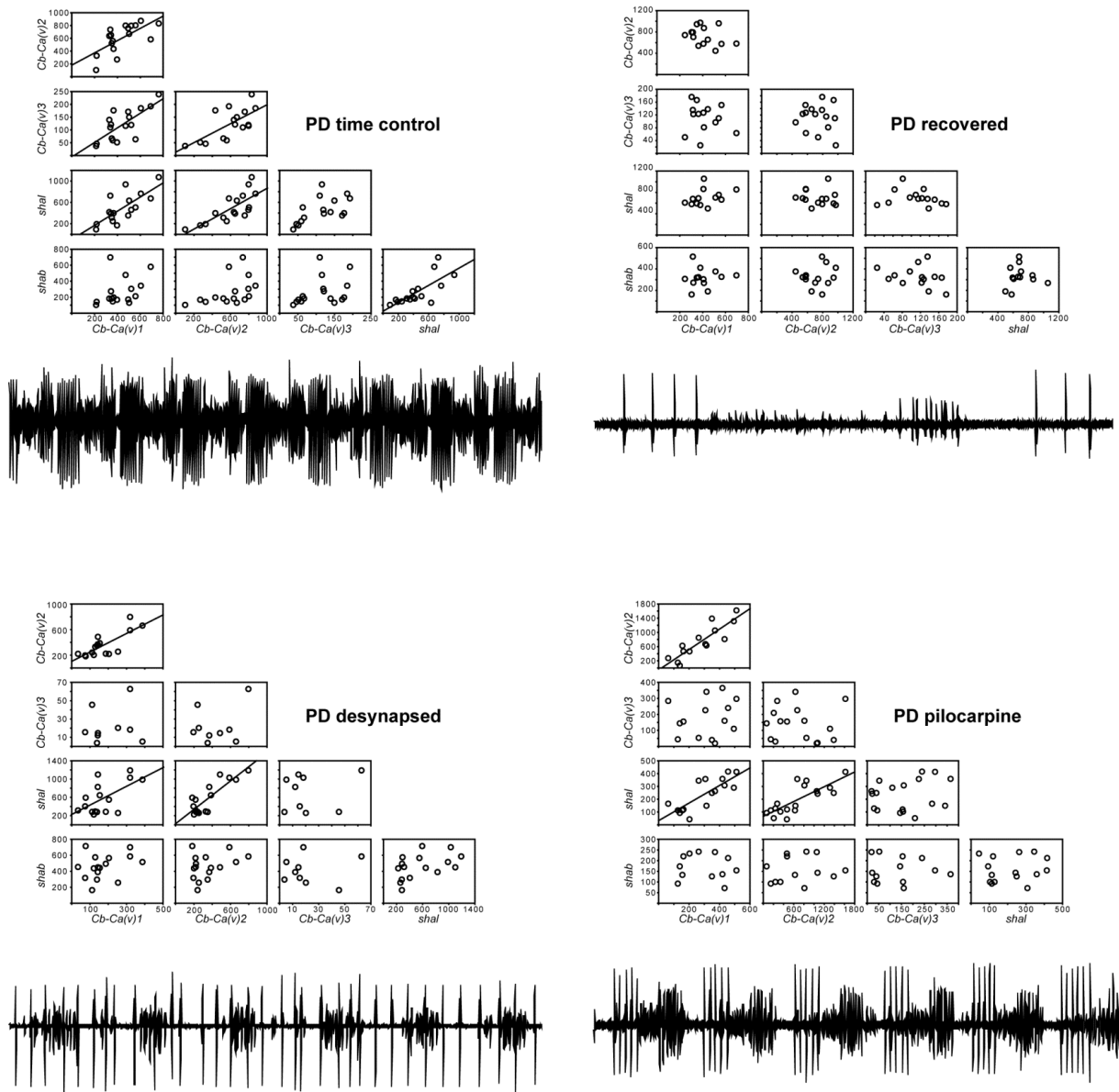
Figure 3. Correlations among ion channel expression levels of the STG pacemaker cell, PD under various conditions. Open circles represent the mRNA levels of an individual cell. Regression lines are shown for significant correlations (Pearson's test P<0.05). Under each group of channel correlations is an extracellular recording of the lvn to show the typical pyloric activity under each condition. To determine factors that PD channel correlations may be dependent on, neuromodulation and activity were decoupled. *Time-control* are intact networks incubated for 3 days to take into account biological changes due to long incubation periods. *Recovered* are decentralized networks that regained the pyloric network function following several days of incubation. *Desynapsed* have neuromodulatory input but activity was disrupted by blocking glutamatergic synapses using picrotoxin (PTX). *Pilocarpine* artificially maintains activity through one modulator, the muscarinic agonist pilocarpine, not the normal descending inputs.

APPENDIX 1. Temporal, S., et al., (2012) Neuromodulation independently determines correlated channel expression and conductance levels in motor neurons of the stomatogastric ganglion. *J Neurophysiology* 107" 718-727

Neuromodulation independently determines correlated channel expression and conductance levels in motor neurons of the stomatogastric ganglion

Simone Temporal,[3]* Mohati Desai,[1]* Olga Khorkova,[1] Gladis Varghese,[1] Aihua Dai,[3] David J. Schulz,[3] and Jorge Golowasch[1,2]

[1]*Federated Department of Biological Sciences, New Jersey Institute of Technology and Rutgers University, Newark;* [2]*Department of Mathematical Sciences, New Jersey Institute of Technology, Newark, New Jersey; and* [3]*Department of Biological Sciences, University of Missouri, Columbia, Missouri*

Temporal S, Desai M, Khorkova O, Varghese G, Dai A, Schulz DJ, Golowasch J. Neuromodulation independently determines correlated channel expression and conductance levels in motor neurons of the stomatogastric ganglion. *J Neurophysiol* 107: 718–727, 2012. First published October 12, 2011; doi:10.1152/jn.00622.2011.—Neuronal identity depends on the regulated expression of numerous molecular components, especially ionic channels, which determine the electrical signature of a neuron. Such regulation depends on at least two key factors, activity itself and neuromodulatory input. Neuronal electrical activity can modify the expression of ionic currents in homeostatic or nonhomeostatic fashion. Neuromodulators typically modify activity by regulating the properties or expression levels of subsets of ionic channels. In the stomatogastric system of crustaceans, both types of regulation have been demonstrated. Furthermore, the regulation of the coordinated expression of ionic currents and the channels that carry these currents has been recently reported in diverse neuronal systems, with neuromodulators not only controlling the absolute levels of ionic current expression but also, over long periods of time, appearing to modify their correlated expression. We hypothesize that neuromodulators may regulate the correlated expression of ion channels at multiple levels and in a cell-type-dependent fashion. We report that in two identified neuronal types, three ionic currents are linearly correlated in a pairwise manner, suggesting their coexpression or direct interactions, under normal neuromodulatory conditions. In each cell, some currents remain correlated after neuromodulatory input is removed, whereas the correlations between the other pairs are either lost or altered. Interestingly, in each cell, a different suite of currents change their correlation. At the transcript level we observe distinct alterations in correlations between channel mRNA amounts, including one of the cell types lacking a correlation under normal neuromodulatory conditions and then gaining the correlation when neuromodulators are removed. Synaptic activity does not appear to contribute, with one possible exception, to the correlated expression of either ionic currents or of the transcripts that code for the respective channels. We conclude that neuromodulators regulate the correlated expression of ion channels at both the transcript and the protein levels.

voltage clamp; ion channel; mRNA; correlation; crab

NEURONAL IDENTITY DEPENDS on the molecular composition that determines morphology and function, and it is regulated at multiple levels (Hobert et al. 2010). The distinct activity pattern of individual neurons is due to the regulation of neuronal excitability as determined principally by the activity of voltage-gated ionic currents. The generation of these currents is the result of the pattern of gene expression of voltage-gated channels as well as the posttranscriptional and posttranslational events that influence the biophysical properties of the channels inserted in the membrane (Hille 2001). Furthermore, extensive plasticity in neuronal excitability results from both activity-dependent (Cudmore and Turrigiano 2004; Desai et al. 1999; Li et al. 2004; Loebrich and Nedivi 2009; Zhang and Linden 2003) and activity-independent mechanisms (Khorkova and Golowasch 2007; MacLean et al. 2003, 2005). These mechanisms include forms of plasticity of intrinsic excitability (intrinsic plasticity) that either alter or homeostatically maintain the output of these cells depending on conditions (Zhang and Linden 2003). Recently, the coordinated expression of conductances (or conductance properties) and the contribution of such coordination to neuronal functions have been reported in an increasing number of systems (Bergquist et al. 2010; Coggan et al. 2010; Del Negro et al. 2002; Khorkova and Golowasch 2007; MacLean et al. 2003; McAnelly and Zakon 2000; Schulz et al. 2006, 2007). At this point, however, neither the role of this coregulation of ionic currents nor the level at which correlations are controlled is well known. It also is not known if, within a functional network, ionic currents are globally regulated among all functionally related neurons or if they are regulated at the individual neuron level. In this study, we examined at what level these current correlations are controlled. We did this by looking at the correlated distributions of ionic currents and of the mRNA that code for the channels that carry these currents in two identified neurons. We used the well-defined pyloric neuronal network of the crab *Cancer borealis*, in which individual neurons can unambiguously be identified.

The stomatogastric ganglion (STG) of *C. borealis* contains 25–26 neurons (Kilman and Marder 1996) that are identifiable on the basis of their anatomic projections (Maynard and Dando 1974). These neurons belong to two distinct neuronal networks that form central pattern generators (CPGs) producing different rhythmic motor patterns. The faster pyloric rhythm (cycle frequency of 0.5–2.0 Hz) is composed of six neuronal subtypes that produce rhythmic activity driven by the pacemaker activity of one neuron (the anterior burster, AB neuron), which is strongly electrically coupled to two pyloric dilator (PD) neurons. Thus this group of three neurons acts as a single pacemaker unit. This rhythmic activity pattern is conditionally

dependent on the release of neuromodulators from neurons located in adjacent ganglia that project into the STG (Luther et al. 2003; Thoby-Brisson and Simmers 2002). These substances have paracrine actions on pyloric neurons and are thought to regulate activity via short- and long-term actions (Khorkova and Golowasch 2007; Swensen and Marder 2001).

Individual neurons of the STG CPGs have distinct biophysical properties as well as gene expression profiles. For example, individually identified neurons of the pyloric network have highly variable kinetics and conductance density levels of the hyperpolarization-activated current, I_H (Peck et al. 2006), and the transient K$^+$ current, I_A (Goldman et al. 2001; Golowasch et al. 1999; Khorkova and Golowasch 2007; Peck et al. 2001). Particular pyloric neurons also differ in the quantitative relationships of expression of voltage-gated channel genes (Baro et al. 1997; Schulz et al. 2006, 2007), with different cell types expressing different relative amounts of voltage-gated channel mRNA and distinct correlations of channel mRNA levels (Schulz et al. 2007). These results suggest a differential regulation (and coregulation) of ion channel gene transcription in distinct STG neuron types. Together, the overall regulation of ion channel gene expression and posttranscriptional processing must play a substantial role in generating the unique output of each cell type.

In this study, we characterized the correlations of ionic currents expressed by two key neuronal subtypes of the pyloric network, the PD and lateral pyloric (LP) neurons, under different neuromodulatory conditions using a combination of electrophysiological and molecular analyses. We also examined the role of synaptic interactions and altered activity in the modification of these correlations.

METHODS

Adult male Jonah crabs (*C. borealis*) were purchased from local fishermen (Newark, NJ) and kept in cooled seawater aquaria at ~12°C. Animals were anesthetized by cooling for 15–30 min on ice. The foregut was removed, and the STG, with a portion of the nerves attached, were isolated as previously described (Harris-Warrick 1992; Selverston et al. 1976).

The removal of neuromodulatory input (i.e., decentralization) was accomplished by either transection of the stomatogastric nerve (*stn*) or by blocking action potential transmission along the *stn*, which carries all known neuromodulatory inputs from adjacent ganglia (esophageal and commissural ganglia) to the STG (Fig. 1*A*). To block transmission, a Vaseline well was built around the desheathed nerve, and either the well was filled with isotonic (750 mM) sucrose plus 10^{-6} M tetrodotoxin (Biotium), or the *stn* was cut as close to the STG as possible. Preparations in which experiments lasted more than 12 h (such as decentralization experiments) were maintained in organotypic culture at 6°C between recording sessions during which the preparation was bathed in physiological saline.

Electrophysiology. Neurons were identified and intracellularly recorded from exactly as described previously (Zhao et al. 2010). Extracellular recordings were performed with differential recordings using an AC amplifier (model 1700; A-M Systems) and two tungsten wires, one placed inside a Vaseline well built around a motor nerve (either the lateral ventricular nerve, *lvn*, or the pyloric dilator nerve, *pdn*, or both) and the other placed in the bath outside the well. Ionic currents were measured at 11–13°C in two-electrode voltage clamp, with current injection electrode resistances of 18–22 MΩ and voltage recording electrode resistances of 20–28 MΩ. K$^+$ currents were measured in standard *C. borealis* physiological saline. The high-threshold, voltage-gated outward potassium currents, I_{HTK}, were activated from a holding voltage of −40 mV. The voltage-gated transient current, I_A, was activated with depolarizing steps from a holding voltage of −80 mV. The high-threshold currents activated during the I_A activation protocol were removed by subtracting the currents previously measured from a holding potential of −40 mV. The hyperpolarization-activated current, I_H, was measured using 8-s-long hyperpolarizing pulses from a holding potential of −40 mV.

Ionic conductance of I_{HTK} and I_A was determined by dividing the current levels measured at +20 mV by the driving force, assuming a K$^+$ reversal potential (E_K) of −80 mV, and ionic conductance of I_H was similarly determined using a current measured at −110 mV and a reversal potential (E_H) of −10 mV (Haedo and Golowasch 2006; Khorkova and Golowasch 2007).

After ionic currents were measured under control conditions, the preparations were either treated with 10^{-5} M picrotoxin or decentralized and placed at 6°C for 24 h. The currents were measured again using the same protocols, and the neurons were subsequently processed for RNA extraction (see below).

mRNA quantification. Quantitative PCR was performed as described by Schulz et al. (2006). Briefly, total RNA was isolated using the RNeasy microcolumn-based RNA extraction kit (Qiagen, Valencia, CA), reverse transcribed using SuperScript III reverse transcriptase (Invitrogen), and used as a template in real-time RT-PCR with
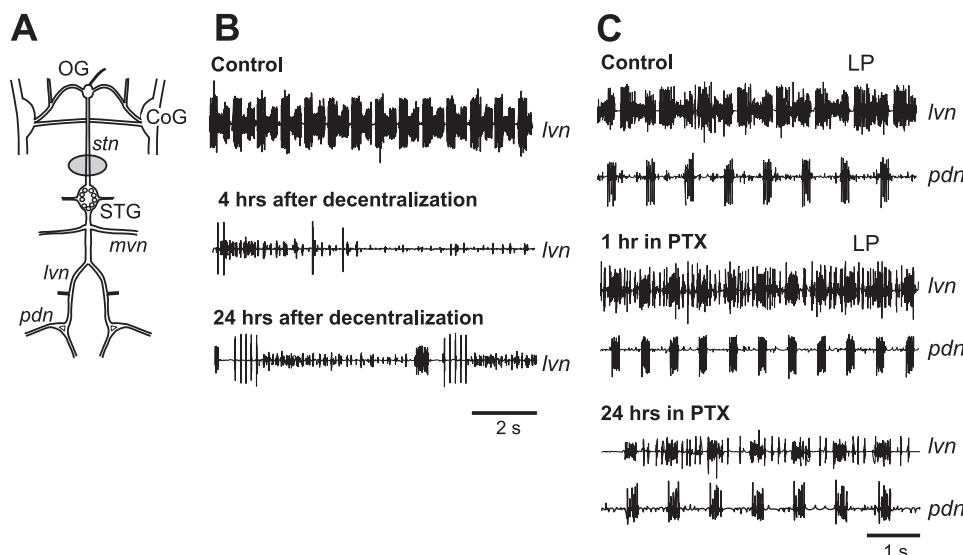

Fig. 1. Stomatogastric nervous system and activity changes under different modulatory conditions. *A*: the stomatogastric nervous system. OG, esophageal ganglion; CoG, commissural ganglion; STG, stomatogastric ganglion; *stn*, stomatogastric nerve; *lvn*, lateral ventricular nerve; *pdn*, pyloric dilator nerve; *mvn*, medial ventricular nerve. The circle around *stn* represents a Vaseline well used to block action potential transmission (METHODS). *B*: effect of the removal of neuromodulatory input to the STG. Pyloric activity is temporarily lost after decentralization (4 h). Activity is slower but can be identified as pyloric 24 h after decentralization. *C*: effect of the removal of glutamatergic inhibitory synapses with picrotoxin (PTX). The lateral pyloric (LP) neuron becomes, and remains, tonic over 24 h.

SYBR green (SABiosciences, Frederick, MA). Primers specific for real-time PCR detection of *Shal*, *BK-KCa*, *H*, and 18S rRNA with SYBR green were developed and designed using Primer3 software and are the same as previously reported (Schulz et al. 2006, 2007).

Statistics. Comparisons of overall levels of mRNA and conductance density were made using a one-way ANOVA followed by post hoc Tukey's *t*-test pairwise comparisons (Systat; Aspire Software International, Ashburn, VA). Correlation (parametric Pearson's product moment and nonparametric Spearman's rank correlation test) and linear regression analyses were carried out using Sigmastat (Systat). We compared correlation coefficients between experimental groups for a given pairwise correlation by performing a Fisher transformation of ρ using

$$\rho' = (0.5)\log_e \left| \frac{1 + \rho}{1 - \rho} \right|,$$

and then calculating a Fisher's z statistic as follows:

$$z = \frac{\rho'_1 - \rho'_2}{\sqrt{\dfrac{1}{n_1 - 3} + \dfrac{1}{n_2 - 3}}}.$$

Finally, slopes of relationships between conductances and between mRNA levels were compared between experimental groups with a modified ANCOVA (GraphPad Prism version 5; GraphPad Software, San Diego, CA).

RESULTS

As has been shown previously (Luther et al. 2003; Thoby-Brisson and Simmers 2002), decentralization of the STG leads to the rapid but reversible loss of rhythmic activity of the pyloric network (Fig. 1*B*). The rhythmic pyloric activity recovers to levels and characteristics similar to those observed under control conditions with a delay of hours to days (Luther et al. 2003). The removal of most chemical synapses in the ganglion, which are primarily inhibitory glutamatergic, was accomplished using 10^{-5} M picrotoxin, which disrupts the triphasic pyloric rhythm (Bidaut 1980; Marder and Eisen 1984), making the follower neurons (LP and other neurons) fire tonically, but leaves the pacemaker's activity (monitored by the PD neurons' activity on both the *lvn* and *pdn*) intact over the course of 24 h (Fig. 1*C*). Picrotoxin blocks inhibitory chemical synapses, which produces drastic changes in activity of LP but not PD neurons. This allows us to decouple activity-dependent mechanisms from neuromodulator-dependent correlations of mRNA and conductance levels.

Ion channel conductances are correlated across channel types. We hypothesized that, as shown previously for PD neurons (Khorkova and Golowasch 2007), ionic conductances are expressed in other pyloric neurons in a correlated fashion. To test this, we measured three ionic currents, I_{HTK}, I_A, and I_H in PD and LP neurons and estimated the ionic conductances (g_{HTK}, g_A, and g_H). Control PD neurons expressed pairwise correlations (Fig. 2, *top* row) very similar to those described previously (Khorkova and Golowasch 2007). Table 1 lists all coefficients of determination (R^2) and Pearson product moment coefficients (ρ) for each pairwise conductance comparison. We performed the same measurements in another identified neuron, the LP neuron, and found that these three conductances were all similarly correlated in a pairwise manner (Fig. 3, *top* row, and Table 1). The nonparametric Spearman's rank correlation test was also used and gave nearly identical results to the

Pearson product moment correlation test; thus we report only the latter tests in this report.

To determine what factors may control these correlations, we treated these preparations in two different ways designed to disrupt the major inputs these cells receive within the STG: in one we used picrotoxin to block the synaptic input these two cells receive, and in the other we blocked all neuromodulatory input to the cells (decentralization). For the picrotoxin group, we treated the entire stomatogastric nervous system (Fig. 1*A*) with 10^{-5} M picrotoxin.

In this process of removing synaptic inhibition to LP, we greatly alter its firing pattern (Fig. 1*C*). Despite these manipulations, we observed that all pairwise correlations of the three ionic currents were maintained with similar correlation coefficients in both PD (Fig. 2) and LP neurons (Fig. 3, Table 1). Even though the g_{HTK}-g_H pair for the LP neurons shows a marginally higher *P* value (0.056) than the cutoff of 0.05, we accepted it as indicative of a significant correlation.

For the "decentralized" group, significant differences between the two cell types were observed after 24 h: in PD neurons, only the pairwise g_A vs. g_H correlation was maintained, whereas the g_{HTK} vs. g_A and the g_{HTK} vs. g_H correlations were lost (Fig. 2, Table 1); in contrast, in LP neurons, all of the correlations were maintained, but the correlation coefficient for g_A vs. g_H was significantly lower in decentralized relative to control groups (Fig. 3, Table 1).

In addition to the presence or absence of a significant correlation between conductances, we determined whether correlations that were maintained between conditions (e.g., the same correlation present in control and picrotoxin groups) differed in the slope of the relationship. Despite the fact that correlations were maintained among conductance pairs across experimental groups, there were significant changes in a subset of these relationships in both PD and LP cells (Table 2). There was a significant decrease in the slope of g_{HTK} vs. g_A between the control and picrotoxin-treated groups, as well as a significant increase in the g_A vs. g_H slope of the decentralized relative to the control group in PD cells. However, there was no change in the slope of the relationship between g_{HTK} and g_H in control and picrotoxin-treated PD cells. For LP cells, the slope of the g_{HTK} vs. g_A relationship was lower in picrotoxin-treated LP cells, whereas the slope of all three relationships was lower in decentralized LP cells relative to controls (Table 2).

Ion channel correlations at the mRNA level: distinct from conductance correlations. Pairwise comparison of channel mRNA levels under control conditions revealed a three-way correlation between *BK-KCa*, *H*, and *Shal* in PD neurons (Fig. 4, Table 3), consistent with the correlations observed at the ionic conductance level described above. Surprisingly, LP neurons showed no correlation of the *BK-KCa–Shal* pair, whereas the other two channel mRNA pairs showed strong and statistically significant correlation levels (Fig. 5, Table 3). Again, as before, to determine what factors may control these correlations, we treated one group of preparations with 10^{-5} M picrotoxin for 24 h, decentralized a second group for 24 h, and measured channel mRNA levels in both. We observed that PD neurons treated with picrotoxin showed similarly strong and statistically significant correlations in all three pairs as in the control preparations (Fig. 4, Table 3). Consistent with the correlations observed under control conditions, in LP neurons treated with picrotoxin, the *BK-KCa–Shal* pair showed
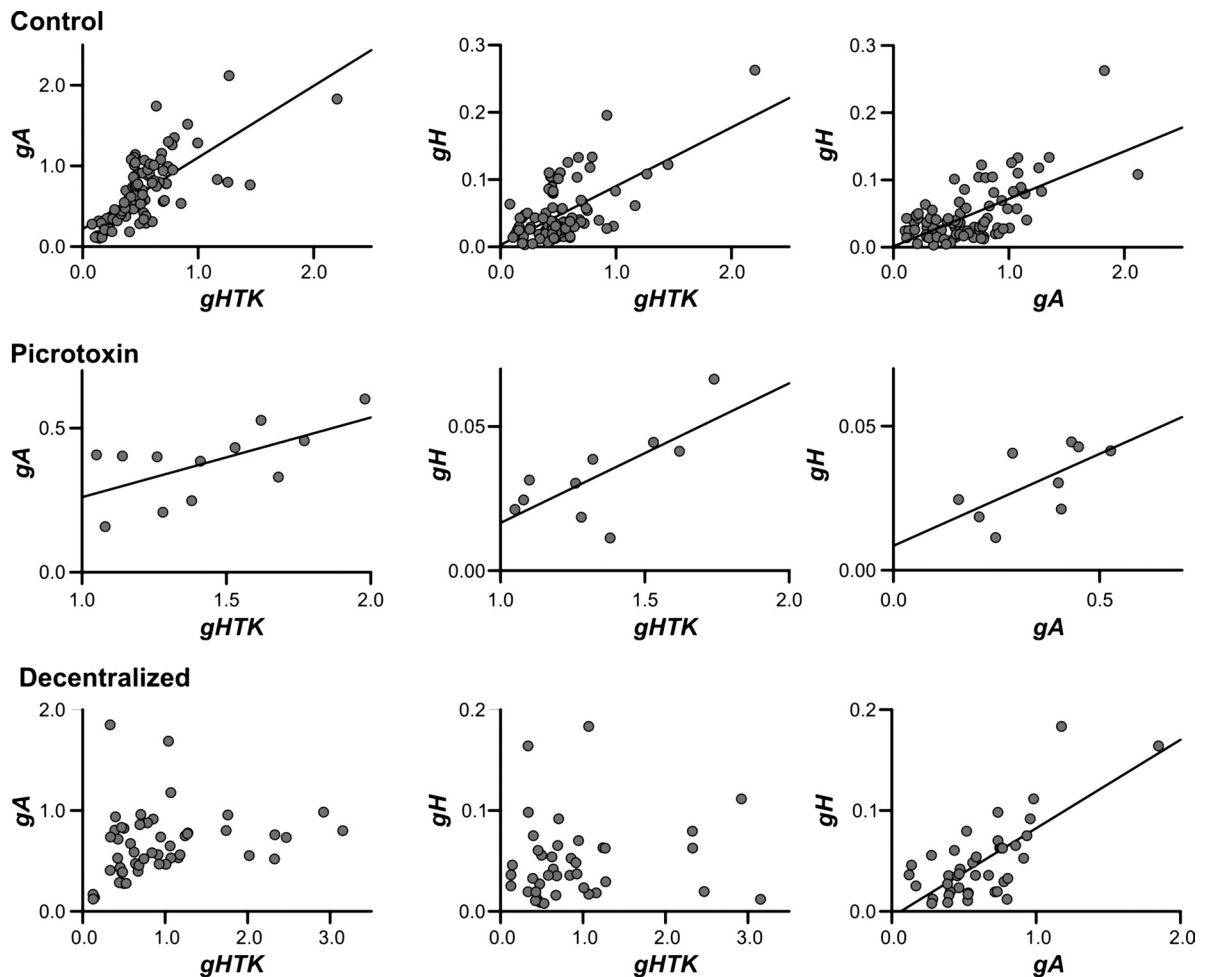
Fig. 2. Ionic conductance correlations in pyloric dilator (PD) neurons. Conductances of the high-threshold K^+ current (g_{HTK}), transient K^+ current (g_A), and hyperpolarization-activated inward current (g_H) are graphed in all pairwise combinations. Each point represents a different cell. Regression lines are shown only for significant correlations (Pearson correlation analysis, $P < 0.05$). Measurements were obtained under the 3 conditions indicated: control (*top* row), after 24 h in 10^{-5} M PTX (*middle* row), and 24 h after decentralization (*bottom* row). Ionic conductances are reported in μS.

no correlation, whereas the other two channel mRNA pairs did (Fig. 5, Table 3).

Finally, we evaluated the pairwise channel mRNA correlation levels in the decentralized preparation group and found another surprise: in the LP neurons, the *BK-KCa–Shal* pair that

had shown no statistically significant correlations in either the control or picrotoxin group now showed a moderate but statistically significant correlation. The other two channel mRNA pairs (*BK-KCa–H* and *Shal–H*) on the other hand, were mixed. There was no significant change in *BK-KCa–H* correlation, but

Table 1. *Ion channel conductance-level correlations*

	g_{HTK} vs. g_A			g_{HTK} vs. g_H			g_A vs. g_H		
	R^2	ρ (P value)	n	R^2	ρ (P value)	n	R^2	ρ (P value)	n
				PD neuron conductances					
Controls	0.481	**0.693**[a] (**<0.001**)	95	0.376	**0.613**[a] (**<0.001**)	94	0.409	**0.640**[a] (**<0.001**)	89
Picrotoxin	0.397	**0.630**[a] (**0.028**)	12	0.517	**0.719**[a] (**0.019**)	10	0.422	**0.722**[a] (**0.050**)	9
Decentralized	0.055	0.234 (0.102)	50	0.009	0.094 (0.562)	40	0.517	**0.719**[a] (**<0.001**)	41
				LP neuron conductances					
Controls	0.631	**0.794**[a] (**<0.001**)	76	0.405	**0.637**[a] (**<0.001**)	69	0.514	**0.717**[a,b] (**<0.001**)	70
Picrotoxin	0.396	**0.630**[a] (**0.038**)	11	0.383	**0.619**[a] (**0.056**)	10	0.795	**0.892**[a] (**<0.001**)	10
Decentralized	0.443	**0.665**[a] (**<0.001**)	31	0.213	**0.462**[a] (**0.022**)	24	0.276	**0.526**[b] (**0.006**)	26

Coefficients of determination (R^2) and Pearson product moment correlation coefficients (ρ) of pyloric dilator (PD) and lateral pyloric (LP) neurons (n = no. of neurons) were determined under control, picrotoxin, and decentralized conditions for pairs of ion channel conductance levels: g_{HTK}, high-threshold K^+ current conductance; g_A, transient K^+ current conductance; g_H, hyperpolarization-activated inward current conductance. Boldface indicates a significant ($P < 0.05$) correlation in the Pearson's correlation analysis. [a,b]Different superscript letters between 2 groups indicate significant differences among correlation coefficients of these groups. Correlation coefficient analysis was not performed with groups in which a significant correlation was not found.
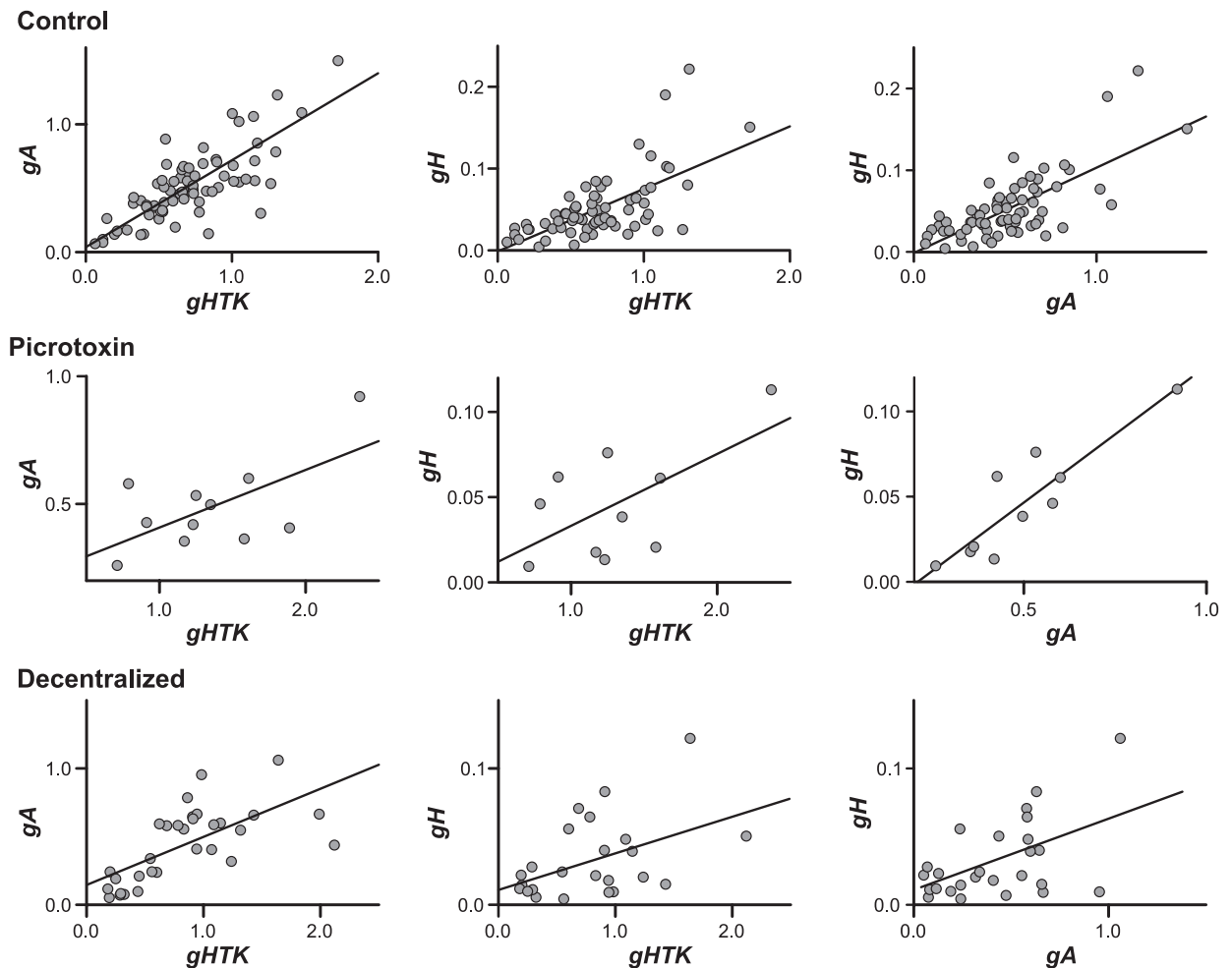
Fig. 3. Ionic conductance correlations in LP neurons. Conductances g_{HTK}, g_A, and g_H are graphed in all pairwise combinations. Each point represents a different cell. Regression lines are shown only for significant correlations (Pearson correlation analysis, $P < 0.05$). Measurements were obtained under the 3 conditions indicated: control (*top* row), after 24 h in 10^{-5} M PTX (*middle* row), and 24 h after decentralization (*bottom* row). Ionic conductances are reported in μS.

there was a significant decrease in the correlation coefficient of the *Shal–H* relationship (Fig. 5, Table 3).

We also determined whether the slopes of the relationships changed for mRNA correlations across treatment groups (Table 4). There was a significant decrease in both the *BK-KCa* vs. *H* and *Shal* vs. *H* relationships from control to the picrotoxin

group, whereas the slope of the relationship between *BK-KCa* and *Shal* was maintained in PD cells. In decentralized PD cells, there was a significant decrease in the slope of the *BK-KCa* vs. *Shal* and *BK-KCa* vs. *H* relationships relative to control, and the *Shal* vs. *H* relationship was lost. For LP cells, there was a significant increase in the *Shal* vs. *H* relationship in picrotoxin, whereas the *BK-KCa*

Table 2. *Slopes for pairwise conductance-level relationships*

	g_{HTK} vs. g_A			g_{HTK} vs. g_H			g_A vs. g_H		
	Slope	SD	n	Slope	SD	n	Slope	SD	n
	PD neuron conductances								
Controls	**0.8875**[a]	0.10	95	0.087[a]	0.011	94	**0.013**[a]	0.012	91
Picrotoxin	**0.2765**[b]	0.11	12	0.048[a]	0.017	10	0.064[a,b]	0.028	9
Decentralized	NS	NS	50	NS	NS	40	**0.088**[b]	0.014	41
	LP neuron conductances								
Controls	**0.68**[a]	0.06	76	**0.076**[a]	0.011	69	**0.104**[a]	0.012	70
Picrotoxin	**0.23**[b]	0.09	11	0.042[a,b]	0.019	10	**0.16**[a]	0.029	10
Decentralized	**0.35**[b]	0.07	31	**0.027**[b]	0.011	24	**0.055**[b]	0.018	26

Conductances were measured under control, picrotoxin, and decentralized conditions, and slopes for significantly correlated conductances were analyzed across groups via modified analysis of covariance (ANCOVA). Boldface indicates comparisons in which the conditions result in significantly different slopes from one another ($P < 0.05$). [a,b]Different superscript letters for slope values indicate pairs for which the difference is significant (thus pairs with the same superscript are not different). NS, no significant pairwise correlation was found between the 2 conductance levels in a given treatment group.
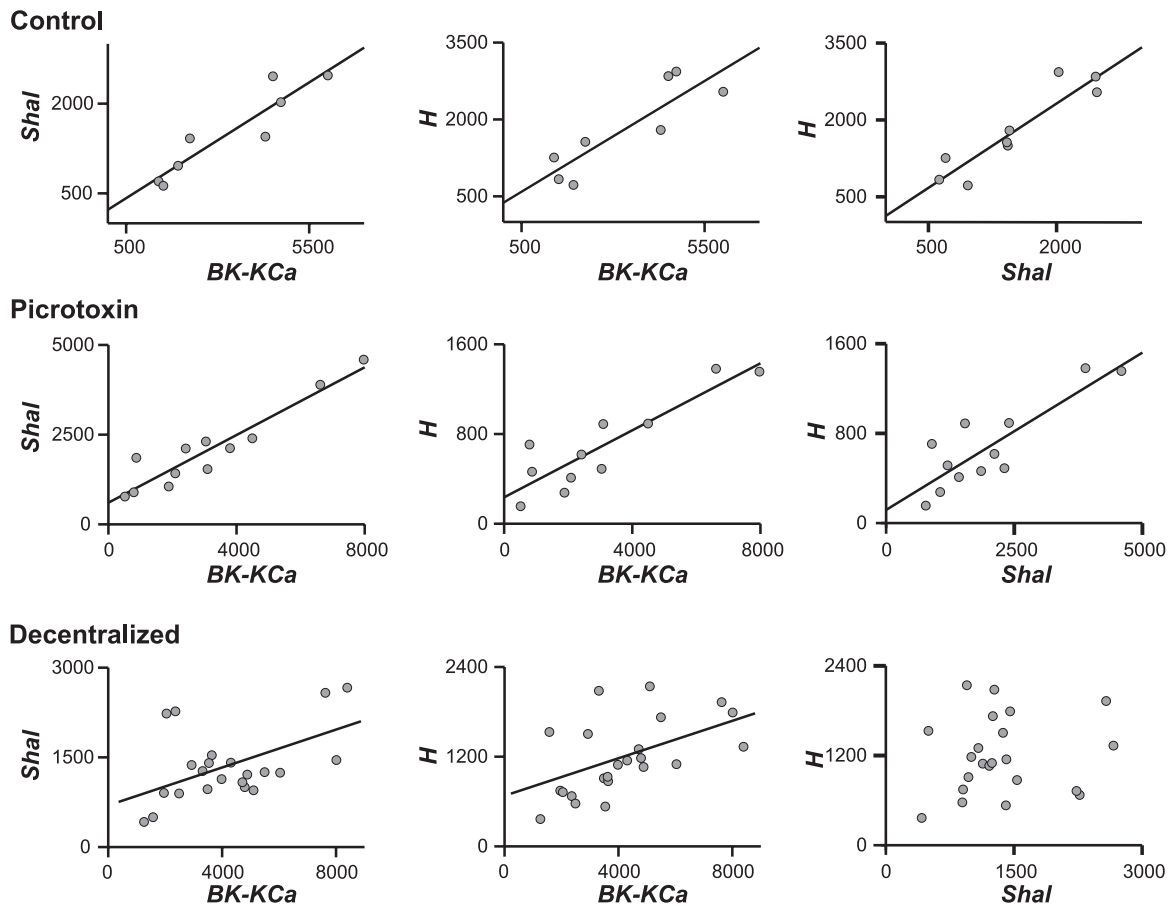
Fig. 4. Channel mRNA correlations in PD neurons. mRNA levels of *BK-KCa*, *Shal*, and *H* are graphed in all pairwise combinations. Each point represents a different cell. Regression lines are shown only for significant correlations (Pearson correlation analysis, $P < 0.05$). Measurements were obtained under the 3 conditions indicated: control (*top* row), after 24 h in 10^{-5} M PTX (*middle* row), and 24 h after decentralization (*bottom* row). Numbers indicate mRNA copy numbers.

vs. *H* relationship was unchanged. No significant changes were seen in the slopes of mRNA relationships relative to control in decentralized LP cells, although a novel *BK-KCa* vs. *Shal* relationship was detected.

DISCUSSION

Neurons have the ability to generate a functional output that is stable over long time scales. To ensure this, neurons express plasticity in their intrinsic properties and excitability (Daoudal and Debanne 2003; Davis 2006; Frick and Johnston 2005; Haedo and Golowasch 2006; Thoby-Brisson and Simmers 2002; Turrigiano and Nelson 2004; Zhang and Linden 2003), which manifests itself via changes in ionic channel properties (Zhang and Linden 2003), but the levels at which this is regulated, and the molecular mechanisms involved, remain to be understood. It has been shown previously that ionic chan-

Table 3. *Ion channel mRNA-level correlations*

	BK-KCa vs. Shal			BK-KCa vs. H			Shal vs. H		
	R^2	ρ (P value)	n	R^2	ρ (P value)	n	R^2	ρ (P value)	n
					PD neuron mRNA				
Controls	0.848	**0.921[a] (0.001)**	9	0.755	**0.869[a] (0.005)**	8	0.847	**0.920[a] (<0.001)**	9
Picrotoxin	0.886	**0.941[a] (<0.001)**	12	0.791	**0.889[a] (<0.001)**	11	0.728	**0.853[a] (<0.001)**	12
Decentralized	0.238	**0.487[b] (0.021)**	22	0.303	**0.550[b] (0.006)**	23	0.014	0.118 (0.600)	22
					LP neuron mRNA				
Controls	0.089	0.298 (0.216)	19	0.602	**0.705[a] (0.001)**	16	0.782	**0.884[a] (<0.001)**	18
Picrotoxin	0.034	0.186 (0.585)	11	0.649	**0.806[a] (0.005)**	10	0.932	**0.965[a] (<0.001)**	9
Decentralized	0.357	**0.598 (0.015)**	16	0.328	**0.573[a] (0.020)**	16	0.328	**0.573[b] (0.020)**	16

R^2 and ρ of PD and LP neurons were determined under control, picrotoxin, and decentralized conditions for pairs of ion channel mRNA levels. Boldface indicates a significant ($P < 0.05$) correlation in the Pearson's correlation analysis. [a,b]Different superscript letters between 2 groups indicate significant differences among correlation coefficients of these groups. Correlation coefficient analysis was not performed with groups in which a significant correlation was not found.
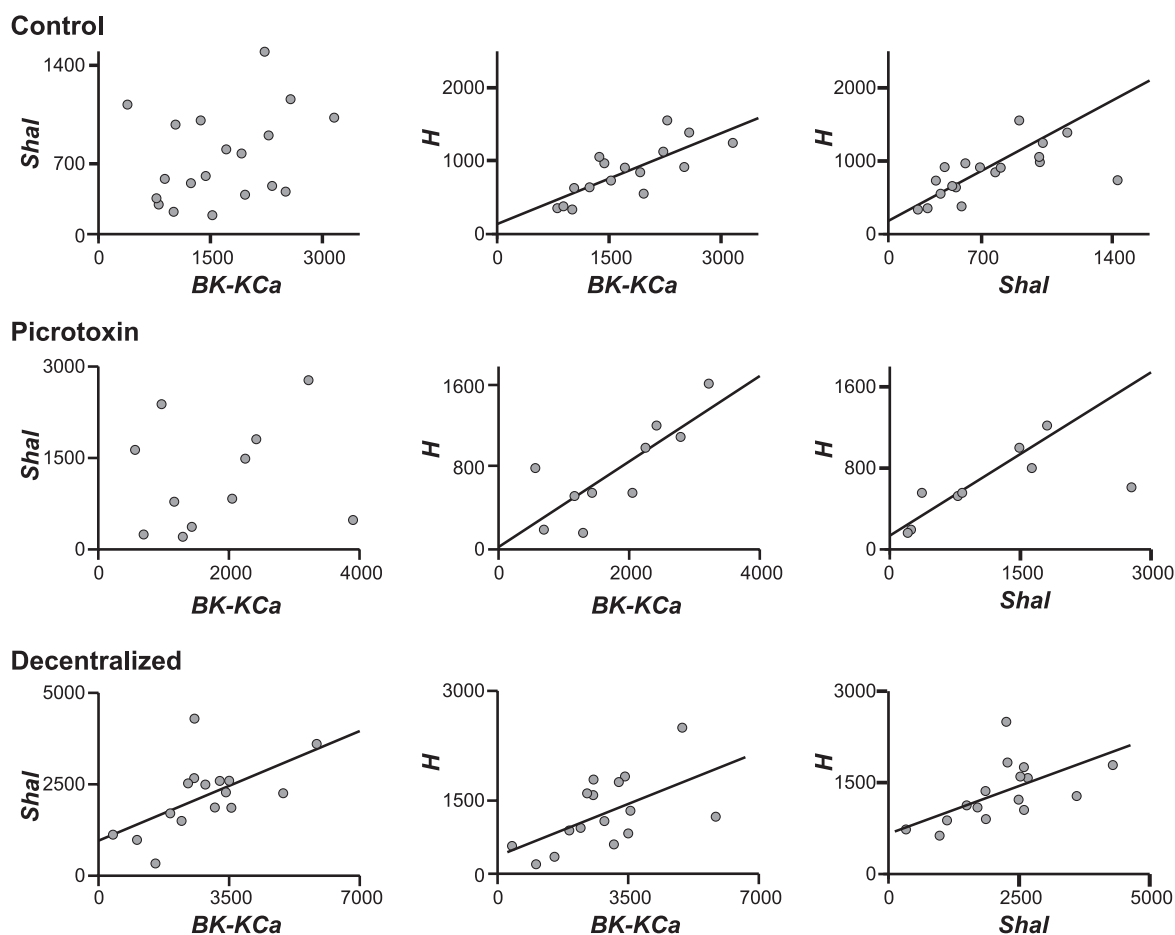
Fig. 5. Channel mRNA correlations in LP neurons. mRNA levels of *BK-KCa*, *Shal*, and *H* are graphed in all pairwise combinations. Each point represents a different cell. Regression lines are shown only for significant correlations (Pearson correlation analysis, $P < 0.05$). Measurements were obtained under the three conditions indicated: control (*top* row), after 24 h in 10^{-5} M PTX (*middle* row), and 24 h after decentralization (*bottom* row). Numbers indicate mRNA copy numbers.

nels may be codependent at both the mRNA (Schulz et al. 2007) and the conductance levels (Khorkova and Golowasch 2007; MacLean et al. 2003) and that such codependence may be related to the homeostatic regulation of function in the pyloric network (Ball et al. 2010; Burdakov 2005; Franklin et al. 2010; Khorkova and Golowasch 2007; MacLean et al. 2005). The purpose of this study was twofold: first, to deter-

mine whether the apparent coregulation of ionic channel expression is cell-type specific, and second, to determine how neuromodulatory input and synaptic activity affects the correlated expression of ionic channels at both the ionic conductance and mRNA levels. We have shown that *1*) neurons comodify ion channel mRNA (*BK-KCa*, *Shal*, and *H*) levels in a cell-specific manner: under control conditions (i.e., neuro-

Table 4. *Slopes for pairwise ion channel mRNA-level relationships*

	BK-KCa vs. Shal			BK-KCa vs. H			Shal vs. H		
	Slope	SD	*n*	Slope	SD	*n*	Slope	SD	*n*
	PD neuron mRNA								
Controls	**0.39**[a]	0.07	8	**0.43**[a]	0.10	8	**1.10**[a]	0.18	9
Picrotoxin	**0.47**[a]	0.05	12	**0.15**[b]	0.03	11	**0.28**[b]	0.05	12
Decentralized	**0.14**[b]	0.06	22	**0.14**[b]	0.05	23	NS	NS	22
	LP neuron mRNA								
Controls	NS	NS	19	0.35[a]	0.88	18	**0.57**[a]	0.08	18
Picrotoxin	NS	NS	11	0.42[a]	0.11	10	**1.74**[b]	0.18	9
Decentralized	0.43	0.05	16	0.21[a]	0.08	16	1.14[a,b]	0.44	16

mRNA levels were measured under control, picrotoxin, and decentralized conditions, and slopes for significantly correlated conductances were analyzed across groups via modified ANCOVA. Boldface indicates comparisons in which the conditions result in significantly different slopes from one another ($P < 0.05$). [a,b]Different superscript letters for slope values indicate pairs for which the difference is significant (thus pairs with the same superscript are not different). NS, no significant pairwise correlation was found between the 2 mRNA levels in a given treatment group.

modulatory and synaptic input present), PD neurons express these three mRNA species in a three-way correlated manner, whereas LP neurons appear to do so only for the pairs *Shal* vs. *H* and *BK-KCa* vs. *H* and not for the *BK-KCa* vs. *Shal* pair. *2*) Removal of neuromodulatory input can destroy, induce, or alter the strength or slope of the correlated expression of ion channel mRNA in a cell-specific manner: in PD neurons, all correlated pairs either lose or have significantly weakened correlations, whereas LP neurons show a gain in the correlation of *BK-KCa* vs. *Shal* but weakening of the correlations of the other two pairs examined. *3*) At the conductance level, three-way pairwise correlations appear to be common to both cell types examined, but the response to the loss of neuromodulatory input is cell-type specific (i.e., different between PD and LP neurons) and is also distinct from that observed at the mRNA level. *4*) Finally, chemical synaptic activity does not seem to play a role, at least for the two cell types examined, in controlling the correlated expression of the ionic currents we measured at either the mRNA or the conductance levels. Of these results, only the three-way pairwise correlations and the absence of activity-dependent regulation of ionic conductances in PD neurons have been shown previously (Khorkova and Golowasch 2007). Yet, it was previously unclear whether these effects acted solely at the level of membrane conductances or whether they extended to multiple levels of cellular organization such as mRNA for ion channels. Furthermore, it was not known whether these relationships would exist in multiple neurons in the network, including a "follower" neuron such as LP, or be limited to critical pacemaker cells such as PD.

There is a substantial overlap in correlations among conductances and those among mRNA levels; in PD cells, correlations were consistent in six of nine relationships between conductances and mRNA, whereas in LP cells, seven of nine were consistent. These results therefore implicate a functional link between regulation at the mRNA level and membrane conductance, which has previously been seen for LP but not PD neurons (Schulz et al. 2006). Yet, one of the more striking outcomes of our study is that the correlations seen among channel mRNA types and those among ionic conductances, although both seemingly influenced strongly by neuromodulation, can themselves be distinct. These results indicate that neuromodulation plays a role, at least in part, in coordinating regulation across multiple levels of cellular organization. Nevertheless, our work suggests that modulators can have distinct and independent effects on, and perhaps independent pathways for, regulation of transcription and posttranslational mechanisms involved in generating membrane currents. This is consistent with recent studies demonstrating variation in similar kinds of relationships between mRNA and protein, presumably as a result of transcriptional and nontranscription-level variation (Foss et al. 2011). Although it is an obvious notion that mRNA abundance does not simply equate to mature protein or channel activity, this is, to our knowledge, the first demonstration of separate control by neuromodulators of membrane ion channel conductances and their mRNA. Given that our manipulations remove the input to the STG of a large number of neuromodulators [at last count, at least 27 (Marder and Bucher 2007)], it is conceivable that different modulators have distinct actions at different levels. However, it is interesting to note that a single peptidergic modulator (proctolin) has been shown to revert fully, in an activity-independent manner, all the effects

of decentralization on conductance correlations in PD neurons (Khorkova and Golowasch 2007). Our results are significant in that they reveal important differences in how the correlated expression of ionic currents ultimately comes about, suggesting multiple levels of potential regulation: at the very least, at the levels of transcription, and also at some level between the beginning of translation and the full integration of the channel proteins into the plasma membrane.

What are the possible mechanisms underlying this phenomenon? Cotranscription is a process by which the close proximity of molecular elements and genes involved in transcription increases the likelihood of them being simultaneously expressed (Sutherland and Bickmore 2009). This would result in ion channels appearing to be "tracking" each other's expression levels. If transcription is the point at which this process of coexpression occurs, the many modifications and variations that can occur along the way as the ion channel transcripts are processed, transported, and translated, and the expressed channel proteins are then modified and exported into the plasma membrane, could explain the lack of perfect inter-ion channel correlation across preparations (Tables 1 and 3). Furthermore, this could provide an explanation for the lower level of correlation observed in most pairs at the conductance rather than at the mRNA level (when significant correlations exist). Nevertheless, it appears that correlations in expression may also be implemented downstream of transcription. For instance, in LP neurons (control conditions), the *BK-KCa* vs. *Shal* pair, and in PD neurons (decentralized conditions), the *Shal* vs. *H* pair, show no apparent correlation at the transcription level but a high level of correlation at the conductance level. Mechanisms to explain this could be the cotranslational interaction of ion channels similar to what occurs during ion channel subunit assembly (Shi et al. 1996), the cotrafficking into the plasma membrane (Vanoye et al. 2010), the coassembly of ion channels into macromolecular complexes (e.g., Arcangeli 2011; Frank 2011; Zhang et al. 2011), or the direct interactions between ion channels via nonconducting properties (Kaczmarek 2006). The results observed by MacLean et al. (2003) in which the transfection of lobster PD neurons with *Shal* mRNA resulted in the activity-independent enhanced coexpression of the *H* current, suggest that the control of coexpression does occur at a translational or posttranslation level. We did not measure transcription per se, but only steady-state mRNA levels, and thus the correlations of mRNA types could be the result of posttranscriptional regulation of mRNA stability. Therefore, our results indicate that neuromodulators may regulate either transcription directly or the stability of mRNA in a concerted manner.

The loss of cotranscription observed in PD neurons after decentralization could be attributed to neuromodulators activating a transcription regulation pathway that affects the coexpression of ion channels at any of the steps mentioned above. Interestingly, our data suggest that in different neuronal cell types, this process is different (i.e., inverse, such as in LP neurons), suggesting that neuromodulators may also act to repress cotranscription. Although activity is known to influence the expression of ion channels in a wide variety of systems, including the pyloric network (Cudmore and Turrigiano 2004; Desai et al. 1999; Golowasch et al. 1999; Haedo and Golowasch 2006; Li et al. 2004; Loebrich and Nedivi 2009; Turrigiano et al. 1994; Zhang and Linden 2003), the

coexpression of the ion channels examined in this work appears not to be influenced by synaptic activity. Our results do not rigorously rule out activity as a factor, but STG neurons are known to be sensitive to patterned activity (Golowasch et al. 1999; Haedo and Golowasch 2006; Turrigiano et al. 1994), and synaptic activity is known to dramatically influence these patterns of activity in certain neurons (LP neurons, for example, see Fig. 1). Thus our results are consistent with a lack of effect of activity on the correlated expression of ion channels, which was also demonstrated previously for PD neurons (Khorkova and Golowasch 2007).

What functional role does coexpression of ion channels serve? Given the high level of variability in the conductances of distinct ionic currents between neurons of the same type (see range along the axes of any of our graphs herein), it appears that coexpression of ionic currents is one way to reduce the global variability of the system by linking multiple highly variable currents to each other. It has been shown theoretically that this can indeed stabilize specific activity features (Ball et al. 2010; Burdakov 2005; Franklin et al. 2010; MacLean et al. 2005). The loss of correlations between ionic conductances may be an evolutionary adaptation of the neurons in this system to permit the independent modification of their levels as the pyloric network recovers its lost activity. By modifying the process that keeps these conductances linked to each other, constraints on the system may be eased to make it better able to visit alternative activity states that may result in the restoration of rhythmic neuronal activity and behavioral output.

DISCLOSURES

No conflicts of interest, financial or otherwise, are declared by the author(s).

AUTHOR CONTRIBUTIONS

Author contributions: S.T., M.D., O.K., G.V., and A.D. performed experiments; S.T., M.D., O.K., G.V., A.D., D.J.S., and J.G. analyzed data; S.T., M.D., O.K., D.J.S., and J.G. interpreted results of experiments; S.T., M.D., D.J.S., and J.G. drafted manuscript; S.T., M.D., O.K., G.V., A.D., D.J.S., and J.G. edited and revised manuscript; S.T., M.D., O.K., G.V., A.D., D.J.S., and J.G. approved final version of manuscript; M.D., D.J.S., and J.G. prepared figures; D.J.S. and J.G. conception and design of research.

REFERENCES

Arcangeli A. Ion channels and transporters in cancer. 3. Ion channels in the tumor cell-microenvironment cross talk. *Am J Physiol Cell Physiol* 301: C762–C771, 2011.

Ball JM, Franklin CC, Tobin AE, Schulz DJ, Nair SS. Coregulation of ion channel conductances preserves output in a computational model of a crustacean cardiac motor neuron. *J Neurosci* 30: 8637–8649, 2010.

Baro DJ, Levini RM, Kim MT, Willms AR, Lanning CC, Rodriguez HE, Harris-Warrick RM. Quantitative single-cell-reverse transcription-PCR demonstrates that A-current magnitude varies as a linear function of *shal* gene expression in identified stomatogastric neurons. *J Neurosci* 17: 6597–6610, 1997.

Bergquist S, Dickman DK, Davis GW. A hierarchy of cell intrinsic and target-derived homeostatic signaling. *Neuron* 66: 220–234, 2010.

Bidaut M. Pharmacological dissection of pyloric network of the lobster stomatogastric ganglion using picrotoxin. *J Neurophysiol* 44: 1089–1101, 1980.

Burdakov D. Gain control by concerted changes in I_A and I_H conductances. *Neural Comput* 17: 991–995, 2005.

Coggan JS, Prescott SA, Bartol TM, Sejnowski TJ. Imbalance of ionic conductances contributes to diverse symptoms of demyelination. *Proc Natl Acad Sci USA* 107: 20602–20609, 2010.

Cudmore RH, Turrigiano GG. Long-term potentiation of intrinsic excitability in LV visual cortical neurons. *J Neurophysiol* 92: 341–348, 2004.

Daoudal G, Debanne D. Long-term plasticity of intrinsic excitability: learning rules and mechanisms. *Learn Mem* 10: 456–465, 2003.

Davis GW. Homeostatic control of neural activity: from phenomenology to molecular design. *Annu Rev Neurosci* 29: 307–323, 2006.

Del Negro CA, Koshiya N, Butera RJ Jr, Smith JC. Persistent sodium current, membrane properties and bursting behavior of pre-Botzinger complex inspiratory neurons in vitro. *J Neurophysiol* 88: 2242–2250, 2002.

Desai NS, Rutherford LC, Turrigiano GG. Plasticity in the intrinsic excitability of cortical pyramidal neurons. *Nat Neurosci* 2: 515–520, 1999.

Foss EJ, Radulovic D, Shaffer SA, Goodlett DR, Kruglyak L, Bedalov A. Genetic variation shaped protein networks mainly through non-transcriptional mechanisms. *PLoS Biol* 9: e1001144, 2011.

Frank RA. Endogenous ion channel complexes: the NMDA receptor. *Biochem Soc Trans* 39: 707–718, 2011.

Franklin CC, Ball JM, Schulz DJ, Nair SS. Generation and preservation of the slow underlying membrane potential oscillation in model bursting neurons. *J Neurophysiol* 104: 1589–1602, 2010.

Frick A, Johnston D. Plasticity of dendritic excitability. *J Neurobiol* 64: 100–115, 2005.

Goldman MS, Golowasch J, Marder E, Abbott LF. Global structure, robustness, and modulation of neuronal models. *J Neurosci* 21: 5229–5238, 2001.

Golowasch J, Abbott LF, Marder E. Activity-dependent regulation of potassium currents in an identified neuron of the stomatogastric ganglion of the crab *Cancer borealis*. *J Neurosci* 19: RC33, 1999.

Haedo RJ, Golowasch J. Ionic mechanism underlying recovery of rhythmic activity in adult isolated neurons. *J Neurophysiol* 96: 1860–1876, 2006.

Harris-Warrick RM. *Dynamic Biological Networks: the Stomatogastric Nervous System*. Cambridge, MA: MIT Press, 1992.

Hille B. *Ion Channels of Excitable Membranes*. Sunderland, MA: Sinauer Associates, 2001.

Hobert O, Carrera I, Stefanakis N. The molecular and gene regulatory signature of a neuron. *Trends Neurosci* 33: 435–445, 2010.

Kaczmarek LK. Non-conducting functions of voltage-gated ion channels. *Nat Rev Neurosci* 7: 761–771, 2006.

Khorkova O, Golowasch J. Neuromodulators, not activity, control coordinated expression of ionic currents. *J Neurosci* 27: 8709–8718, 2007.

Kilman VL, Marder E. Ultrastructure of the stomatogastric ganglion neuropil of the crab, *Cancer borealis*. *J Comp Neurol* 374: 362–375, 1996.

Li CY, Lu JT, Wu CP, Duan SM, Poo MM. Bidirectional modification of presynaptic neuronal excitability accompanying spike timing-dependent synaptic plasticity. *Neuron* 41: 257–268, 2004.

Loebrich S, Nedivi E. The function of activity-regulated genes in the nervous system. *Physiol Rev* 89: 1079–1103, 2009.

Luther JA, Robie AA, Yarotsky J, Reina C, Marder E, Golowasch J. Episodic bouts of activity accompany recovery of rhythmic output by a neuromodulator- and activity-deprived adult neural network. *J Neurophysiol* 90: 2720–2730, 2003.

MacLean JN, Zhang Y, Goeritz ML, Casey R, Oliva R, Guckenheimer J, Harris-Warrick RM. Activity-independent coregulation of I_A and I_h in rhythmically active neurons. *J Neurophysiol* 94: 3601–3617, 2005.

MacLean JN, Zhang Y, Johnson BR, Harris-Warrick RM. Activity-independent homeostasis in rhythmically active neurons. *Neuron* 37: 109–120, 2003.

Marder E, Bucher D. Understanding circuit dynamics using the stomatogastric nervous system of lobsters and crabs. *Annu Rev Physiol* 69: 291–316, 2007.

Marder E, Eisen JS. Transmitter identification of pyloric neurons: electrically coupled neurons use different transmitters. *J Neurophysiol* 51: 1345–1361, 1984.

Maynard DM, Dando MR. The structure of the stomatogastric neuromuscular system in *Callinectes sapidus*, *Homarus americanus*, and *Panulirus argus* (Decapoda Crustacea). *Philos Trans R Soc Lond B Biol Sci* 268: 161–220, 1974.

McAnelly ML, Zakon HH. Coregulation of voltage-dependent kinetics of Na^+ and K^+ currents in electric organ. *J Neurosci* 20: 3408–3414, 2000.

Peck JH, Gaier E, Stevens E, Repicky S, Harris-Warrick RM. Amine modulation of I_h in a small neural network. *J Neurophysiol* 96: 2931–2940, 2006.

Peck JH, Nakanishi ST, Yaple R, Harris-Warrick RM. Amine modulation of the transient potassium current in identified cells of the lobster stomatogastric ganglion. *J Neurophysiol* 86: 2957–2965, 2001.

Schulz DJ, Goaillard JM, Marder E. Variable channel expression in identified single and electrically coupled neurons in different animals. *Nat Neurosci* 9: 356–362, 2006.

Schulz DJ, Goaillard JM, Marder EE. Quantitative expression profiling of identified neurons reveals cell-specific constraints on highly variable levels of gene expression. *Proc Natl Acad Sci USA* 104: 13187–13191, 2007.

Selverston AI, Russell DF, Miller JP. The stomatogastric nervous system: structure and function of a small neural network. *Prog Neurobiol* 7: 215–290, 1976.

Shi G, Nakahira K, Hammond S, Rhodes KJ, Schechter LE, Trimmer JS. Beta subunits promote K^+ channel surface expression through effects early in biosynthesis. *Neuron* 16: 843–852, 1996.

Sutherland H, Bickmore WA. Transcription factories: gene expression in unions? *Nat Rev Genet* 10: 457–466, 2009.

Swensen AM, Marder E. Modulators with convergent cellular actions elicit distinct circuit outputs. *J Neurosci* 21: 4050–4058, 2001.

Thoby-Brisson M, Simmers J. Long-term neuromodulatory regulation of a motor pattern-generating network: maintenance of synaptic efficacy and oscillatory properties. *J Neurophysiol* 88: 2942–2953, 2002.

Turrigiano G, Abbott LF, Marder E. Activity-dependent changes in the intrinsic properties of cultured neurons. *Science* 264: 974–977, 1994.

Turrigiano GG, Nelson SB. Homeostatic plasticity in the developing nervous system. *Nat Rev Neurosci* 5: 97–107, 2004.

Vanoye CG, Welch RC, Tian C, Sanders CR, George AL Jr. KCNQ1/KCNE1 assembly, co-translation not required. *Channels (Austin)* 4: 108–114, 2010.

Zhang J, Bal M, Bierbower S, Zaika O, Shapiro MS. AKAP79/150 signal complexes in G-protein modulation of neuronal ion channels. *J Neurosci* 31: 7199–7211, 2011.

Zhang W, Linden DJ. The other side of the engram: experience-driven changes in neuronal intrinsic excitability. *Nat Rev Neurosci* 4: 885–900, 2003.

Zhao S, Golowasch J, Nadim F. Pacemaker neuron and network oscillations depend on a neuromodulator-regulated linear current. *Front Behav Neurosci* 4: 21, 2010.

APPENDIX 2. Ransdell JL, Nair SS, Schulz DJ (2012) Rapid homeostatic plasticity of intrinsic excitability in a central pattern generator network stabilizes functional neural network output. *Journal of Neuroscience* 32: 9649-9658. [Featured in "This Week in The Journal"].

Cellular/Molecular

Rapid Homeostatic Plasticity of Intrinsic Excitability in a Central Pattern Generator Network Stabilizes Functional Neural Network Output

Joseph L. Ransdell,[1] **Satish S. Nair,**[2] **and David J. Schulz**[1]

[1]Division of Biological Sciences and [2]Department of Electrical and Computer Engineering, University of Missouri-Columbia, Columbia, Missouri 65211

Neurons and networks undergo a process of homeostatic plasticity that stabilizes output by integrating activity levels with network and cellular properties to counter longer-term perturbations. Here we describe a rapid compensatory interaction among a pair of potassium currents, I_A and I_{KCa}, that stabilizes both intrinsic excitability and network function in the cardiac ganglion of the crab, *Cancer borealis*. We determined that mRNA levels in single identified neurons for the channels which encode I_A and I_{KCa} are positively correlated, yet the ionic currents themselves are negatively correlated, across a population of motor neurons. We then determined that these currents are functionally coupled; decreasing levels of either current within a neuron causes a rapid increase in the other. This functional interdependence results in homeostatic stabilization of both the individual neuronal and the network output. Furthermore, these compensatory increases are mechanistically independent, suggesting robustness in the maintenance of neural network output that is critical for survival. Together, we generate a complete model for homeostatic plasticity from mRNA to network output where rapid post-translational compensatory mechanisms acting on a reservoir of channels proteins regulated at the level of gene expression provide homeostatic stabilization of both cellular and network activity.

Introduction

The balance of plasticity and stability in generating appropriate output is a matter of fundamental importance in the nervous system across all functional levels. These processes occur even at the most fundamental level, the excitability of individual neurons, and yet little is known about mechanisms governing these processes (Marder, 2011; Turrigiano, 2011). Early work identified such processes of "homeostatic plasticity" of intrinsic excitability (LeMasson et al., 1993; Turrigiano et al., 1994, 1995; Golowasch et al., 1999), but subsequent focus more intensely shifted to determining how stabilization of synapses is accomplished through synaptic scaling (Turrigiano, 2012). Recently, a resurgence of interest in plasticity of intrinsic excitability has accompanied work on synaptic scaling (Debanne and Poo, 2010; Misonou, 2010; Turrigiano, 2011).

Fewer studies on homeostatic plasticity have considered functional compensation in the context of endogenous network activity. The most dramatic example may be complete recovery of motor network output following loss of central inputs as a result

of changes in conductances in the crustacean stomatogastric ganglion (STG) (Thoby-Brisson and Simmers, 1998, 2002). Knockouts of K$^+$ channels in mice have been shown to have modest effects on phenotype and cellular output as a result of compensation by other K$^+$ channels (Guo et al., 2005; Nerbonne et al., 2008). Additionally, overexpression of A-type K$^+$ channels in STG neurons results in little change in neuronal output as a result of compensatory increases in H-current (MacLean et al., 2003, 2005). However, these examples feature mechanisms that act over longer time scales of days to weeks. While initial reports of plasticity in intrinsic excitability were found over shorter time scales (Desai et al., 1999; Golowasch et al., 1999), surprisingly little is known of the role these mechanisms may play in short-term ongoing activity of biologically intact networks, specifically where an expectation for rapid conservation of output could be argued, such as in central pattern generators (CPGs).

Compensation in CPG circuits may be inferred from the fact that normal populations of unmanipulated motor neurons of two invertebrate CPGs, the cardiac and stomatogastric ganglia, show correlations in expression levels of mRNAs for ion channels (Schulz et al., 2007; Tobin et al., 2009) and membrane conductances (Khorkova and Golowasch, 2007; Temporal et al., 2012). One relationship detected in previous work (Tobin et al., 2009) is a positive correlation between *BKKCa* and *shaker* mRNA levels in neurons of the cardiac ganglion. These channels encode calcium-activated and A-type K$^+$ currents, respectively. However, it is unclear how a neuron would use two similar hyperpolarizing conductances additively to generate or maintain its output. In this study we focused on elucidating the functional relationship between these two conductances in motor neurons of the crab

cardiac ganglion. We discovered a striking discrepancy in the relationship of these channels across functional levels: mRNAs for these channels were positively correlated, while their conductances were negatively correlated. Therefore, we propose a comprehensive hypothesis for plasticity of excitability from mRNA to network output whereby rapid compensation provides stabilization of cellular and network activity.

Materials and Methods

Preparations. Cancer borealis crabs of either sex were purchased and shipped overnight from The Fresh Lobster Company (Gloucester, MA). Crabs were kept between 24 h and 2 weeks in artificial sea water at 12°C before use. Crabs were anesthetized in ice for 15 min before the dissection. The dissection took place in chilled physiological saline comprised of 440 mM NaCl, 26 mM MgCl₂ 13 mM CaCl₂, 11.2 mM Trizma base, 11 mM KCl, and 5 mM maleic acid (pH = 7.4). When we wanted to isolate individual large cells, individual strands of bulking nylon were used to ligate the nerve on both sides of a large cell soma. To impale large cells, each cell was individually desheathed using a tungsten needle (Fine Science Tools).

Quantitative single-cell RT-PCR. Quantitative RT-PCR was performed as previously described (Schulz et al., 2006a; Tobin et al., 2009). Primers specific for real-time PCR detection of *shal*, *BKKCa*, *shab*, and *shaker* using Sybr Green were developed and designed using Primer3 software and are the same as previously reported (Schulz et al., 2006a; Tobin et al., 2009). Briefly, total RNA was isolated using RNeasy micro column-based RNA extraction kit (Qiagen), reverse transcribed using SuperScript III reverse transcriptase (Invitrogen), and used as a template in real-time RT-PCR with Sybr Green (SABiosciences) in a RotorGene 3000 real-time PCR machine (Corbett Research). Previous studies have determined that in LC motor neurons, correlations can be equally well detected among channel mRNA levels with and without normalization of real-time results to 18S rRNA (Tobin et al., 2009). Values reported here are total copy numbers from a single neuron, and are not normalized with respect to 18S levels.

Pharmacology. Pharmacological blockers were dissolved in physiological saline and perfused onto the cardiac ganglion using a Rabbit peristaltic pump (Rainin Instruments) at a rate of 1.5 ml/min or added to the preparation from a stock solution via pipette. The following pharmacological agents were used: tetraethylammonium dissolved in saline at 25 mM, 4-aminopyridine dissolved in saline at 1 mM, cadmium chloride dissolved in saline at 250 μM (Acros Organics), tetrodotoxin dissolved in saline at 1 μM (Alomone Laboratories), BAPTA-AM dissolved DMSO and applied at 30 μM in saline, ryanodine dissolved DMSO and applied at 100 μM in saline, staurosporine dissolved in DMSO and applied at 5 μM in saline, okadaic acid dissolved in DMSO and applied at 500 nM in saline (Ascent Scientific), cyclosporine A dissolved in DMSO and applied at 2 μM in saline (Tocris Biosciences). All DMSO applications resulted in a final concentration of DMSO that was <1% (range: 0.000025% to 0.5%).

Pharmacological agents used to investigate intracellular mechanisms involved in the compensatory response (BAPTA-AM, ryanodine, okadaic acid, cyclosporine A, staurosporine) were applied to the cardiac ganglion 1 h prior (2 h prior with ryanodine) to the application of the blocker which caused the compensation (TEA or 4AP). A cell or preparation was exposed only to one channel blocker type (TEA or 4AP) for a given experiment.

Current measurements. All experiments were performed in physiological saline cooled to 12°C. To measure current magnitudes and activation properties, two-electrode voltage-clamp (TEVC) experiments were performed by impaling a large cell with two glass electrodes filled with 3 M KCl (8–17 MΩ resistance) and an Axoclamp 2A amplifier (Molecular Devices). All recordings were made from anterior large cell somata; action potential conductances were blocked (unless noted otherwise) by tightening thread ligatures on both sides of the large cell soma, preserving space clamp. TEVC protocols were created, driven and recorded with clampex 9.2 software (Molecular Devices). Current recordings were analyzed with Clampfit 9.2 software (Molecular Devices). Current and voltage traces were sometimes filtered with a lowpass boxcar filter using 7

smoothing points. Most voltage clamps were modified from those used previously in STG preparations (Golowasch and Marder, 1992; Khorkova and Golowasch, 2007; Temporal et al., 2012). High threshold potassium current (I_{HTK}) magnitude was measured using a leak subtracted TEVC protocol with a holding potential of −40 mV and 16 voltage steps from −55 mV to +20 mV (5 mV intervals). A-type potassium current (I_A) magnitude was measured by subtracting the I_{HTK} current traces from a TEVC protocol that is identical except for a holding potential of −80 mV. Calcium-activated potassium current (I_{KCa}) was isolated by subtracting postcadmium (250 μM CdCl₂, 1 h) I_{HTK} current traces from precadmium I_{HTK} current traces (isolating the cadmium-sensitive outward current). Delayed rectifier potassium current (I_{Kd}) was isolated using the I_{HTK} TEVC protocol after cadmium exposure (250 μM CdCl₂, 1 h). All current magnitude measurements were taken at 0 mV on an I-V plot made from the current traces.

Large cell excitability and network output. Cardiac network output was monitored with a single intracellular recording (using same equipment as TEVC protocols) taken from one of the three anterior large cells and an extracellular differential recording made with a model 1700 A-M Systems AC amplifier and two stainless steel wires; one placed inside and one outside a vaseline well located around the central nerve of the CG (see Fig. 1). Pharmacological blockers (TEA or 4AP) were perfused on the entirety of the CG with the exception of the four small cell and two posterior large cell somata. These cells were isolated from the perfusion by a vaseline well placed around these cells and the posterior branch point containing regular physiological saline (see Fig. 1). Using this experimental configuration we monitored the effect of the LC compensatory response (isolated to the best of our ability from small cells) in the context of the functioning network. Network activity was recorded in 10 min intervals before and during blocker perfusion. These recordings were analyzed using Spike2 v6.00 software (Cambridge Electronic Design).

LC intrinsic excitability was examined under similar conditions except 10^{-6} M TTX saline was placed in the vaseline well around the four small cell and two posterior LC somata. This eliminated spontaneous network activity and small cell excitatory input into the anterior LCs. Excitability in the anterior LCs was then monitored using two-electrode current-clamp (TECC) protocols run before and every 5 min after TEA or 4AP perfusion. TECC protocol was a six step depolarizing current injection (from 1 to 6 nA) lasting six seconds per step and six seconds between steps.

Statistics. All statistical tests were performed with SigmaPlot v11.0 (Systat, Aspire Software International). All data were confirmed to be of normal distribution as required by statistical analyses used. Relationships between channel mRNAs and ionic currents were analyzed using Pearson's correlation test, and coefficients of determination were calculated from the resulting correlation coefficients. In the case of Figure 2, C and D, a potential outlier was identified that could be anchoring a false positive for the Pearson's test (see arrows). Analyses on these datasets were performed both with and without the data point in question and both results reported. Bonferroni corrections were used for multiple comparisons in the correlation analyses, and the p value adjusted to 0.017 for statistical significance (three comparisons each for mRNA and ionic currents). Changes in current magnitude before and after pharmacological block were analyzed in one of two ways. Raw currents were analyzed before and after blockade via paired *t* tests, and these are reported in Figure 3. In Figure 5, significant changes in a current relative to baseline were expressed as a percent change from zero, and analyzed via one-sample *t* test with the hypothesized population mean set to 0. Overall changes in burst duration, spikes per burst, and spike frequency within the burst reported in Figure 4 were analyzed with repeated-measures ANOVA.

Results

The crustacean cardiac ganglion as a model for central pattern generator network activity

The rhythmic pumping of the heart in decapod crustaceans such as the crab, *Cancer borealis* (our model organism), is neurogenic
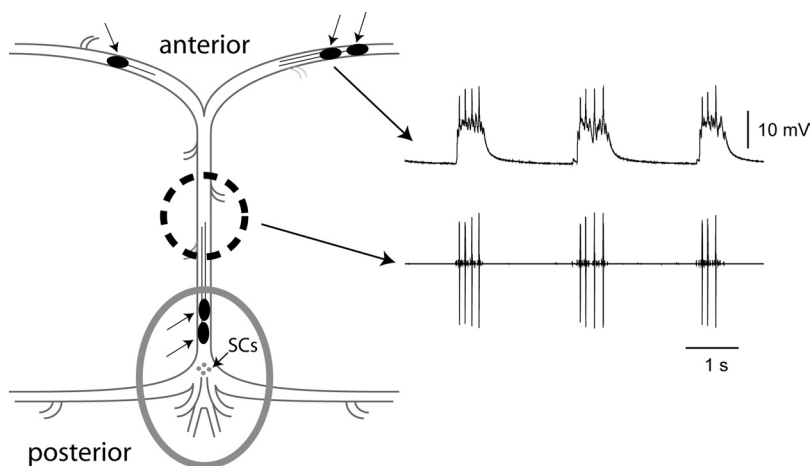
Figure 1. The crustacean cardiac ganglion. When dissected from the animal, the cardiac ganglion can be pinned flat and simultaneous recordings of network activity and intracellular recordings can be obtained. Five large cell somata (dark ovals marked with arrowheads) are distributed throughout the ganglion. Individual or pairs of large cells can be isolated for voltage clamp with thread ligature, or for pharmacological treatment with a vaseline well. The recording shows a simultaneous extracellular and intracellular recording of network activity. The bursting of the network is seen at the site indicated by the dotted circle and corresponds to the extracellular (bottom) trace. Burst output of a single LC motor neuron is seen in the top trace, taken from an intracellular recording of a LC soma. This rhythmic motor activity corresponds directly to the contraction of the single-chambered crab heart muscle, showing an *in vitro* maintenance of biological network activity. The gray oval represents a vaseline well used in pharmacological blocker experiments. During measurements of individual LC excitability (Fig. 4A), this well was used to apply TTX to the small cell pacemaker neurons (SCs, small gray circles) to silence the network activity but preserve output capability in anterior LCs. During measurements of compensation during ongoing network activity, this cell was used to protect SCs from blocker application in the bath (Fig. 4B).

in nature, and under the control of a simple central pattern generator network called the cardiac ganglion (Alexandrowicz, 1932) (Fig. 1). The ganglion consists of only nine neurons: four "small cell" interneurons (SCs) that generate the pacemaker activity and five "large cell" motor neurons (LCs) that innervate the heart musculature (Hartline, 1967; Tazaki and Cooke, 1983c). The SCs of the cardiac ganglion are endogenous oscillators, i.e., they undergo spontaneous and rhythmic generation of a depolarizing wave of membrane potential that leads to a bursting phenotype of multiple spikes per burst (Tazaki and Cooke, 1983b; Cooke, 2002). The LCs of the CG produce bursts of action potentials as a result of synaptic pacemaker input from the SCs, ultimately leading to muscle contraction (Hartline, 1967; Tazaki and Cooke, 1979, 1983a,c; Berlind, 1989). The behavioral output of the ganglion represents a direct correlation of the influence of LCs on heart muscle (Sakurai and Wilkens, 2003; García-Crescioni et al., 2010), and thus a direct measure of heart activity. Yet the entire network can be dissected out intact, and maintained in physiological saline for extended periods of recording while continuing to produce its endogenous rhythmic output. The motor neurons are all individually identifiable, and due to their distributed nature within the ganglion (Fig. 1), we can perform pharmacological manipulations on one or multiple motor neurons, either in isolation or in the intact, functional network (Tazaki and Cooke, 1983a; Cooke, 2002). The underlying burst potentials of the LCs represent functional output at the motor neuron level, and our preliminary modeling studies show how the simplicity of this model system can be used to study functional implications of the relationships between mRNAs and ionic conductances on cellular output (Ball et al., 2010; Franklin et al., 2010).

Relationship between I_A and I_{KCa} in a population of large cell motor neurons

Potassium currents were measured using protocols developed for the STG cells of the same species (Golowasch and Marder, 1992).

The total outward current of LC motor neurons consists primarily of three K^+ currents (Fig. 2B) (Golowasch and Marder, 1992): A-type transient K^+ current (I_A), calcium-activated K^+ current (I_{KCa}), and delayed rectifier K^+ current (I_{Kd}). I_{KCa} and I_{Kd} can be found in one combined current trace elicited from holding potentials at -40 mV or higher, and is termed here as the high-threshold K^+ current (I_{HTK}), while the A-type current can be measured by subtracting I_{HTK} from the total outward current elicited from a holding potential of -80 mV.

We first examined the relationships among mRNA levels in single identified LC motor neurons for three channel genes that correspond to these three K^+ currents (Atkinson et al., 1991; Tsunoda and Salkoff, 1995; Kim et al., 1998): *BKKCa* (I_{KCa}), *shaker* (I_A), and *shab* (I_{Kd}). We detected a significant correlation between *BKKCa* and *shaker* mRNA levels across a population of 20 LC motor neurons (Fig. 2A, left), but no correlations among any other channel mRNAs (Fig. 2A, middle, right). A fourth channel mRNA encoding an A-type K^+ current, *shal*, also was significantly positively correlated to *BKKCa* mRNA levels ($p < 0.005$; $R^2 = 0.58$), as well as to *shaker* ($p < 0.002$; $R^2 = 0.42$) but not to *shab*, suggesting an overall relationship between I_{KCa} and I_A, but not with I_{Kd}, in these cells.

We next examined the relationships among the ionic currents encoded by these channel genes across a population of LC motor neurons. I_A, I_{KCa}, and I_{Kd} were all measured in each cell across a population of LC motor neurons. A similar pattern of correlated current levels was seen as with the mRNA with one striking distinction: only I_A and I_{KCa} showed a significant correlation (Fig. 2A), but the correlation was strongly negative as opposed to positive as seen in the mRNA measurements. No significant correlations were found between I_A and I_{Kd}, or I_{KCa} and I_{Kd} (Fig. 2A). Because of the striking difference between the mRNA correlation (positive), and the current correlation (negative), we were most interested in pursuing the relationship between I_A and I_{KCa}, but had concerns about the effects of pharmacological blockers used to measure I_{KCa} (Fig. 3F); we use Cd^{2+} to block calcium currents that evoke I_{KCa} to measure this current via subtraction from I_{HTK}, as we have not identified any blockers specific to I_{KCa} in our preparation despite many attempts. Therefore, we decided to use the peak I_{HTK} as an indicator of I_{KCa} abundance in these experiments.

I_{HTK} (HighThreshold K^+) is known from previous work (Golowasch and Marder, 1992; Haedo and Golowasch, 2006; Khorkova and Golowasch, 2007) to, in large part, consist of I_{KCa}, particularly the transient portion, as I_{Kd} shows no transient peak that could account for the peak in I_{HTK} (Fig. 2B). We also determined that measurements of the peak I_{HTK} were likely sufficient to reveal the relationship between I_{KCa} and I_A, as the only transient peak seen in the currents that underlie I_{HTK} belongs to I_{KCa} (Fig. 2B, right). Peak I_{HTK} also shows the same negative relationship with I_A as does I_{KCa} (Fig. 2C, left), and peak I_{KCa} itself very strongly correlates with peak I_{HTK} (Fig. 2C, middle), but not I_{Kd} (Fig. 2C, right). Accordingly, for the remainder of the study, we

used I_{HTK} peak current from baseline as a measure of I_{KCa} abundance, to allow for measurement of all K^+ currents under the least manipulative pharmacological blocker regime, i.e., without the need to block voltage-gated calcium currents.

I_{KCa} and I_A are rapidly upregulated within the same LC motor neuron

Because the focus of the study was on the negative relationship between I_A and I_{KCa}, we decided to repeat the initial measurements in a new population of LC motor neurons to confirm the original finding before examining the functional impact of this relationship. In a distinct population of 20 LC motor neurons, we once again found a strong negative relationship between I_A and I_{KCa} (as revealed by I_{HTK} measurements; Fig. 3A), confirming our original finding. This strongly suggested a causal relationship between I_A and I_{KCa}. Specifically, we hypothesized that if these two currents are functionally interrelated, then a decreased level of I_A should result in an increased level of I_{KCa} and vice versa. We tested this hypothesis by blocking one current in this pair and determining whether there was an effect on the magnitude of the other. We measured baseline levels of I_A in a given cell, then used tetraethylammonium (TEA) to block the HTK-current for 60 min, and then measured I_A again post-TEA. 60 min of exposure to TEA significantly increased peak ($p < 0.001$; paired t test) A-current (Fig. 3B,C). The converse experiment was performed using 4-aminopyridine (4AP) for 60 min to block I_A. The peak ($p < 0.003$) of I_{HTK} was significantly increased following 60 min of 4-AP blockade (Fig. 3B,C). Additionally, these results appear to be due to an overall increase in conductance, since no change was seen in the voltages of activation of I_A and I_{HTK} concomitant with the changes in total current as a result of the block experiments (Fig. 3D). No consistent or significant effects of TEA and 4-AP on neuronal input resistance were observed in these cells (ΔR_{IN} TEA: -1.87 ± 2.5 MΩ, ΔR_{IN} 4-AP: -0.52 ± 1.7 MΩ).

Our initial data strongly implicate I_{KCa} and I_A as the key pair of currents involved in this response. Since I_{HTK} is a mixed current comprised predominantly of I_{KCa} and I_{Kd}, and both of these currents are blocked by TEA, we determined whether the changes seen in I_{HTK} as a result of 4AP blockade were attributable to just one or to both of these currents. Most convincingly, while 4AP block significantly increases I_{HTK} (Fig. 3C), 1 h of exposure to 4AP had no significant effect on I_{Kd} magnitude itself (Fig. 3E, left). Unfortunately, we have not identified a blocker specific to I_{KCa} in our preparation to directly test the effects of blocking this current on changes in I_A. However, we can indirectly block I_{KCa} by using CdCl$_2$ to block voltage-gated Ca^{2+} channels that trigger I_{KCa}. Blocking with Cd^{2+} completely eliminates I_{KCa} in these cells, and causes a significant increase in I_A after 1 h of exposure that is very similar to that seen with TEA (Fig. 3E, right). Together, these data strongly suggest that the relationship between
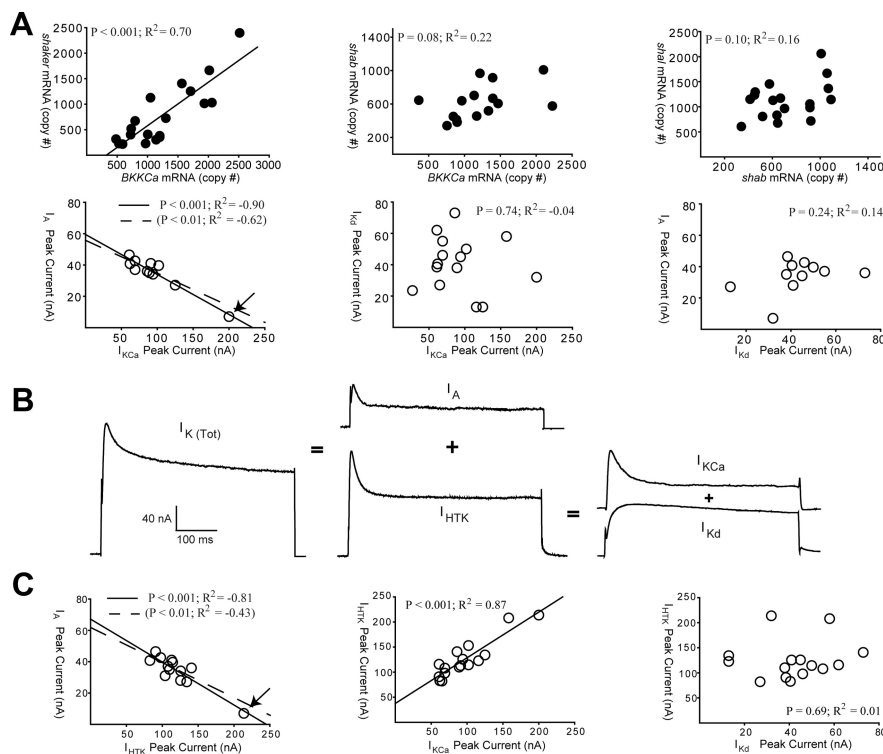

Figure 2. Relationships among channel gene mRNA levels and among ionic currents in a normal population of large cell motor neurons. **A**, Correlations between mRNA levels from single identified LC motor neurons for BKKCa, shaker, and shab channel genes (top row) and the corresponding K$^+$ current correlations from single identified LC motor neurons for I_{KCa}, I_A, and I_{Kd} (bottom row). Each point represents values from a single neuron. Regression lines shown only for significant correlations as revealed by Pearson's test, for which the p value and R^2 values are reported in each plot. When two regression lines are present, the solid line and top set of statistics refers to the entire dataset, while the dotted line and the bottom set of statistics represents the correlation with the single point indicated by the arrow removed. Despite having this outlier removed, the correlation is still significant and largely unchanged. **B**, The total K$^+$ current ($I_{K(Tot)}$) in LC motor neurons consists primarily of three distinct K$^+$ currents: A-type K$^+$ (I_A), and the high-threshold K$^+$ current (I_{HTK}) that can be subdivided into calcium-activated K$^+$ (I_{KCa}) and delayed rectifier K$^+$ (I_{Kd}). **C**, Correlations between currents reveal that I_{HTK} peak is highly representative of I_{KCa} levels, but not of I_{Kd}. With these results, we use I_{HTK} peak levels as an indicator of I_{KCa} for any given cell for the remainder of the study. Statistics as in **A**.

I_A and I_{HTK} identified in the experiments (Fig. 3) are the result of a causal relationship between the levels of I_A and I_{KCa} in a given motor neuron.

I_A and I_{KCa} act in a compensatory fashion to stabilize cellular excitability and network output

The negative correlation we measured between I_A and I_{KCa} in the normal population, together with the rapid change in currents seen within a cell after TEA and 4AP block, led us to hypothesize that levels of I_A and I_{KCa} may be acting in a compensatory fashion to stabilize both cellular and network output. To determine whether such a functional compensation exists, we followed over time the activity of both isolated LCs, as well as LCs in an intact network, with either 4AP or TEA blockade, and then determined whether the output of the cells and of the network changed over the course of the blockade and the potential compensation.

As seen in Figure 4, A and B, TEA blockade caused a substantial increase in the excitability of the LC motor neuron in the initial 10–20 min. However, over the time course of the measured increase in I_A seen in previous experiments (Fig. 2C) there was a compensatory change in the output of the cell and of the network toward the baseline level of activity. In isolated LCs (Fig. 4A), both TEA and 4AP application shifted the cells from a less excitable state to a state characterized by large sustained burst potentials. However, over the time course of compensation, the
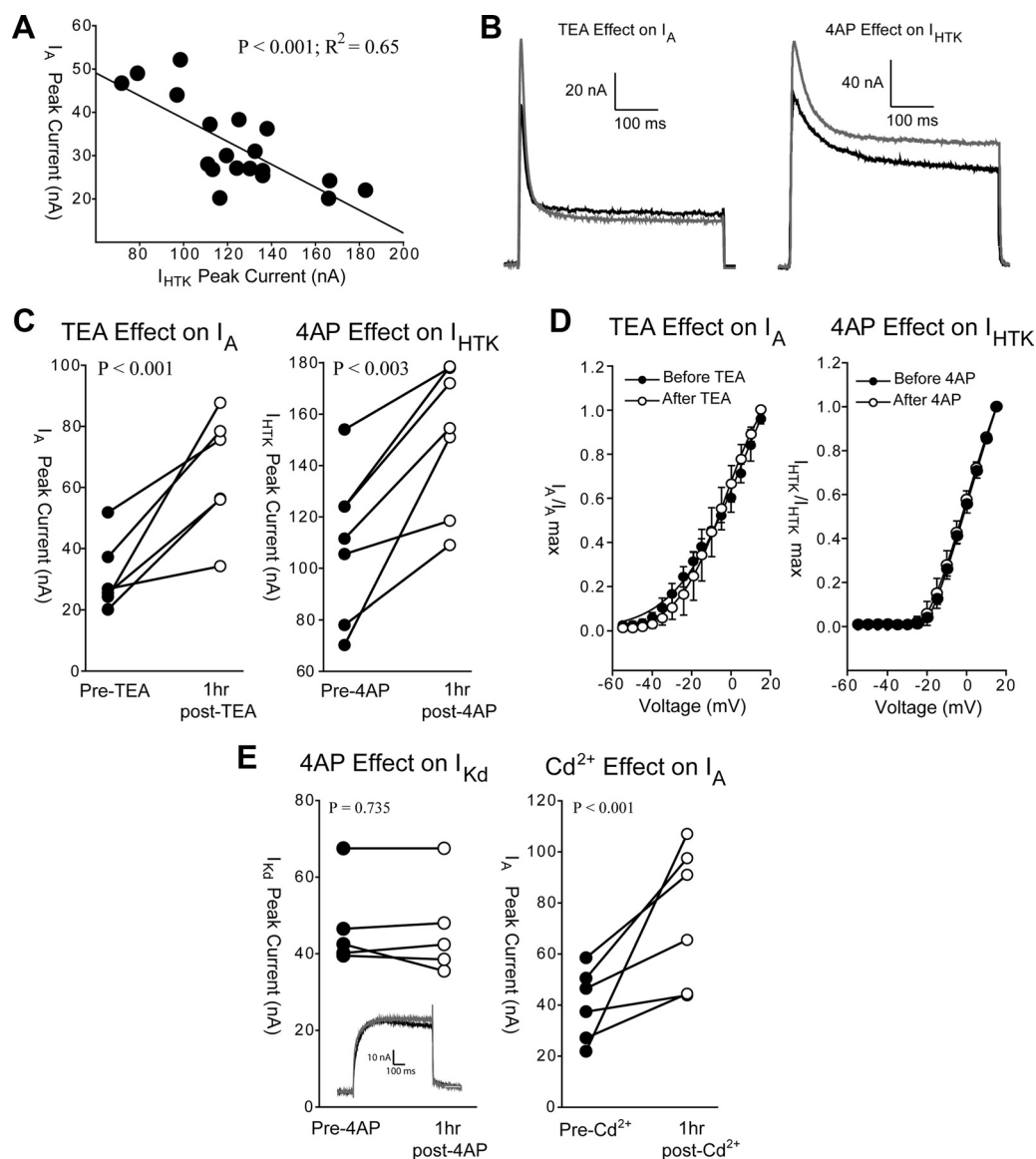
Figure 3. Reciprocal interaction of I_A and I_{HTK} levels in LC motor neurons. **A**, Correlation between peak I_A and I_{HTK} across a second population of LC motor neurons distinct from those in Figure 2. Statistics represent results of a Pearson's test ($n = 20$). **B**, Representative recordings of the increase in I_A after TEA exposure (left) and the increase in I_{HTK} after 4AP exposure (right). Black trace is the control, gray trace is the same cell after 60 min exposure to blocker. **C**, Quantified effects of TEA (left) and 4AP (right) on the peak I_A and I_{HTK} respectively in $N = 6$ cells. The same cell before (black) and after (white) is connected with a solid line. Statistics represent paired t test on mean current before and after blocker. **D**, Activation characteristics, expressed as I/I_{max} for an $N = 5$ cells, of I_A (left) and I_{HTK} (right) before and after block with TEA and 4AP, respectively. Each point represents mean $\pm$ SD. **E**, Effects of 4AP on I_{Kd} (left; $N = 5$) and Cd^{2+} on I_A (right; $N = 6$). Insert in the left panel shows representative traces of I_{Kd} before (black) and after (gray) exposure to 4AP. Legends and statistics as in **C**.

excitability of isolated cells returned to control levels, losing the large burst potentials and showing firing patterns similar to those before the application of the blocker (Fig. 4A).

In the intact network, TEA often caused a complex multiphase bursting output in treated LCs (Fig. 4B; 10 min recording). Given this somewhat complex pattern of bursting, we determined that measurements of burst duration across a population of these cells represented the clearest means to quantify changes in output over time. Over the course of 60–90 min, TEA blockade resulted in a significant change in burst duration ($p < 0.01$; ANOVA; Fig. 4C, left), initially increasing to nearly twice as long as control before re-establishing a stable burst duration indistinguishable from that at the control level (Fig. 4B).

In the companion experiment with 4AP blockade in the intact network, we see a similar effect of compensation as in the LC motor neuron output (seen in Fig. 4B,C). 4AP block does not

cause the same change in burst duration as with TEA. Rather, 4AP blockade initially causes a significant increase in spike frequency and the number of spikes fired per burst ($p < 0.01$; ANOVA). Over the time course of the blockade, this spike frequency and number of spikes per burst returns to control levels (Fig. 4D). These data indicate that the changes seen in the level of I_A and I_{KCa} as a result of TEA and 4AP block, respectively, are a functional compensatory response that stabilizes the output of the cells and of the network as a whole. However, the roles of I_A and I_{KCa} are not simply functionally redundant; blocking either current causes an initial change in the output of the cell that is not the same. These results implicate distinct roles for these two currents in addition to their ability to partially compensate for one another. However, we do not rule out the possibility that there could be other currents or mechanisms involved in the compensatory effect.

Compensatory changes in I_A and I_{KCa} follow distinct regulatory pathways

We then set out to determine the underlying mechanisms implementing the compensation in these currents. We first investigated whether the change in I_{KCa} elicited by 4AP blockade was dependent on intracellular calcium. To check this, we co-applied the calcium chelator BAPTA with the blocker. When BAPTA was co-applied with 4AP, there was no change in I_{HTK}, in contrast to the characteristically significant increase in I_{HTK} with 4AP blockade (Fig. 5A). We also confirmed that this effect was not simply due to an effect of BAPTA on the calcium-dependence of I_{KCa}; BAPTA alone did not result in a significant reduction of I_{HTK} (data not shown; see also Turrigiano et al., 1994). More specifically, the calcium dependence of the increase in I_{HTK} was attributable to the release from intracellular calcium stores since co-application of 4AP and the intracellular calcium release blocker ryanodine also prevented the compensatory increase in I_{HTK} normally seen with 4AP blockade (Fig. 5A). These results suggest that the compensatory increase in I_{KCa} is dependent on intracellular calcium signaling mechanisms that depend on the release of intracellular calcium stores.

Because relatively rapid changes in current magnitude can often be attributed to changes in phosphorylation states of ion channels and associated regulatory proteins, we examined the effects of phosphatase and kinase inhibitors on the ability of the blockers to elicit the compensatory changes in these currents. Okadaic acid is a broad spectrum inhibitor of serine/threonine protein phosphatases (Cohen et al., 1990). While application of okadaic acid alone did not affect baseline levels of I_{HTK} (data not shown), co-application of okadaic acid with 4AP also abolished the compensatory increase in I_{HTK} (Fig. 5A), suggesting the action of a serine/threonine protein phosphatase in this compensatory effect. Because calcineurin is a well known Ca^{2+}-dependent protein serine/threonine phosphatase (Klee et al., 1998), we used cyclosporine A to inhibit calcineurin activity in our system. Cyclosporine alone did not affect baseline levels of I_{HTK} (data not shown), but combined application of 4AP with cyclosporine eliminated the compensatory increase in I_{HTK} (Fig. 5A), indicating that the increase in I_{HTK} is dependent, at least in part, on the activity of calcineurin.
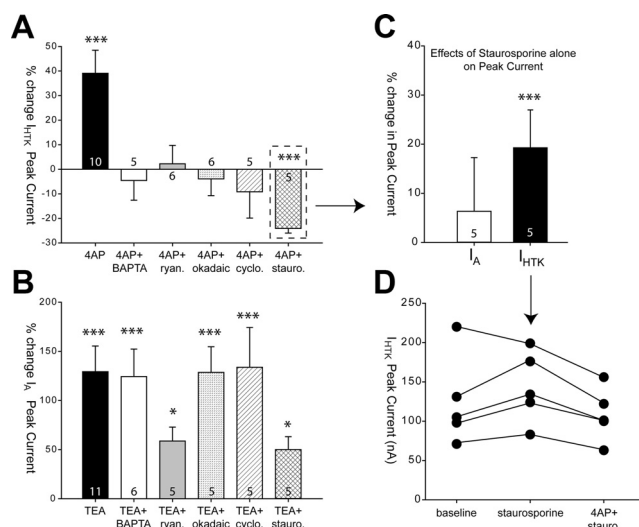
In complete contrast, the compensatory influence of TEA on I_A appears to be implemented via mechanistically distinct pathways compared with those we found for the 4AP block on I_{HTK}. The increase of I_A in response to TEA blockade is neither calcium-dependent (Fig. 5B) nor dependent on the activity of serine/threonine phosphatases (Fig. 5B). Parallel experiments showed that BAPTA, ryanodine, okadaic acid and cyclosporine,

when co-applied with TEA, failed to prevent a significant increase in I_A (Fig. 5B). The only exception was that the application of ryanodine in conjunction with TEA appeared to reduce the magnitude of increase in I_A, although this effect was not statistically significant with respect to TEA alone ($p = 0.103$; t test), or TEA plus BAPTA ($p = 0.08$).

We also examined the effects of inhibiting kinase activity on the compensatory effects of 4AP and TEA blockade. Staurosporine is a potent, cell-permeable protein kinase C inhibitor which also partially inhibits other kinases such as PKA, PKG, and CaMKII (Rüegg and Burgess, 1989). Co-application of staurosporine with 4AP appears to cause a significant decrease in I_{HTK} (Fig. 5A).

Figure 4. I_A and I_{KCa} engage in a compensatory relationship that stabilizes neuronal excitability and network output. **A**, Representative recordings of the effects on the excitability of individual LC motor neurons isolated from network activity after exposure to TEA (left) and 4AP (right). Because the pacemaker neurons of the network were silenced with TTX in this experiment, DC current injections were used to elicit activity in LC motor neurons (current traces shown at top). **B**, Representative recordings of the effects of TEA (left) and 4AP (right) exposure on network output over time. Pacemaker cells were shielded from exposure to the blocker (see Fig. 1), while the 3 upper motor neurons were exposed to blocker. Paired intracellular (top traces) and extracellular recordings were made over the time course of the experiment. **C**, Quantified effects of TEA and 4AP effects on burst characteristics of LC motor neurons in the intact network. Bars represent mean ± SD of N = 5 preparations at 10 min intervals. The first 10 min interval is baseline without blocker, and subsequent bins represent cumulative time after blocker exposure.

Figure 5. Use of pharmacological inhibitors to probe mechanisms of changes in I_A and I_{KCa}. *A*, Effects of BAPTA, ryanodine, okadaic acid, cyclosporine, and staurosporine (referred to as the treatment) on the induction of increased I_{HTK} with 4AP exposure. All bars are mean ± SD, sample sizes as shown in bars. All results are percentage change in peak I_{HTK} with 4AP + treatment relative to treatment alone (see Materials and Methods). None of the treatments caused a change in baseline levels of I_{HTK} with the exception of staurosporine (dotted box; see *C*). *** represents a significant ($p < 0.001$) difference from 0 via one-sample t test. *B*, Effects of BAPTA, ryanodine, okadaic acid, cyclosporine, and staurosporine on the induction of increased I_A with TEA exposure. All results are percentage change in peak I_A with TEA + treatment relative to treatment alone (see Materials and Methods). None of the treatments caused a change in baseline levels of I_A. ***$p < 0.001$ and *$p < 0.01$ represent a significant difference from 0 via one-sample t test. *C*, Effects of staurosporine alone on baseline levels of I_A and I_{HTK}. *** represents a significant ($p < 0.001$) difference from 0 via one-sample t test. *D*, Overall effects of staurosporine alone and then 4AP + staurosporine on I_{HTK}. Each individual cell is connected with a solid line across the treatments.

However, this is a more complex result than that for the other pharmacological blockers. Unlike any of the other pharmacological blockers used in this study, staurosporine was the only one to cause a change in baseline levels of I_{HTK} when applied alone (Fig. 5*C*). Therefore, combined application of 4AP and staurosporine results in a relative decrease in I_{HTK} compared to that with staurosporine alone, but the net effect of 4AP + staurosporine is a restoration of I_{HTK} to baseline levels (Fig. 5*D*).

Once again, the effects of staurosporine on I_A in the context of TEA blockade contrast with those for 4AP and I_{HTK}. There is no effect of staurosporine on baseline levels of I_A (Fig. 5*C*), and while staurosporine co-applied with TEA results in an apparent decrease in the magnitude of the effect on I_A, there is still a significant increase in I_A with staurosporine present (Fig. 5*B*), which is not statistically significant from the effect of TEA alone ($p = 0.08$; t test).

Discussion

Rapid compensation between I_A and I_{KCa} preserves both cellular and network outputs

We have identified a naturally occurring coregulatory relationship between potassium currents (I_A and I_{KCa}) in an intact CPG network that results in homeostatic compensation of neuronal excitability as well as network function. Furthermore, we have determined that these compensatory changes in K^+ current magnitudes are independently regulated by distinct mechanisms. Compensatory increases in I_{KCa} are calcium-dependent and due, at least in part, to the activity of calcineurin-based phosphatase activity. Conversely, compensatory increases in I_A are indepen-

dent of all of the regulatory pathways implicated in the I_{KCa} response. These effects are also fairly rapid, acting over the course of 60–90 min to stabilize the activity of a critical CPG network responsible for cardiac muscle contraction and heart beat generation in the animal. While such homeostatic responses and their role in stabilizing synaptic function have been well studied (Bergquist et al., 2010; Turrigiano, 2011), we know much less about the mechanisms underlying homeostatic plasticity of intrinsic excitability and the role this form of plasticity plays in the stabilization of neuronal and motor network output (Turrigiano, 2011).

Even neurons and networks with extremely robust output display highly variable underlying physiological parameters responsible for neuronal output, particularly membrane conductances (Schulz et al., 2006a, 2007; Khorkova and Golowasch, 2007; Goaillard et al., 2009; Temporal et al., 2012). Our work reveals that embedded within this variability are coregulatory relationships that act to stabilize the excitability of the cell, in part by balancing the sum total of major transient outward currents, I_A and I_{KCa}. A similar relationship between I_A and I_{KCa} was reported in the STG. Artificial depolarization of inferior cardiac neurons results in increased I_A and decreased I_{HTK}, which is abolished by Cd^{2+} blockade of calcium channels (Golowasch et al., 1999). These experiments did not reveal a naturally existing correlation between these currents (Golowasch et al., 1999), suggesting that excitability in the STG may be a more complex interaction among multiple conductances, or perhaps between conductances and their constitutive neuromodulation (Harris-Warrick, 2011). Although it is not known what effect this has on network output in the STG, our complementary results suggest that such homeostatic mechanisms may be common among motor neurons in different CPGs.

Distinct intracellular pathways mediate compensation

The mechanisms involved in the regulation of the compensatory response mediated by I_{KCa} after 4AP block in the CG network are consistent with work supporting changes in K^+ current density in a homeostatic fashion (Desai et al., 1999; Schulz et al., 2006b; Debanne and Poo, 2010; Misonou, 2010). In particular, the mechanisms we see for the compensatory increase in I_{KCa} are similar to those found in regulation of excitability in cultured hippocampal neurons (Misonou et al., 2004, 2005; Misonou and Trimmer, 2004). Increased excitability in these cultured neurons results in calcineurin-dependent dephosphorylation of Kv2.1 channels, leading to a functional potentiation of these channels via a shift in activation voltage, and to restoration of excitability (Misonou et al., 2004). While our data strongly suggest that I_{KCa} is primarily responsible for the observed change in I_{HTK}, we cannot conclusively rule out a role for I_{Kd} (similar to Kv2.1). However, cyclosporine has been shown to alter I_{KCa} channels directly (Hay, 1998), and calcineurin is known to have widespread effects on neuronal plasticity and excitability beyond its effects on Kv2.1 activity (Groth et al., 2003). The effects seen in our experiments likely can be attributed to an overall increase in the maximal conductance of I_{KCa}, as we see no changes in either activation curves or any consistent or significant changes in input resistances of these cells (O'Leary et al., 2010).

The mechanisms underlying compensatory increases in I_A are less clear, but distinct from the pathways involved in the upregulation of I_{KCa}. Unlike for I_{KCa}, the increase in I_A is neither calcium-dependent, nor influenced by the activity of calcineurin or any other phosphatases that would be affected by treatment with okadaic acid (Cohen et al., 1990). Indeed, blocking neither
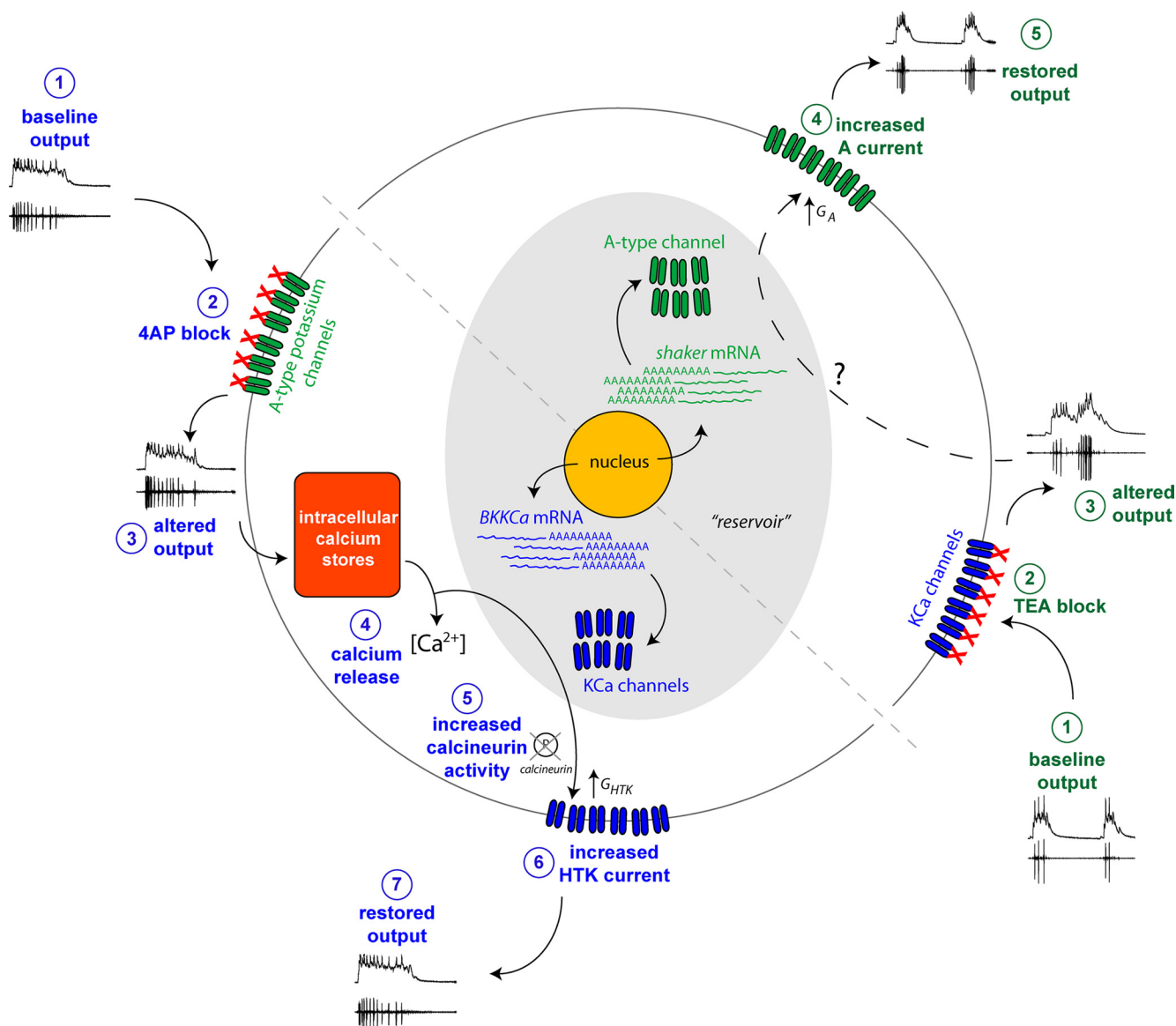
Figure 6. A working model for the induction of homeostatic plasticity of intrinsic excitability via rapid compensation between I_A and I_{KCa}. This model summarizes all of the data in the current study and provides a framework for interpretation and future experimentation. The two halves of the cell represent the distinct mechanisms induced by a block of I_A with 4AP (left, blue pathway) and a block of I_{KCa} with TEA (right, green pathway). Blue Pathway (4AP blockade): The baseline activity (1) is disrupted by the block of A-type channels with 4AP (2), causing an alteration in the excitability of the cell and its output in the network, in this case rapid initial firing frequency (3). This change presumably results in the release of calcium from intracellular stores (4) that increases activity of the calcium-dependent phosphatase calcineurin (5). Calcineurin activity induces an increase in I_{KCa} (6), restoring the excitability of the cell and re-establishing motor neuron activity in the intact network (7). Green Pathway (TEA blockade): Baseline network activity (1) is disrupted via TEA blockade (2), causing substantial changes in the output properties of the motor neuron and the network (3). While the intracellular mechanisms remain unclear at this point, a subsequent increase in I_A that is independent of the pathway invoked by 4AP blockade compensates for loss of I_{KCa}, restoring output of the neurons and the network (5). This compensation is rapid (on the order of 1 h), suggesting that there is an already existing "reservoir" or channel protein available that is maintained via positive coregulation at the transcription/mRNA level of the channel genes responsible for I_{KCa} and I_A (Gray Oval).

phosphatase nor kinase activity by two broad spectrum blockers was able to prevent an increase in I_A as a result of TEA blockade, possibly precluding the contribution of phosphorylation state to this half of the compensation story. However, we were able to dampen the effect by blocking release of intracellular calcium with ryanodine, as well as by inhibiting kinase activity, suggesting a more complex path of regulation in this response. Given the potential nonspecific effects of pharmacological treatment, we cannot rule out at least some role for a kinase in this pathway. For example, Kv1.2 potassium channels are known to be affected by cAMP/protein kinase A pathways which enhance their conductance, in part by altering trafficking of these channels (Connors et al., 2008). Our staurosporine treatment may result in only partial

inhibition of PKA (Rüegg and Burgess, 1989), which could explain the intermediate effects seen on the A-type current compensation. Regardless, the fact that I_A and I_{KCa} are regulated by distinct pathways demonstrates an inherent robustness to this homeostatic response, which may be characteristic of networks responsible for critical functions, such as CPGs.

Reservoirs of channel proteins might implement rapid compensation

Our data also begin to shed light on a striking disparity between levels of regulation in this system. Namely, we see an entirely different relationship at the level of mRNA for the channel genes *BKKCA* and *shaker* (positive correlation), than we do for the

currents I_{KCa} and I_A that these channels most directly encode (negative correlation). Indeed, to date every correlation we have found between channel mRNAs at the single cell level has been a positive correlation (Schulz et al., 2007; Tobin et al., 2009; Temporal et al., 2012). These data include measurements of at least nine different channel genes in seven different motor neuron types in the crustacean stomatogastric and cardiac ganglia (S. Temporal and D. J. Schulz, unpublished data), for a total of no fewer than 60 correlations in channel expression detected among channel transcript levels, and every one has thus far been positive. In addition, our data impact the present, although admittedly limited, understanding of the relationship between channel mRNA and ionic current in a given neuron. Namely, that mRNA for a given K^+ channel correlates positively with its corresponding ionic conductance (Schulz et al., 2006). Although both of these measurements were not made in the same cells in this study, logic dictates that there cannot simply be a positive relationship between mRNA and conductance for both K^+ currents in this study. Clearly, and not particularly surprisingly, our data demonstrate that more complexity lies within the relationship of mRNA and ionic conductance than a one-for-one tracking between these disparate levels of function in all cell types. However, our data continue to support the concept that correlation among mRNA levels (Schulz et al., 2007; Tobin et al., 2009) underlies a functional relationship at the conductance level.

So then why do we see only positively correlated mRNA levels for channel genes in these motor networks? The linkage to cellular and network output in our study enables us to propose a new hypothesis in this regard. We hypothesize that rapid compensation of intrinsic excitability, such as that reported in this study, is implemented via an already existing pool of protein. That is, protein pools for the two opposing channels must already be available in relatively equivalent numbers, even if they are not functionally equally represented. This requires that mechanisms must occur at the level of gene regulation to ensure a sufficient "reservoir" of protein capable of compensating for the loss of a given channel. Thus, regardless of whether channels act in concert to set neuronal output (Ball et al., 2010; Franklin et al., 2010), or act in a compensatory fashion, the overall gene regulation between the two must be relatively balanced. Such a reservoir perspective is reminiscent of mechanisms seen for synaptic vesicle protein dynamics (Fernández-Alfonso et al., 2006), or extrasynaptic AMPA receptors that serve as a reservoir during synaptic plasticity (Hayashi et al., 2000; Zhu et al., 2000). Interestingly, insertion of AMPA receptor during synaptic plasticity is also under the control of phosphorylation-dependent processes (Lin et al., 2009). Therefore, this hypothesis provides a compelling framework for future investigation of the relationship between mRNA levels and ionic conductance, as well as the interplay between gene expression and post-transcriptional mechanisms involved in homeostatic plasticity of intrinsic excitability over different time scales.

Putting it all together
Our findings represent one of the first comprehensive demonstrations of rapid homeostatic plasticity of intrinsic excitability that results in a stabilization of output in a mature, intact network of a CPG. These rapid compensatory increases are mechanistically independent, suggesting robustness in the maintenance of neural network output that is critical for survival. Furthermore, this study reveals a distinct mechanism for compensation that leads us to at least one working model of homeostatic plasticity in this system (Fig. 6). We hypothesize that one pathway to func-

tional compensation in this system relies on intracellular calcium concentration as a measure of cell excitability (Kennedy, 1989; Ross, 1989; LeMasson et al., 1993). A block of A-type K^+ channels leads to an increase in the excitability of the cell, causing release of intracellular calcium stores. This calcium influx alters calcineurin activity, resulting in dephosphorylation of targets, perhaps the KCa-channels themselves, that increases I_{KCa}. This ultimately restores the outward current balance that was lost during decreased I_A and thus restores excitability. The corresponding mechanism responsible for compensatory increases in I_A (Fig. 6) is presently unknown, but is likely to involve distinct mechanisms for monitoring excitability (Dirnagl et al., 2003), as well as other candidate mechanisms that alter A-type conductances (Connors et al., 2008). Finally, we hypothesize that positive coregulation of mRNA numbers for channel genes may ultimately provide a reservoir of channel protein (Fig. 6) for implementing compensation over rapid time scales during which *de novo* synthesis may be insufficient to implement full compensation.

References

Alexandrowicz JS (1932) The innervation of the heart of the crusacea. I. Decapoda. Q J Microsc Sci 75:181–249.

Atkinson NS, Robertson GA, Ganetzky B (1991) A component of calcium-activated potassium channels encoded by the *Drosophila* slo locus. Science 253:551–555.

Ball JM, Franklin CC, Tobin AE, Schulz DJ, Nair SS (2010) Coregulation of ion channel conductances preserves output in a computational model of a crustacean cardiac motor neuron. J Neurosci 30:8637–8649.

Bergquist S, Dickman DK, Davis GW (2010) A hierarchy of cell intrinsic and target-derived homeostatic signaling. Neuron 66:220–234.

Berlind JA (1989) Feedback from motor neurones to pacemaker neurones in lobster cardiac ganglion contributes to regulation of burst frequency. J Exp Biol 141:277–294.

Cohen P, Holmes CF, Tsukitani Y (1990) Okadaic acid: a new probe for the study of cellular regulation. Trends Biochem Sci 15:98–102.

Connors EC, Ballif BA, Morielli AD (2008) Homeostatic regulation of Kv1.2 potassium channel trafficking by cyclic AMP. J Biol Chem 283:3445–3453.

Cooke IM (2002) Reliable, responsive pacemaking and pattern generation with minimal cell numbers: the crustacean cardiac ganglion. Biol Bull 202:108–136.

Debanne D, Poo MM (2010) Spike-timing dependent plasticity beyond synapse—pre- and post-synaptic plasticity of intrinsic neuronal excitability. Front Synaptic Neurosci 2:21.

Desai NS, Rutherford LC, Turrigiano GG (1999) Plasticity in the intrinsic excitability of cortical pyramidal neurons. Nat Neurosci 2:515–520.

Dirnagl U, Simon RP, Hallenbeck JM (2003) Ischemic tolerance and endogenous neuroprotection. Trends Neurosci 26:248–254.

Fernández-Alfonso T, Kwan R, Ryan TA (2006) Synaptic vesicles interchange their membrane proteins with a large surface reservoir during recycling. Neuron 51:179–186.

Franklin CC, Ball JM, Schulz DJ, Nair SS (2010) Generation and preservation of the slow underlying membrane potential oscillation in model bursting neurons. J Neurophysiol 104:1589–1602.

García-Crescioni K, Fort TJ, Stern E, Brezina V, Miller MW (2010) Feedback from peripheral musculature to central pattern generator in the neurogenic heart of the crab Callinectes sapidus: role of mechanosensitive dendrites. J Neurophysiol 103:83–96.

Goaillard JM, Taylor AL, Schulz DJ, Marder E (2009) Functional consequences of animal-to-animal variation in circuit parameters. Nat Neurosci 12:1424–1430.

Golowasch J, Marder E (1992) Ionic currents of the lateral pyloric neuron of the stomatogastric ganglion of the crab. J Neurophysiol 67:318–331.

Golowasch J, Abbott LF, Marder E (1999) Activity-dependent regulation of potassium currents in an identified neuron of the stomatogastric ganglion of the crab Cancer borealis. J Neurosci 19:RC33.

Groth RD, Dunbar RL, Mermelstein PG (2003) Calcineurin regulation of neuronal plasticity. Biochem Biophys Res Commun 311:1159–1171.

Guo W, Jung WE, Marionneau C, Aimond F, Xu H, Yamada KA, Schwarz TL, Demolombe S, Nerbonne JM (2005) Targeted deletion of Kv4.2 elimi-

nates I(to,f) and results in electrical and molecular remodeling, with no evidence of ventricular hypertrophy or myocardial dysfunction. Circ Res 97:1342–1350.

Haedo RJ, Golowasch J (2006) Ionic mechanism underlying recovery of rhythmic activity in adult isolated neurons. J Neurophysiol 96:1860–1876.

Harris-Warrick RM (2011) Neuromodulation and flexibility in Central Pattern Generator networks. Curr Opin Neurobiol 21:685–692.

Hartline DK (1967) Impulse identification and axon mapping of the nine neurons in the cardiac ganglion of the lobster Homarus americanus. J Exp Biol 47:327–340.

Hay M (1998) Cyclosporine A modulation of Ca++ activated K+ channels in cardiac sensory afferent neurons. Brain Res 786:243–247.

Hayashi Y, Shi SH, Esteban JA, Piccini A, Poncer JC, Malinow R (2000) Driving AMPA receptors into synapses by LTP and CaMKII: requirement for GluR1 and PDZ domain interaction. Science 287:2262–2267.

Kennedy MB (1989) Regulation of neuronal function by calcium. Trends Neurosci 12:417–420.

Khorkova O, Golowasch J (2007) Neuromodulators, not activity, control coordinated expression of ionic currents. J Neurosci 27:8709–8718.

Kim M, Baro DJ, Lanning CC, Doshi M, Moskowitz HS, Farnham J, Harris-Warrick RM (1998) Expression of Panulirus shaker potassium channel splice variants. Receptors Channels 5:291–304.

Klee CB, Ren H, Wang X (1998) Regulation of the calmodulin-stimulated protein phosphatase, calcineurin. J Biol Chem 273:13367–13370.

LeMasson G, Marder E, Abbott LF (1993) Activity-dependent regulation of conductances in model neurons. Science 259:1915–1917.

Lin DT, Makino Y, Sharma K, Hayashi T, Neve R, Takamiya K, Huganir RL (2009) Regulation of AMPA receptor extrasynaptic insertion by 4.1N, phosphorylation and palmitoylation. Nat Neurosci 12:879–887.

MacLean JN, Zhang Y, Johnson BR, Harris-Warrick RM (2003) Activity-independent homeostasis in rhythmically active neurons. Neuron 37:109–120.

MacLean JN, Zhang Y, Goeritz ML, Casey R, Oliva R, Guckenheimer J, Harris-Warrick RM (2005) Activity-independent coregulation of IA and Ih in rhythmically active neurons. J Neurophysiol 94:3601–3617.

Marder E (2011) Variability, compensation, and modulation in neurons and circuits. Proc Natl Acad Sci U S A 108:15542–15548.

Misonou H (2010) Homeostatic regulation of neuronal excitability by K(+) channels in normal and diseased brains. Neuroscientist 16:51–64.

Misonou H, Trimmer JS (2004) Determinants of voltage-gated potassium channel surface expression and localization in Mammalian neurons. Crit Rev Biochem Mol Biol 39:125–145.

Misonou H, Mohapatra DP, Park EW, Leung V, Zhen D, Misonou K, Anderson AE, Trimmer JS (2004) Regulation of ion channel localization and phosphorylation by neuronal activity. Nat Neurosci 7:711–718.

Misonou H, Mohapatra DP, Trimmer JS (2005) Kv2.1: a voltage-gated k+ channel critical to dynamic control of neuronal excitability. Neurotoxicol 26:743–752.

Nerbonne JM, Gerber BR, Norris A, Burkhalter A (2008) Electrical remodelling maintains firing properties in cortical pyramidal neurons lacking KCND2-encoded A-type K+ currents. J Physiol 586:1565–1579.

O'Leary T, van Rossum MC, Wyllie DJ (2010) Homeostasis of intrinsic excitability in hippocampal neurones: dynamics and mechanism of the response to chronic depolarization. J Physiol 588:157–170.

Ross WN (1989) Changes in intracellular calcium during neuron activity. Annu Rev Physiol 51:491–506.

Rüegg UT, Burgess GM (1989) Staurosporine, K-252 and UCN-01: potent but nonspecific inhibitors of protein kinases. Trends Pharm Sci 10:218–220.

Sakurai A, Wilkens JL (2003) Tension sensitivity of the heart pacemaker neurons in the isopod crustacean Ligia pallasii. J Exp Biol 206:105–115.

Schulz DJ, Goaillard JM, Marder E (2006a) Variable channel expression in identified single and electrically coupled neurons in different animals. Nat Neurosci 9:356–362.

Schulz DJ, Baines RA, Hempel CM, Li L, Liss B, Misonou H (2006b) Cellular excitability and the regulation of functional neuronal identity: from gene expression to neuromodulation. J Neurosci 26:10362–10367.

Schulz DJ, Goaillard JM, Marder EE (2007) Quantitative expression profiling of identified neurons reveals cell-specific constraints on highly variable levels of gene expression. Proc Natl Acad Sci U S A 104:13187–13191.

Tazaki K, Cooke IM (1979) Isolation and characterization of slow, depolarizing responses of cardiac ganglion neurons in the crab, Portunus sanguinolentus. J Neurophysiol 42:1000–1021.

Tazaki K, Cooke IM (1983a) Separation of neuronal sites of driver potential and impulse generation by ligaturing in the cardiac ganglion of the lobster, Homarus americanus. J Comp Physiol A Neuroethol Sens Neural Behav Physiol 151:329–346.

Tazaki K, Cooke IM (1983b) Neuronal mechanisms underlying rhythmic bursts in crustacean cardiac ganglia. Symp Soc Exp Biol 37:129–157.

Tazaki K, Cooke IM (1983c) Topographical localization of function in the cardiac ganglion of the crab, Portunus sanguinolentus. J Comp Physiol A Neuroethol Sens Neural Behav Physiol 151:311–328.

Temporal S, Desai M, Khorkova O, Varghese G, Dai A, Schulz DJ, Golowasch J (2012) Neuromodulation independently determines correlated channel expression and conductance levels in motor neurons of the stomatogastric ganglion. J Neurophysiol 107:718–727.

Thoby-Brisson M, Simmers J (1998) Neuromodulatory inputs maintain expression of a lobster motor pattern-generating network in a modulation-dependent state: evidence from long-term decentralization in vitro. J Neurosci 18:2212–2225.

Thoby-Brisson M, Simmers J (2002) Long-term neuromodulatory regulation of a motor pattern-generating network: maintenance of synaptic efficacy and oscillatory properties. J Neurophysiol 88:2942–2953.

Tobin AE, Cruz-Bermudez ND, Marder E, Schulz DJ (2009) Correlations in ion channel mRNA in rhythmically active neurons. PLoS One 4:e6742.

Tsunoda S, Salkoff L (1995) The major delayed rectifier in both *Drosophila* neurons and muscle is encoded by Shab. J Neurosci 15:5209–5221.

Turrigiano G (2011) Too many cooks? Intrinsic and synaptic homeostatic mechanisms in cortical circuit refinement. Annu Rev Neurosci 34:89–103.

Turrigiano G (2012) Homeostatic synaptic plasticity: local and global mechanisms for stabilizing neuronal function. Cold Spring Harb Perspect Biol 4:a005736.

Turrigiano G, Abbott LF, Marder E (1994) Activity-dependent changes in the intrinsic properties of cultured neurons. Science 264:974–977.

Turrigiano G, LeMasson G, Marder E (1995) Selective regulation of current densities underlies spontaneous changes in the activity of cultured neurons. J Neurosci 15:3640–3652.

Zhu JJ, Esteban JA, Hayashi Y, Malinow R (2000) Postnatal synaptic potentiation: delivery of GluR4-containing AMPA receptors by spontaneous activity. Nat Neurosci 3:1098–1106.

APPENDIX 3. Nahar J, Lett KM, Schulz DJ (2012) Restoration of descending inputs fails to rescue activity following deafferentation of a motor network. *Journal of Neurophysiology* 108: 871-881.

Restoration of descending inputs fails to rescue activity following deafferentation of a motor network

Jebun Nahar,* Kawasi M. Lett,* and David J. Schulz
Department of Biological Sciences, University of Missouri, Columbia, Missouri

Nahar J, Lett KM, Schulz DJ. Restoration of descending inputs fails to rescue activity following deafferentation of a motor network. *J Neurophysiol* 108: 871–881, 2012. First published May 2, 2012; doi:10.1152/jn.00183.2012.—Motor networks such as the pyloric network of the stomatogastric ganglion often require descending neuromodulatory inputs to initiate, regulate, and modulate their activity and their synaptic connectivity to manifest physiologically appropriate output. Prolonged removal of these descending inputs often results in a compensatory response that alters the inputs themselves, their targets, or both. Using the pyloric network of the crab, *Cancer borealis*, we investigated whether isolation of motor networks would result in alterations that change the responses of these networks to restored modulatory input. We used a reversible block with isotonic sucrose to transiently alter descending inputs into the pyloric network of the crab stomatogastric ganglion. Using this method, we found that blocking neuromodulatory inputs caused a reduced ability for subsequently restored modulatory projections to appropriately generate network output. Our results suggest that this could be due to changes in activity of descending projection neurons as well as changes in sensitivity to neuromodulators of the target neurons that develop over the time course of the blockade. These findings suggest that although homeostatic plasticity may play a critical role in recovery of functional output in a deafferented motor network, the results of these compensatory changes may alter the network such that restored inputs no longer function appropriately.

neuromodulation; homeostatic plasticity; stomatogastric ganglion; decentralization

MOTOR NETWORKS OFTEN CONSIST of central pattern generator circuits (CPGs) that endogenously encode network output features as a result of the intrinsic properties of the constituent neurons as well as their pattern of synaptic connectivity (Grillner 2006; Selverston 2010). Moreover, the ability to generate this endogenous activity often requires both excitatory drive as well as neuromodulatory inputs that tune synaptic and intrinsic properties of the constituent neurons to enable pattern generation (Harris-Warrick 2011), such that loss of these inputs often results in a loss of function, even though the motor networks themselves remain intact.

More recently, a substantial amount of plasticity in this dependence on descending drive and motor output has been observed. For example, in the crustacean stomatogastric ganglion (STG), the pyloric motor network is a CPG that is dependent on descending neuromodulatory inputs to produce a rhythmic motor output (Moulins and Cournil 1982). Yet although the pyloric motor output ceases soon after the modu-

latory inputs are removed, over a period of 3–7 days (depending on species studied) the pyloric rhythm can recover its functional output in the absence of all descending neuromodulation (Golowasch et al. 1999; Thoby-Brisson and Simmers 1998, 2002). These results suggest that in the absence of the neuromodulatory inputs that produce ongoing activity, the intrinsic motor circuits "retune" themselves so that they are able to produce rhythmic activity by input-independent mechanisms. These mechanisms in the STG include at least in part altering membrane conductances and ion channel expression patterns of individual neurons (Khorkova and Golowasch 2007; Mizrahi et al. 2001; Thoby-Brisson and Simmers 2002). This kind of functional recovery following removal of command inputs is not unique to the STG. Similar phenomena have been reported in recovery of stepping function in spinal cord transected cats (Barbeau and Rossignol 1987; Rossignol et al. 2004a,b), as well as recovery of function in the vestibular system following deafferentation (Darlington and Smith 2000).

Although some properties of these networks have been studied subsequent to recovery, little is known about the functional state of these networks during the process of recovery. In the pyloric network of the STG, loss of neuromodulation is sufficient to change relationships in individual neurons at both the level of ionic conductances and expression of ion channel mRNA prior to recovery taking place, detectable even after 24 h (Khorkova and Golowasch 2007; Temporal et al. 2012). Yet it is unclear whether these changes prior to recovery have an immediate impact on the ability of the network to generate neuromodulation-induced activity. Our focus in this study is to better understand whether the changes that are initiated as a result of removal of modulatory inputs influence the ability of the system to respond appropriately if descending inputs are ultimately restored. This has particular implication for nerve injury and disease, because if potentially compensatory changes are initiated in networks deprived of afferent input, then the effects of restoring input may be unpredictable. In this study, we investigate the impact of removal and restoration of descending inputs on functional output of the pyloric network of the STG over a 3- to 4-day time frame of deafferentation. Recovery of rhythmic activity in the STG can occur over a time course between 1 and 7 days (Luther et al. 2003; Mizrahi et al. 2001), although the most common that we have observed is on the order of 3–5 days, similar to other reports in the literature (Thoby-Brisson and Simmers 1998, 2002). The time frame of our experiments therefore likely coincides with the initiation of cellular mechanisms involved in the recovery process. We then determine whether changes in the output of

---

* These authors contributed equally to this work.

Address for reprint requests and other correspondence: D. J. Schulz, University of Missouri, Department of Biological Sciences, Columbia, MO 65211 (e-mail: schulzd@missouri.edu).

these restored networks result from changes in presynaptic inputs, target neurons of the pyloric network, or both.

MATERIALS AND METHODS

Animals and the stomatogastric preparation. Adult crabs, *Cancer borealis*, were obtained from The Fresh Lobster Company (Gloucester, MA) and maintained in artificial seawater at 12°C until used. Crabs were anesthetized by keeping them on ice for 30 min before dissection. The complete stomatogastric nervous system (STNS) was dissected out of the animal and pinned out in a Sylgard-coated (Dow Corning) dish containing chilled (12–13°C) physiological saline.

The stomatogastric nervous system consists of the STG motor networks and their associated inputs (Fig. 1). The output of the pyloric network of the STG can be most directly monitored via projections of motor neurons through two nerve types, the paired *lvns* and *mvns*. The STG receives central inputs by only a single nerve, the stomatogastric nerve (*stn*), connecting the STG with the rest of the crustacean central nervous system (Fig. 1), including in this preparation the paired commissural ganglia (CoGs) and the oesophageal ganglion (OG). The *stn* of the crab, *Cancer borealis*, contains approximately 60 large axons, as well as a bundle of smaller fibers (Coleman et al. 1992). Of the 60 large fibers, about 40 descend from the paired CoGs, 10 from the OG, and 10 represent ascending interneuron axons from the STG (Coleman et al. 1992; Goldberg et al. 1988). These *stn* inputs are responsible for initiating, maintaining, and altering the activity of the pyloric network (Stein 2009).

Solutions. The physiological saline solution consisted of the following (in mM): 440 NaCl, 11 KCl, 13 CaCl$_2$, 26 MgCl$_2$, and 10 HEPES buffer, pH 7.45. In most experiments, the stomatogastric nerve (*stn*; see Fig. 1) was blocked with a solution composed of isotonic sucrose (750 mM). In some experiments, neuromodulators were superfused to the STG to determine their effects on preparations that previously had *stn* activity blocked with sucrose. These modulators include octopamine (Sigma Chemical, St. Louis, MO), pilo-

carpine (Acros Organics, Geel, Belgium), and proctolin (American Peptide Company, Sunnyvale, CA). Unless otherwise specified, chemicals were obtained from Fisher Chemical. When the STG was superfused with modulators, the *stn* was additionally blocked with 10^{-6} M tetrodotoxin (Alomone Labs, Jerusalem, Israel) in keeping with common practice in STG preparations, as insurance that no propagation of signals up and/or down the *stn* could occur.

Electrophysiology. For electrophysiological recordings, petroleum jelly wells were placed on the nerves from which recordings would be made (*lvn*, lateral ventricular nerve; *mvn*, medial ventricular nerve; *dgn*, dorsal gastric nerve; *stn*, stomatogastric nerve; *son*, superior oesophageal nerve; *ion*, inferior oesophageal nerve). Extracellular recordings from the nerves were made by placing stainless steel pin electrodes in the wells. Signals were amplified and filtered using a differential AC amplifier (A-M Systems, Sequim, WA). Throughout the experiments, both during recordings and incubation times between, the preparations were maintained in chilled (12–13°C) physiological saline. During incubation periods, penicillin and streptomycin (Sigma) were added to the saline to prevent bacterial infection of the culture (50 U/mL penicillin and 50 μg/mL streptomycin). Data were acquired using a Digidata 1322 data acquisition board (Axon Instruments, Sunnyvale, CA). In some preparations, the descending projection neurons were stimulated extracellularly via the stomatogastric nerve (10 Hz, 90 s). The *stn* was stimulated using a Grass S88 stimulator (Grass Instruments, West Warwick, RI). Extracellular nerve stimulation was achieved by placing the wires used to record nerve activity into a stimulus isolation unit (Grass Instruments) that was connected to an S88 stimulator.

The pyloric rhythm was monitored by recording the activities of the lateral pyloric (LP), pyloric constrictor (PY), pyloric dilator (PD), ventricular dilator (VD), and inferior cardiac (IC) neurons on the *lvn* and *mvn* (Fig. 1). Pyloric burst frequencies were derived from the cycle period as determined by the time between two consecutive bursts of PD neurons. The cycle period of the VD neuron was also

Fig. 1. Schematic of the stomatogastric nervous system showing locations of extracellular recording sites as well as representative recordings obtained. Each *dark circle* represents a Vaseline well on a given nerve from which extracellular recordings of spiking activity were made. Corresponding labeled representative traces (made simultaneously) are shown from a control preparation with intact modulatory projections. CoG, commissural ganglion; OG, oesophageal ganglion; ion, inferior oesophageal nerve; son, superior oesophageal nerve; stn, stomatogastric nerve; STG, stomatogastric ganglion; mvn, medial ventricular nerve; lvn, lateral ventricular nerve; dgn, dorsal gastric nerve. In each experiment, at least two wells were placed on the *stn* to facilitate recordings and/or blockade of descending projections. The individual neurons that make up the pyloric rhythm as detected on the *lvn* and the *mvn* (LP, PY, PD, VD, IC) are labeled in a representative pyloric burst. *Inset*: location of the soma of the anterior gastric receptor (AGR) neuron and its axonal projections both into the *dgn* and ascending the *stn* toward the CoGs. With this projection pattern, AGR can be detected in recordings of the *dgn*, *stn*, and *son*. A series of three AGR spikes detected on these nerves are shown on the representative recording with *.
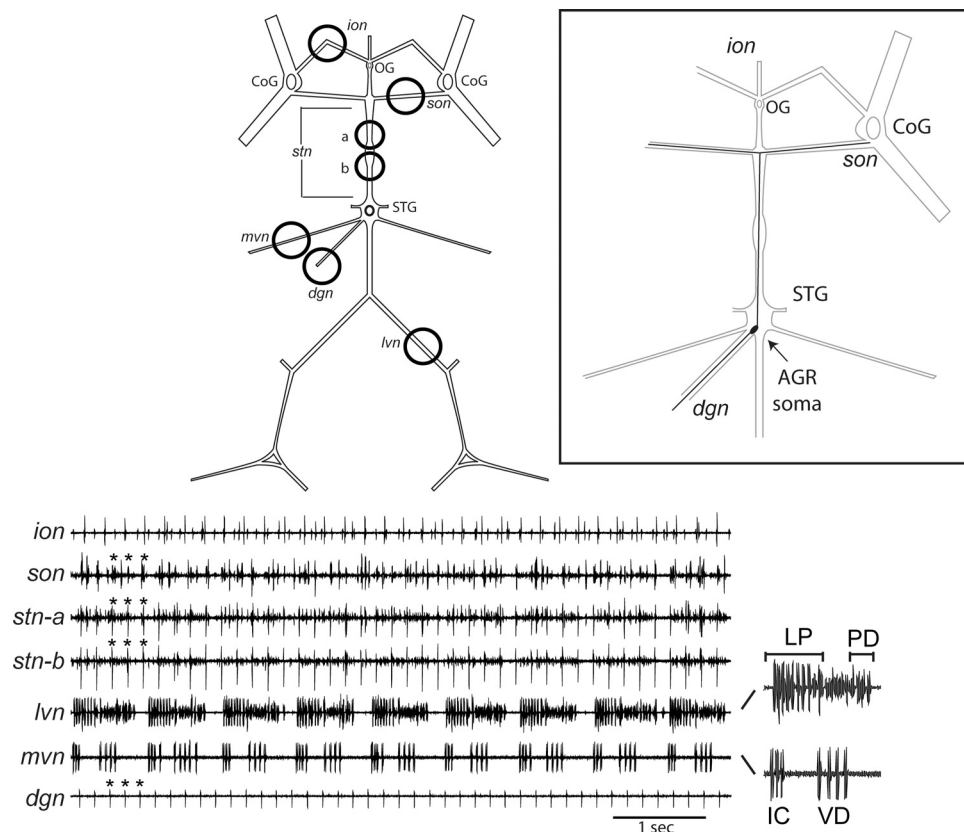
determined as the time between VD bursts measured on the *mvn*. We also used the spiking activity of the anterior gastric receptor (AGR) neuron to monitor the propagation ability of the *stn* across a time course of pharmacologic blockade. AGR is a sensory neuron that has a cell body in close proximity to the STG and projects axon collaterals both centrally, through the *stn* to both CoGs (see Fig. 1, *inset*), and peripherally, through the *dgn* toward the stomach musculature. AGR action potentials can be monitored often as the largest spike on the *stn*, and can also be measured from the paired *sons* and the *dgn* (Smarandache and Stein 2007). Multisweep recordings (Spike2 v6.0, Cambridge Electronic Design, Cambridge, UK) were used to detect AGR spikes at all of these recording sites. If AGR was detectable on the *dgn*, *stn* (both in the blocking well and the other; see Fig. 1), and the *son* after removal of the sucrose blockade, the block was considered as likely not having damaged the *stn* signaling capability. Any preparations for which we could not use AGR to confirm the propagation ability of the *stn* were omitted. Finally, we measured the overall spiking frequency of the units contained within the *son*s. For *son* recordings, we measured the instantaneous firing frequency. However, in some of our recordings, bursting activity of the esophageal OD1 neuron was detected on the *son* (Nagy et al. 1981). When bursting was present, we used average firing frequency of the *son* spikes between bursts of OD1 for a minimum of 10 interburst intervals as the data for *son* spiking frequency.

Data analysis. Pyloric activity was measured as the average burst frequency of consecutive cycles for 10 min in which the range of values did not change visibly and were assumed to represent the steady state. Spiking activity of the AGR and *son* were measured as instantaneous frequency or average firing frequency of a section of the recording (durations ranged from 30 to 240 s). For experiments where the block was removed and pyloric frequency measured (seen in Figs. 3 and 4), relative frequency was plotted as the ratio (for a given preparation) of the frequency at time *x*/control frequency. We chose to express the data this way, when possible, to ensure that differences across groups after restored modulation were not simply due to differences in starting frequency (Spitzer et al. 2008). Differences in mean firing rates or bursting frequencies were compared using un-paired *t*-tests. Correlations were analyzed using Pearson's Product Moment tests. All statistical tests were performed using SigmaPlot v11.0 (Systat Software, Inc., San Jose, CA).

RESULTS

We used a simple blocking regime with isotonic sucrose to examine reversible neuromodulatory blockade effects on the output of the pyloric rhythm. Our data show that sucrose blockade virtually eliminates all pyloric activity on both the *lvn* (LP, PY, and PD activity) and the *mvn* (VD and IC activity) usually within 1 h of application (Fig. 2). Simultaneous recorded activity made from the blocking well (*stn-a*) and posterior to the blocking well (*stn-b*) show a dissociation of spiking activity with the sucrose block in place (Fig. 2, *bottom traces*). *stn-a* recordings with the sucrose block in place show activity for units that largely originate above the block and descend through the *stn*, whereas *stn-b* recordings show units that largely originate below the block that ascend the *stn*. Multisweep analyses of AGR before and after the placement of the block show the inability of AGR spiking to propagate past the sucrose block and into the *son*; AGR spiking is absent on the *son* when the sucrose block is in place (Fig. 3*C*). Taken together, these data indicate that isotonic sucrose is sufficient to block propagation of action potentials through the *stn*, likely resulting in a loss of modulatory drive to the STG during the course of the blockade.

Our hypothesis was that removal of descending neuromodulatory inputs to the STG, and the subsequent change in activity, would alter the properties of the STG neurons, or the descending inputs, or both and result in impaired ability of the descending projections to appropriately drive rhythmic activity following subsequent reconnection of the modulatory drive. We tested this hypothesis using the reversible sucrose block-
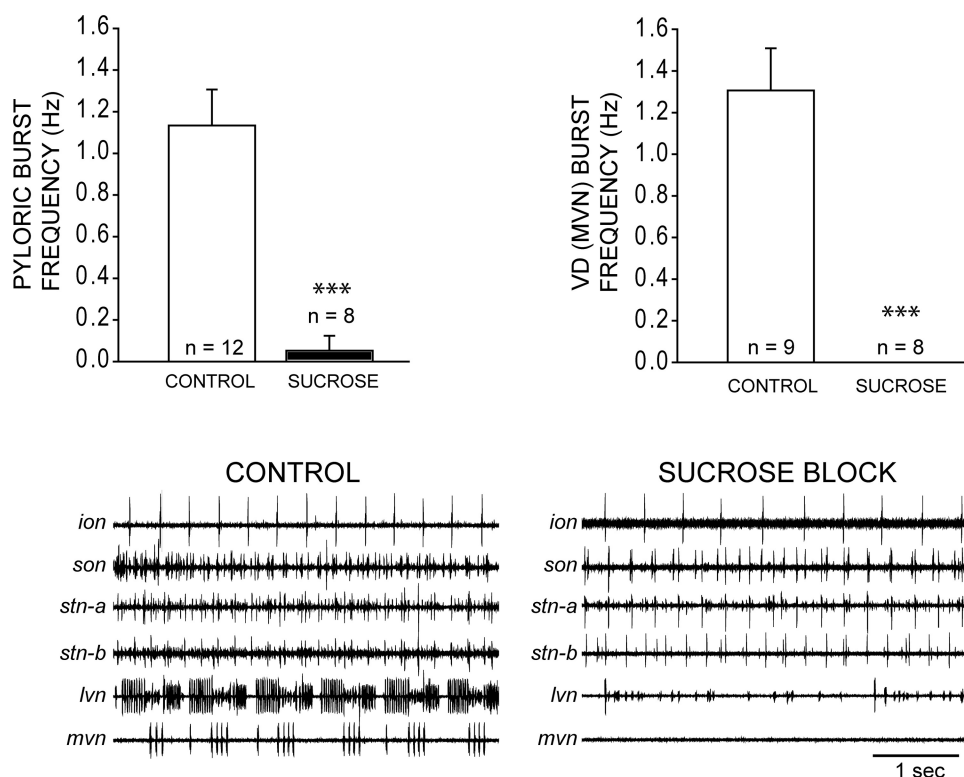

Fig. 2. Effects of blocking the *stn* with isotonic sucrose solution on activity in the stomatogastric nervous system. Acute effects of sucrose blockade on burst frequency of the pyloric rhythm are shown. *Left panel*: the pyloric burst frequency (mean ± SD) as measured by the activity of the *lvn*. *Right panel*: the activity of the *mvn* as represented by VD burst frequency (mean ± SD). *** represents a significant difference relative to control ($P < 0.01$; *t*-test). Representative recordings are provided for stomatogastric nervous system activity under conditions before (control) and 1 h after sucrose block (block intact).
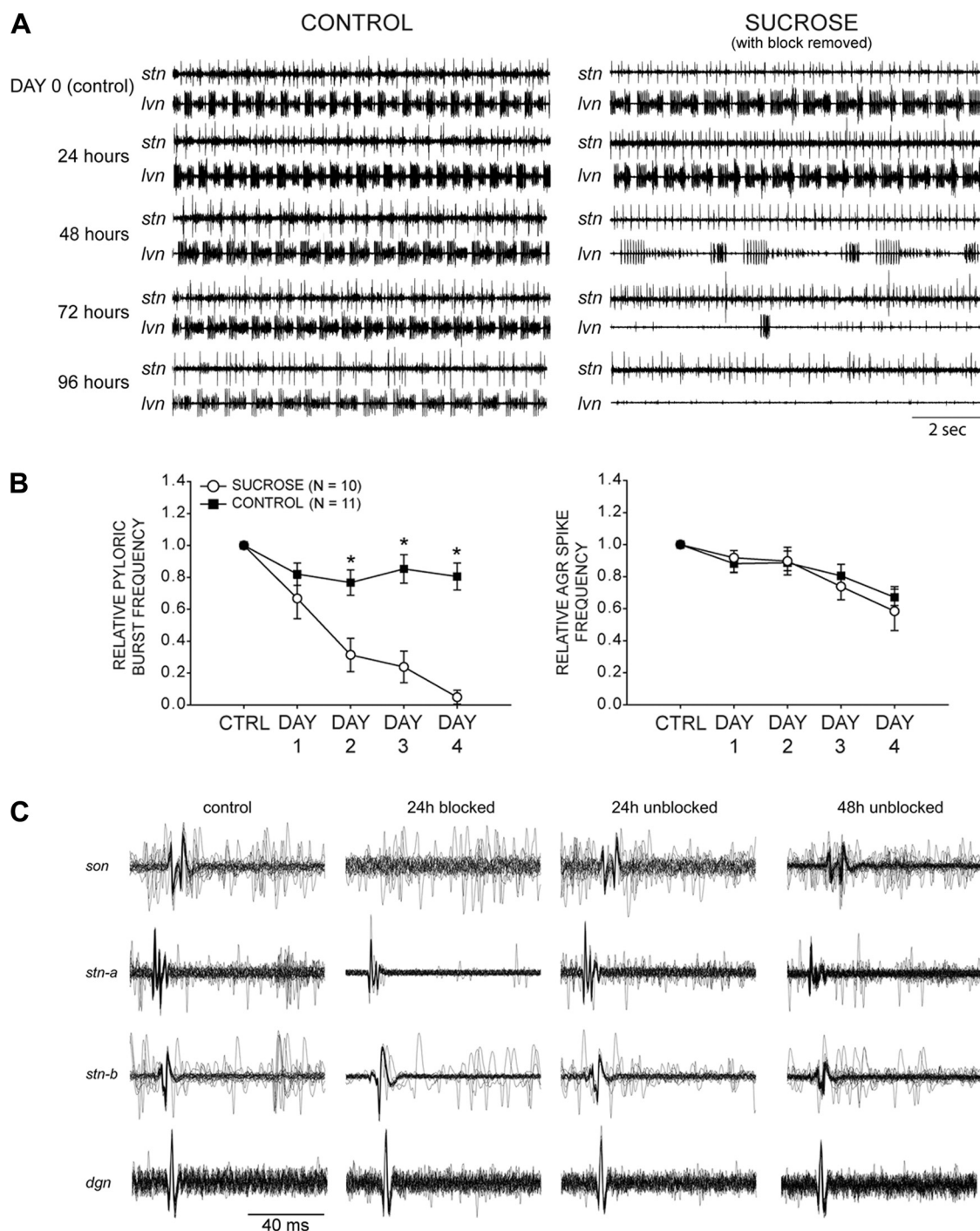
Fig. 3. Effects of *stn* blockade over time on the ability of restored connectivity (when the block is removed) to generate pyloric activity. *A*: representative recordings of *stn* (ascending and descending projections) and *lvn* (pyloric activity) for two preparations over the course of 4 days in culture. All recordings shown have the *stn* unblocked. *CONTROL* preparations were maintained in physiological saline for the entirety of the experiment. *SUCROSE* preparations had the *stn* blocked with isotonic sucrose solution. The block was removed once every 24 h, and a series of recordings (as shown here) made to determine whether rhythmic pyloric activity was restored. Following these recordings, the block was put back into place for the next 24 h. *B*: relative frequency of *lvn* bursting and AGR spiking over time with and without sucrose blockade. Data for the sucrose group were collected while the block was removed. Relative frequency for each preparation was calculated as a proportion of the intact (control, day 0) activity of that preparation, and expressed here as mean ± SD. * represents a significant difference relative to control for a given day ($P < 0.05$; *t*-test). *C*: multisweep recordings of AGR activity showing the reversibility of the sucrose block over time in culture. AGR propagation into the *son* is blocked in sucrose, but restored when sucrose is removed from the blocking well, here shown at 24 and 48 h following the initial sucrose block. *stn-a* was the blocking well in this experiment. During sucrose blockade, AGR action potentials (initiated in the *stn* and propagated both anteriorly and posteriorly) sometimes can propagate into, but not beyond, the blocking well (see 24-h blocked recording).

ade. Descending inputs were blocked over the course of 4 days. Once per 24-h period we removed the *stn* block for 1 h and recorded the activity of the pyloric network in response to this reestablished modulatory connectivity. Representative recordings of *stn* (descending and ascending inputs) and *lvn* (pyloric output) for a single preparation in each treatment group (control and sucrose) across the time course of an experiment are provided in Fig. 3*A*. All of the recordings in Fig. 3*A* and measurements summarized in Fig. 3*B* were made during the time when the sucrose blockade had been *removed* for that day; thus, these preparations all feature potentially intact connections from the descending projections to the STG. None of the preparations used in these experiments, or any subsequent experiments, had yet undergone full recovery of the pyloric rhythm in the absence of descending projections. Thus, in most cases, there was no pyloric activity in the blocked preparations prior to removal of the block.

Other than an initial slight decrease in pyloric burst frequency, control preparations showed consistent and robust pyloric output across the time course of the experiment (Fig. 3*B*, *left*). Conversely, as the preparations spend more time in a decentralized state via sucrose block, they are subsequently less likely to reestablish pyloric output when the block is removed (Fig. 3*B*, *left*). After 24 h, sucrose-blocked preparations were still capable of generating a pyloric rhythm that was not significantly different from the control when the blockade was removed, but after 48 h of blockade there was a significant decrease in pyloric frequency. After 4 days, virtually all pyloric activity was eliminated even with the sucrose block removed (Fig. 3*B*). This effect was not the result of damage to the *stn* by the sucrose blockade. Using the AGR neuron as one indicator of the propagation ability of the *stn*, there was no significant difference in AGR spiking frequency on the *stn* across the time course of the experiment between control and sucrose blocked preparations (see Fig. 3, *A* and *B*, *right*). Furthermore, using AGR as an indicator of *stn* propagation ability, we determined that sucrose likely was not resulting in the death of axons in the *stn* over the time course of the experiment. Figure 3*C* shows a representative multisweep analysis demonstrating the efficacy of the blockade at 24 h, as well as the reestablishment of AGR action potential propagation into the *son* following removal of the blockade at 24 and 48 h. By 48 h, we already saw a substantial decrease in pyloric frequency with the blockade removed (Fig. 3*B*), yet *stn* propagation ability appears to have remained intact.

Our results demonstrate that there is a decrease in the ability of restoring connectivity in the *stn* and the ability of the STG to generate pyloric activity following a period of removal of the inputs. One possible mechanism for the decrease in functional output in reconnected stomatogastric networks is a change in the activity of the descending projections influencing pyloric activity. Therefore, we measured changes in activity of units found on the other nerves that project from the commissural ganglia, *son* and *ion*. The *son* and *ion* contain the projections of many of the modulatory neurons from the CoGs that project down the *stn* (Coleman et al. 1992). The *ion* has only three known units running through it (Hedrich et al. 2011). *Ion* activity in our preparations largely consisted of spiking of an esophageal motor neuron (OMN1), with variable activity of two projection neurons, MCN1 and MCN5. Our analysis of the *ion* revealed no consistent relationships in the

firing of these three units with blockade (data not shown). We did not obtain all of the appropriate recordings to unambiguously identify MCN1 and MCN5 spikes on the *ion*. However, our analysis showed there was substantial variability in the presence or absence of MCN1 and MCN5 activity from preparation to preparation in both control and sucrose-blocked conditions. In other words, we sometimes saw only OMN activity, whereas in some preparations we saw either one or two smaller units on the *ion* that could correspond to MCN1 and/or MCN5. When these units were present in our recordings, they also varied between simply spiking or bursting. Overall, although we could not definitively quantify the MCN1 and MCN5 activity, we detected no consistent qualitative relationships between *ion* unit activity (present or absence) or spiking pattern and pyloric frequency in this study (data not shown), although previously such a relationship was reported (Hedrich et al. 2011). However, we did see a relationship with *son* spiking activity across the time course of our blockade experiments. The *son* contains many more fibers than the *ion*, including both ascending and descending units, making identification of individual units far more challenging. To examine whether more global patterns of activity in the *son* may relate to the activity of the pyloric rhythm, we measured the overall spike frequency in the *son* as it related to the STG activity. The spike frequency of the *son* significantly decreased over the time course of the experiment with sucrose blockade (Fig. 4*A*), in a pattern reminiscent of that seen for the pyloric burst frequency in our earlier experiments (see Fig. 3*B*). We therefore determined whether *son* spiking and pyloric bursting activity were correlated. Our results show that overall pyloric burst frequency and *son* spiking frequency were significantly correlated across blocking conditions in this study (Fig. 4*B*). However, these analyses do not fully explain the relationships seen in our data. When we plotted the relationships among *son* spike frequency, AGR spike frequency, and the pyloric burst frequency in individual preparations, we saw a surprising shift in these relationships. In control preparations maintained in physiological saline for 3 days, we see a significant correlation between *son* spike frequency and pyloric burst frequency (Fig. 4*C*, *top*), but no relationships between AGR and the pyloric output, or *son* and AGR activity (Fig. 4*C*, *middle* and *bottom*). Conversely, preparations in which the *stn* has been blocked with sucrose over the course of 3 days have no relationship between *son* and the pyloric output (Fig. 4*C*, *top* and *middle*), but a significant correlation between AGR spiking and the pyloric burst frequency (Fig. 4*C*, *bottom*). These results show that there is not simply a scaling of all activity in the preparation over time, but rather that there are distinct alterations to spiking activities of projection neurons that correspond to changes in pyloric network output in the STG.

The overall incremental effects of sucrose blockade and removal are summarized in Fig. 5. All of the recordings in Fig. 5 have been made while the sucrose block has been removed and replaced with physiological saline, effectively restoring communication between the descending and ascending neurons in the *stn*. The control recording (Fig. 5, *control*) shows the activity of an intact preparation freshly dissected from the animal. When projections are restored following 24 h of sucrose blockade of the *stn*, the pyloric network generates rhythmic activity that is reduced in bursting frequency from controls (Fig. 5, *24-h block*). At this time point we see con-
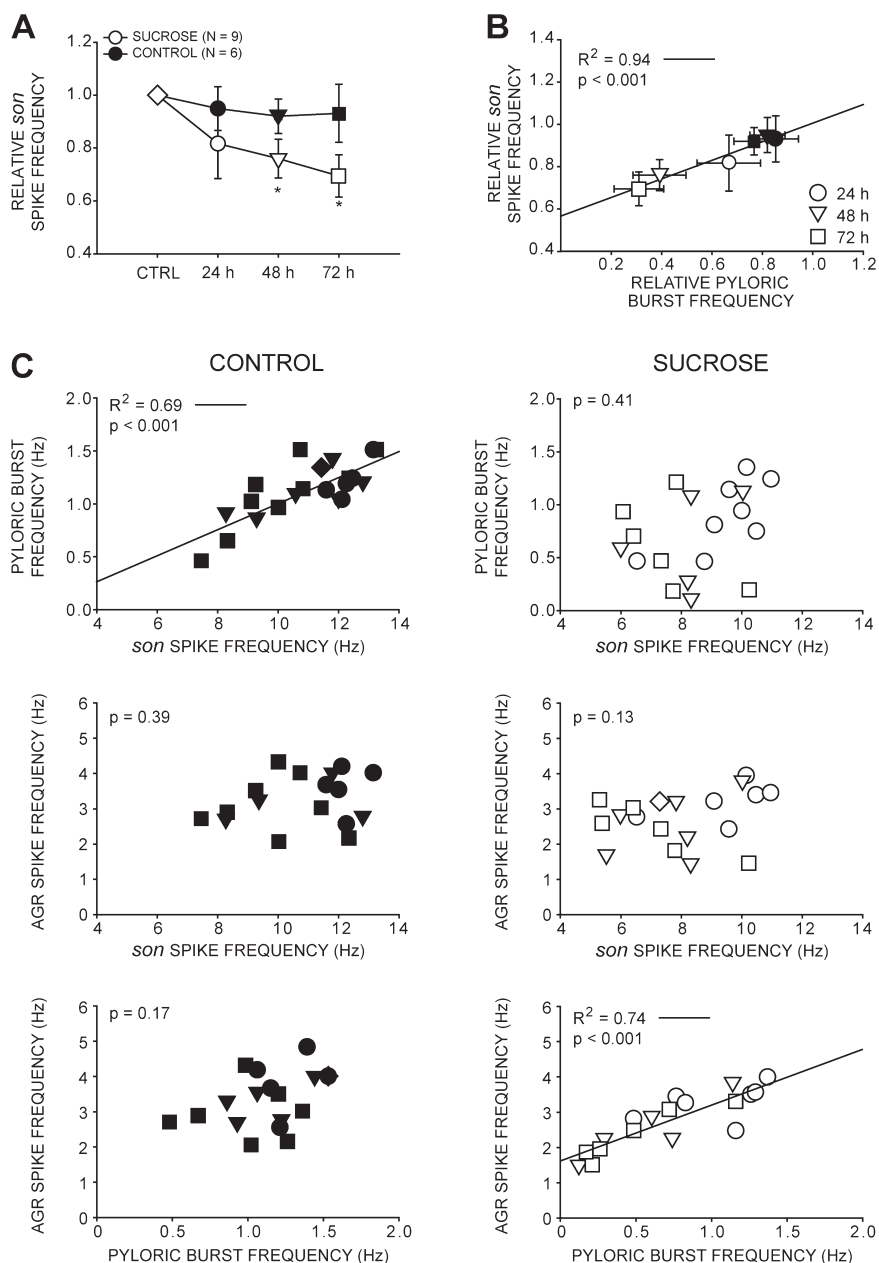
Fig. 4. Effects of *stn* blockade over time on bursting activity of the pyloric rhythm as well as *son* and AGR spiking activity. *A*: relative frequency of *son* spiking over time with blockade. Data were collected while the block was removed. Relative frequency for each preparation was calculated relative to that preparation's control, intact (day 0) activity, and expressed here as mean ± SD. * represents a significant difference relative to control for a given day ($P < 0.05$; *t*-test). *B*: correlation between mean relative pyloric burst frequency and mean *son* spike frequency in sucrose and control preparations over time. Day 0 (control) is omitted because this is the reference point for relative frequency calculation. *C*: correlation among pyloric bursting, AGR, and *son* spike frequencies in control and sucrose blocked preparations for up to 72 h blocked. All data collected while the sucrose block was removed. Statistics reported reflect the outcome of Pearson's correlation tests. Different point markers refer to measurements taken at 24 h, 48 h, and 72 h as shown in the legend of *B*.

served AGR spike propagation via multisweep analyses across the *son, dgn,* and both *stn* recording sites (Fig. 5, *24-h block, right*), ensuring the *stn* remains capable of spike propagation. At 24 h we can also see a reduction in activity on the *son* as well. After 48 h deprived of inputs, removal of the blockade results in further weakened activity on the *lvn* and *mvn*, as well as reduced activity of the *son*. After 72 h deprived of inputs, removal of the blockade is insufficient to restore activity to the pyloric network, although the individual pyloric units can still be seen to be present on the *lvn* recording. Again, spikes are seen propagating through the blocking site (Fig. 5, *72-h block, right*) confirming the viability of the projections, and *son* activity is further decreased (Fig. 5, *72-h block*). However, in this preparation we also saw a substantive change in the activity of the AGR neuron. It begins to fire two independent spikes (instead of a single, tonic spike), one of which propagates through the *son, stn,* and *dgn* that appears to originate in

the *stn*, whereas a second independent spike propagates only in the *dgn* in our recordings (Fig. 5, *72-h block, far right*; see also Daur et al. 2009).

Although our measurements of *son* spiking suggest that the activity of modulatory and interneuron projections may be altered by the sucrose blockade, another possible explanation is that decreased pyloric activity could be the result of a loss in the ability of modulatory projections to release neuromodulator. We tested whether the descending modulatory projections are still capable of releasing neuromodulator after sucrose blockade by stimulating the *stn* both above and below the site of the blockade after 3 days of blockade with sucrose. If sucrose blockade has eliminated the ability of the modulatory projections to influence the pyloric rhythm, then we predict stimulation will be ineffective in producing output changes in the STG. This was not the case; after 3 days of sucrose blockade, electrical stimulation either below the blocking well
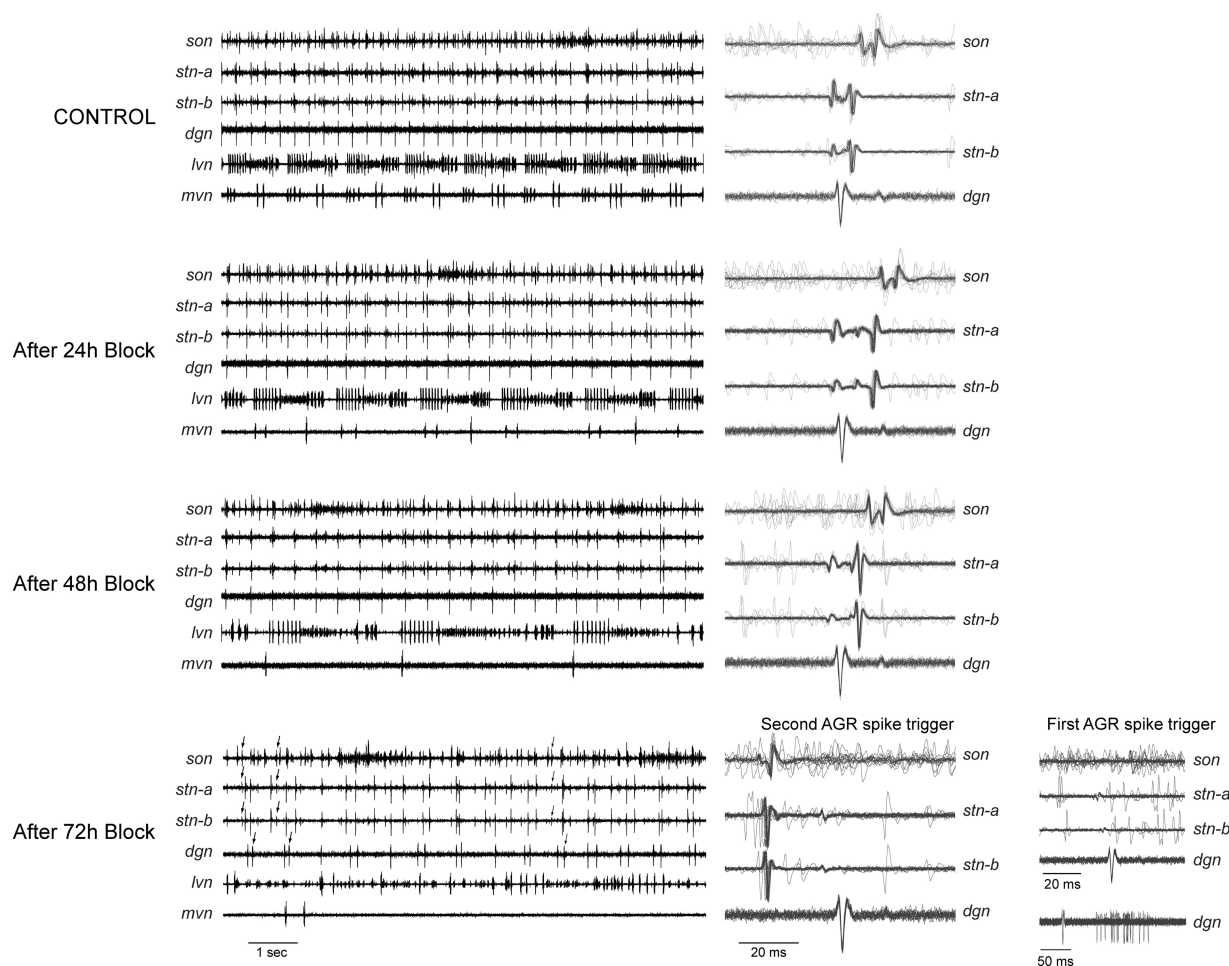
Fig. 5. Representative recordings of a single sucrose-blocked preparation over four time points to illustrate the effects *stn* blockade has on activity of the stomatogastric nervous system. *stn-a* is the blocking well in this experiment. All recordings were made with the sucrose block removed for 30 min. Simultaneous recordings of the *son*, *stn* (two sites), *dgn, lvn,* and *mvn* provided over 72 h of sucrose blockade. In the 72-h panel, representative time-locked AGR spikes are denoted by *arrowheads*. *Right panel*: multisweep recordings for the *son, dgn,* and the two *stn* recording sites (*stn-a* and *stn-b*) triggered from AGR spikes recorded on the *dgn*. In the 72-h trace, the multisweep results show differences from triggering on either the second AGR spike in the spike pairs of the *dgn* (*left*) or the first AGR spike (*right*). *dgn* multisweeps triggered from the first AGR spike are also provided at a longer time scale to show the independence of the first and second AGR spikes on the *dgn*.

(with the block still intact; Fig. 6*A*) or above the blockade (with the block removed; Fig. 6*B*) resulted in similar ability to drive the pyloric frequency. This stimulation effect is reversible, as 20 min after stimulation ceased, the pyloric rhythm had largely returned to its previous baseline levels (Fig. 6, *A* and *B*). These results demonstrate that the *stn* fibers are still capable of releasing neuromodulator to influence pyloric activity. Furthermore, these results provide strong support that we are not damaging *stn* axons via sucrose blockade, because we get the same stimulation effect whether we stimulate above or below where the sucrose blockade was placed.

A third mechanism by which reconnected projections might fail to appropriately generate network output is through altered sensitivity to neuromodulation of the target neurons of the pyloric network. We tested this by analyzing the responses of isolated pyloric networks (subsequent to sucrose blockade) to exogenously applied neuromodulators. After 3 days either with blockade via sucrose, or as an unblocked control preparation, the *stn* of each preparation was blocked with tetrodotoxin to ensure no interaction of the superfused modulator with descending neuromodulation. We then perfused a range of in-

creasing concentrations of the neuropeptide proctolin, the biogenic amine octopamine, or the muscarinic agonist pilocarpine, all of which are known to exogenously activate pyloric activity (Goaillard et al. 2004; Hooper and Marder 1987; Swensen and Marder 2001), on to the isolated STG preparation and recorded pyloric burst output. We found a significant increase in response to proctolin in preparations that had previously been blocked with sucrose for 3 days relative to control (Fig. 7, *top*). At three of four concentrations tested (10^{-8} M, 10^{-7} M, and 10^{-6} M) there was a significantly higher frequency of pyloric burst output in the sucrose-blocked preparations relative to controls. Conversely, there were no significant differences in response to octopamine between sucrose and control preparations (Fig. 7, *middle*). Finally, we found a significant decrease in response to pilocarpine in sucrose-blocked preparations (Fig. 7, *bottom*). Although burst frequency responses of the pyloric rhythm were altered in response to different modulators, there appeared to be no substantial difference in the pattern of the pyloric rhythm elicited by modulators between control and sucrose-blocked preparations. Representative recordings time-scaled to compare one complete pyloric burst
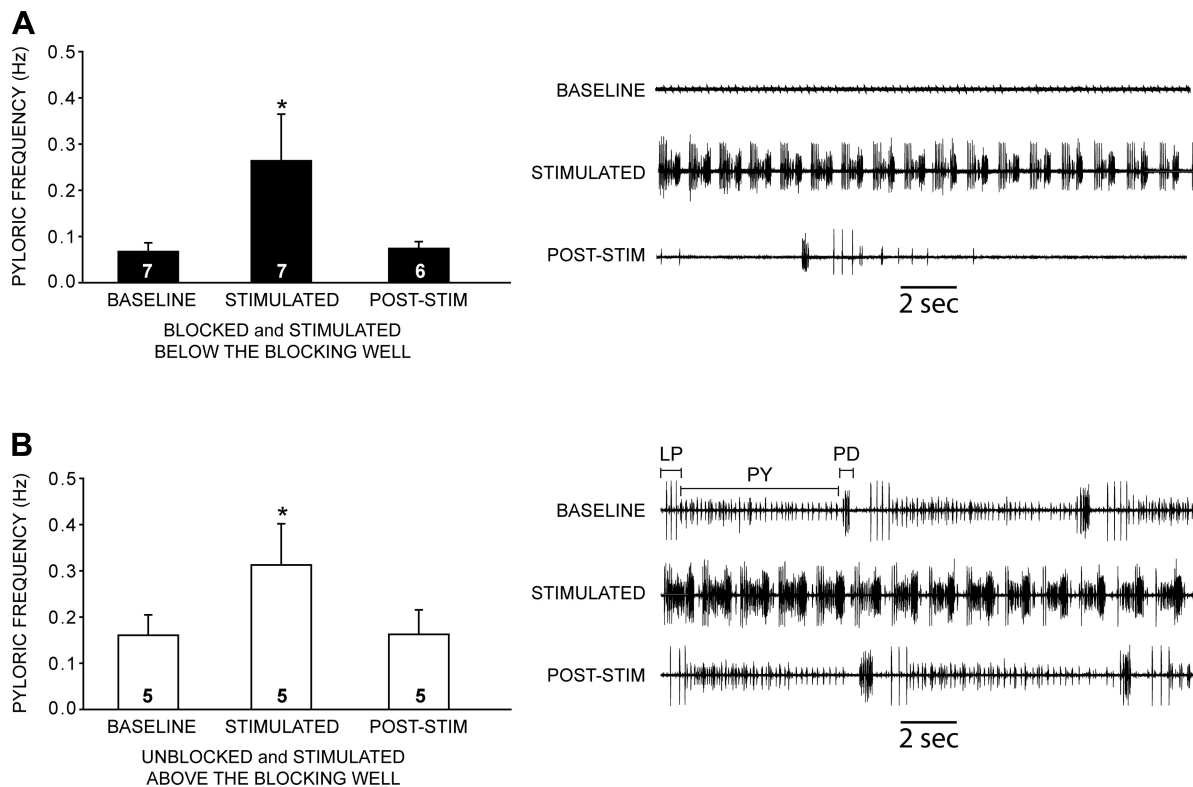
Fig. 6. Effects of *stn* stimulation after 3 days of blockade on pyloric burst frequency. In these experiments, three wells were made on the *stn*; the middle was used for blockade, whereas those above (upper stim) and below (lower stim) were sites of extracellular stimulation. Preps either were maintained with the block intact and the *stn* stimulated below the blocking well (*filled bars*; *A*) or unblocked and stimulated above the blocking well (*open bars*; *B*). *A*: pyloric frequency (mean ± SD) and *lvn* representative recordings of *stn*-stimulated sucrose-blocked preparations with stimulation below the blocking well. *Baseline* recordings were made immediately prior to stimulation. *Stimulated* data were acquired immediately following stimulation of the *stn*. *POST-STIM* data were acquired 20 min after the end of the stimulation. *B*: pyloric frequency and *lvn* representative recordings of preparations with the block removed and stimulation done above the blocking well. Recordings were made in parallel fashion to sucrose block experiments. * represents a significant difference relative to control for a given group ($P < 0.05$; *t*-test). Sample size indicated in each bar. Individual pyloric units (LP, PY, and PD) are labeled as recorded on the *lvn* for reference.

pattern suggest that although proctolin, octopamine, and pilocarpine elicit somewhat distinct patterns (e.g., LP activity levels), no differences were apparent between control and sucrose rhythms for a given modulator (Fig. 7). Together, these results suggest that the sucrose blockade does indeed result in a change in neuromodulator sensitivity of pyloric neurons, perhaps in particular for those neurons involved in the generation and frequency of the bursting of the pyloric rhythm, specifically AB and/or PD.

DISCUSSION

It is only somewhat recently that the occurrence of, and mechanisms underlying, homeostatic compensation in neural circuits have been more widely recognized and studied (Marder and Tang 2010; Turrigiano 2008). Such studies include examples of homeostatic plasticity as compensation for gene knockouts (Bergquist et al. 2010), synaptic scaling (Turrigiano 2008), sensory-modality specific compensation (Deeg and Aizenman 2011), and recovery of function in networks deprived of sensory input (Cullen et al. 2009) and descending command fibers (Golowasch et al. 1999; Tillakaratne et al. 2010). Yet despite the substantial amount that we have learned about homeostatic plasticity in these systems, very few, if any, studies have examined the impact of these homeostatic processes on the subsequent ability of the network to appropriately respond to further perturbation or even reversal of conditions

that initially triggered compensation. Our study is one of the first to examine effects of removal and restoration of inputs to a motor network over the time course of homeostatic compensation. Our data demonstrate that following blockade of modulatory inputs, the system is altered such that removal of the block is insufficient to restore network activity. These effects do not seem to simply be due to damage of the descending *stn* fibers. Using AGR activity as a monitor of *stn* propagation ability (Daur et al. 2009), we found no significant differences in AGR spike propagation ability over time in both control and sucrose preparations, indicating the propagation ability of the *stn* is likely maintained throughout these experiments.

We investigated whether these effects are due to changes in the descending projections themselves, responses of the pyloric network, or both. To determine whether blockade causes a loss of modulator release from descending fibers, we electrically stimulated the *stn* both above and below the blocking well after sucrose blockade. Stimulation was equally effective in eliciting pyloric output regardless of whether the stimulation was below the blockade (with the block intact) or above the blockade (with the block removed). Thus, although we are unable to determine whether quantitative changes occur in modulator release as a result of our blocking manipulation, at least qualitatively we determined that the ability to release neuromodulator is not lost from presynaptic terminals of descending projections, nor is the ability of the STG to respond to released
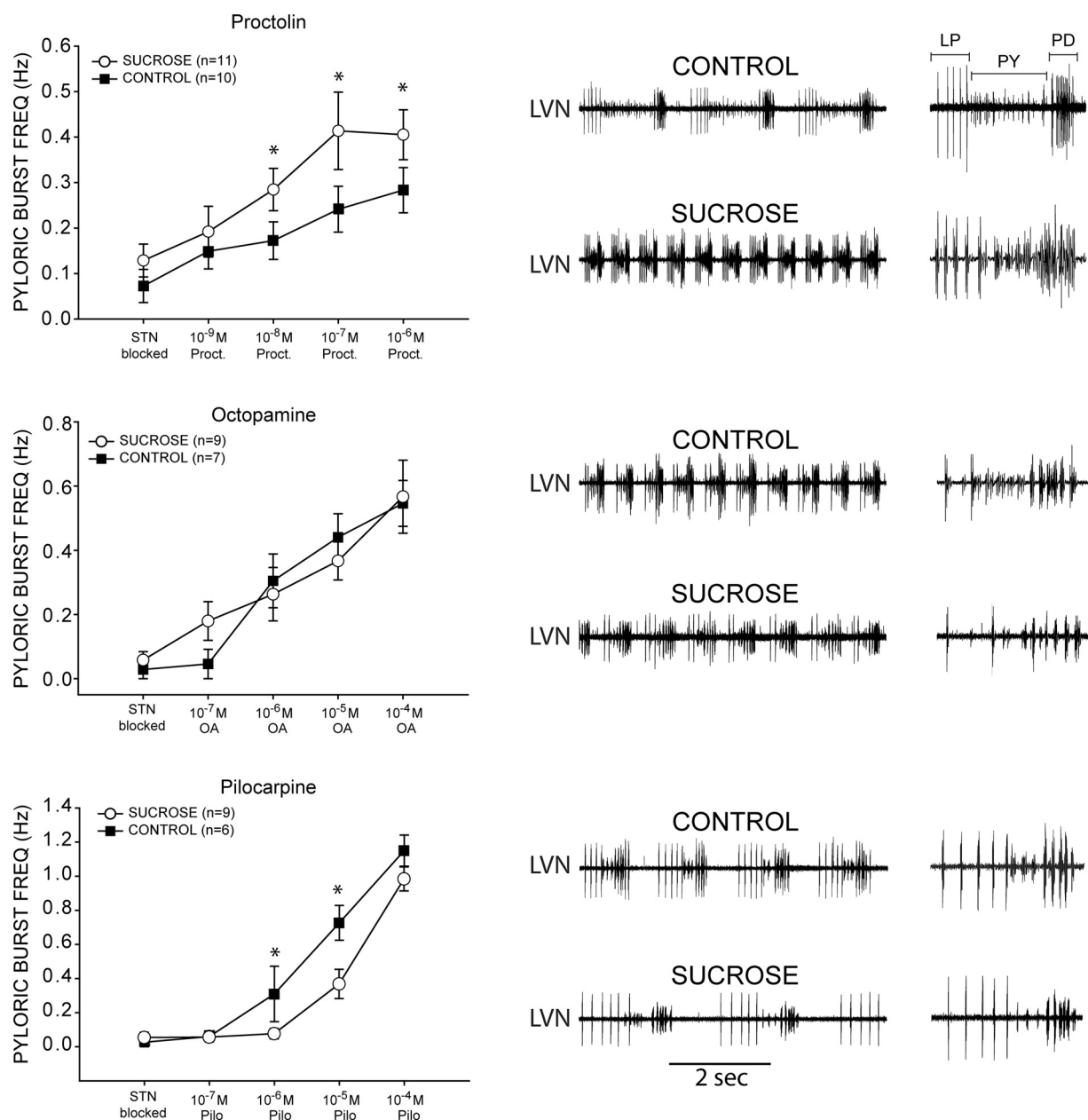
Fig. 7. Effects of exogenously applied neuromodulators on pyloric burst frequency (mean $\pm$ SD) after 3 days of *stn* blockade. After 3 days of sucrose, or time in culture control, the *stn* was completely blocked with tetrodotoxin (TTX) to ensure elimination of any endogenous modulator release. Increasing concentrations of proctolin, octopamine, and pilocarpine were superfused on preparations and pyloric burst frequency measured at steady state for a given concentration. * represents a significant difference relative to control preparations for a given concentration ($P < 0.05$; *t*-test). Representative *lvn* recordings for control and sucrose blocked preparations are shown during the perfusion of 10^{-6} M proctolin (*top*), 10^{-4} M octopamine (*middle*), and 10^{-5} M pilocarpine (*bottom*). A single pyloric burst is scaled for each recording to compare the pattern elicited by modulator application in each treatment group. Individual pyloric units (LP, PY, and PD) are labeled for reference.

modulator lacking. These results also provide support for the maintenance of *stn* propagation ability throughout the study, because stimulation above a removed block was able to trigger effects that traversed the area of blockade.

In addition to blocking descending fibers, the blockade may also influence any ascending feedback from the STG to the commissural ganglia, as represented in our studies by AGR activity (Daur et al. 2009). In this study we consider both possibilities, but do not distinguish between the two. We analyzed the activity of the *son* nerve, which predominantly contains descending projections from the CoGs (Coleman et al.

1992), and found a significant decrease in firing rate on the *son* with increasing duration of blockade that mirrored changes seen in pyloric frequency. Indeed, there was a strong quantitative correlation overall between *son* firing frequency and pyloric burst frequency among control and sucrose blocked preparations. Furthermore, there is a substantial change in the relationship of *son* activity to the pyloric output over the time course of the blockade. In control preparations, *son* spiking and the output of the pyloric network are coupled. Yet as a result of blocking the *stn* projections, this relationship completely disappears, and pyloric output becomes strongly correlated with

the spiking activity of AGR. We have even seen dramatic qualitative changes in the activity of neurons like AGR in this system (Fig. 5, *72-h block*) that may be further indicative of alterations in projections neurons that influence STG activity. We cannot determine from these experiments whether these changes in *son*, AGR, and pyloric network activity are causative or correlative. When combined with the fact that stimulation experiments reveal these projections have not lost the capacity to release modulators, the data overall suggest that disruption of interactions between the STG and the higher ganglia (CoG and OG) may lead to a change in activity underlying modulation, but not the capacity for modulator release, over time.

Finally, we determined whether alteration of descending projections affects response to exogenously applied neuromodulators. Proctolin is a neuropeptide that is a major constituent of releasate of presynaptic fibers of the STN (Billimoria et al. 2005) and is able to exogenously restore network activity to deafferented preparations (Golowasch and Marder 1992; Hooper and Marder 1987). There is a significant increase in the effect of proctolin on pyloric frequency in preparations that have been blocked with sucrose relative to control preparations. It is not possible to determine from our data whether this is a result of increased receptor signaling activity, or downstream targets of modulation such as voltage-gated conductances, or both. However, there was not an increase in pyloric cycle frequency sensitivity for all neuromodulators; octopamine application (Goaillard et al. 2004) did not result in significant differences in pyloric cycle frequency between control and sucrose-blocked preparations, whereas response to pilocarpine (Swensen and Marder 2001) was significantly lower in sucrose-blocked preparations than in controls. These data demonstrate that there is not a uniform change in response to all modulators in the system, but rather distinct responses to different classes of modulatory compounds. This could be the result of changes in modulator receptors, or perhaps intracellular pathways involved in mediating modulator response. However, these data suggest that the convergent target of several modulators in this system, a mixed-inward current elicited by modulator exposure (Golowasch and Marder 1992), may not be the source of the differing responses. Both proctolin and pilocarpine influence this current (Swensen and Marder 2000) in similar fashion, yet our preparations show divergent alterations in the responses to these two modulators.

The changes we see in the ability of restored projections to elicit output following different blockade regimes must represent a change at the cellular level, both in the ability of the STG neurons to respond to neuromodulatory substances, and in presynaptic activity and subsequent release of modulator. It is already established that pyloric neurons alter some intrinsic properties in response to decentralization. These include changes in the magnitude of ionic currents such as I_H (Thoby-Brisson and Simmers 2002), I_A (Khorkova and Golowasch 2007; Mizrahi et al. 2001), I_{Ba}, and I_{KCa} (Khorkova and Golowasch 2007), and disruption of correlations among ionic conductances as well as channel mRNA levels (Khorkova and Golowasch 2007; Temporal et al. 2012). Our results suggest that one possible impact of these changes is that subsequently restored neuromodulation may be ineffective at generating typical output because the downstream targets of modulators have been altered by decentralization. Indeed, due to the fact

that these changes have been documented previously, it is possible that such changes in intrinsic excitability alone are sufficient to account for our results.

Less is known about changes in receptor expression following decentralization in the STG. Our data demonstrate changes in responses to proctolin and pilocarpine in blocked preparations, but at this time we cannot determine whether this is an effect of receptor expression, activity, or signaling, or due to changes in downstream targets. In other systems, changes in receptor expression following deafferentation have been reported, including 5HT-2C receptor expression in mammalian spinal cord (Murray et al. 2010). However, not all systems that undergo homeostatic compensation have corresponding changes in receptor expression. For example, vestibular deafferentation leads to plasticity and compensation, but changes in expression and distribution of γ-aminobutyric acid (GABA) (Gliddon et al. 2005), glutamate (King et al. 2002), glucocorticoid (Lindsay et al. 2005), and cannabinoid (Ashton et al. 2004) receptors have not been detected, despite changes in responses to these compounds.

The interaction of neuromodulation and neural network output is a complex interplay that occurs over multiple time scales. A good deal is known of how neuromodulators affect plasticity in these networks over shorter time scales, as well as influence properties of cells and synapses over more organizational time scales (Harris-Warrick 2011). However, as progress is made toward understanding regenerative processes in nerve injury, it becomes more imperative that potential impacts of changes in isolated or deafferented neural networks as a result of loss of modulatory inputs be more completely understood as well.

DISCLOSURES

No conflicts of interest, financial or otherwise, are declared by the author(s).

AUTHOR CONTRIBUTIONS

J.N., K.M.L., and D.J.S. conception and design of research; J.N. and K.M.L. performed experiments; J.N., K.M.L., and D.J.S. analyzed data; J.N., K.M.L., and D.J.S. interpreted results of experiments; J.N., K.M.L., and D.J.S. edited and revised manuscript; J.N., K.M.L., and D.J.S. approved final version of manuscript; D.J.S. prepared figures; D.J.S. drafted the manuscript.

REFERENCES

Ashton JC, Zheng Y, Liu P, Darlington CL, Smith PF. Immunohistochemical characterisation and localisation of cannabinoid CB1 receptor protein in the rat vestibular nucleus complex and the effects of unilateral vestibular deafferentation. *Brain Res* 1021: 264–271, 2004.

Barbeau H, Rossignol S. Recovery of locomotion after chronic spinalization in the adult cat. *Brain Res* 412: 84–95, 1987.

Bergquist S, Dickman DK, Davis GW. A hierarchy of cell intrinsic and target-derived homeostatic signaling. *Neuron* 66: 220–234, 2010.

Billimoria CP, Li L, Marder E. Profiling of neuropeptides released at the stomatogastric ganglion of the crab, Cancer borealis with mass spectrometry. *J Neurochem* 95: 191–199, 2005.

Coleman MJ, Nusbaum MP, Cournil I, Claiborne BJ. Distribution of modulatory inputs to the stomatogastric ganglion of the crab, Cancer borealis. *J Comp Neurol* 325: 581–594, 1992.

Cullen KE, Minor LB, Beraneck M, Sadeghi SG. Neural substrates underlying vestibular compensation: contribution of peripheral versus central processing. *J Vestib Res* 19: 171–182, 2009.

Darlington CL, Smith PF. Molecular mechanisms of recovery from vestibular damage in mammals: recent advances. *Prog Neurobiol* 62: 313–325, 2000.

Daur N, Nadim F, Stein W. Regulation of motor patterns by the central spike-initiation zone of a sensory neuron. *Eur J Neurosci* 30: 808–822, 2009.

Deeg KE, Aizenman CD. Sensory modality-specific homeostatic plasticity in the developing optic tectum. *Nat Neurosci* 14: 548–550, 2011.

Gliddon CM, Darlington CL, Smith PF. GABA(A) receptor subunit expression in the guinea pig vestibular nucleus complex during the development of vestibular compensation. *Exp Brain Res* 166: 71–77, 2005.

Goaillard JM, Schulz DJ, Kilman VL, Marder E. Octopamine modulates the axons of modulatory projection neurons. *J Neurosci* 24: 7063–7073, 2004.

Goldberg D, Nusbaum MP, Marder E. Substance P-like immunoreactivity in the stomatogastric nervous systems of the crab Cancer borealis and the lobsters Panulirus interruptus and Homarus americanus. *Cell Tissue Res* 252: 515–522, 1988.

Golowasch J, Casey M, Abbott LF, Marder E. Network stability from activity-dependent regulation of neuronal conductances. *Neural Comput* 11: 1079–1096, 1999.

Golowasch J, Marder E. Proctolin activates an inward current whose voltage dependence is modified by extracellular Ca^{2+}. *J Neurosci* 12: 810–817, 1992.

Grillner S. Biological pattern generation: the cellular and computational logic of networks in motion. *Neuron* 52: 751–766, 2006.

Harris-Warrick RM. Neuromodulation and flexibility in central pattern generator networks. *Curr Opin Neurobiol* 21: 685–692, 2011.

Hedrich UB, Diehl F, Stein W. Gastric and pyloric motor pattern control by a modulatory projection neuron in the intact crab *Cancer pagurus*. *J Neurophysiol* 105: 1671–1680, 2011.

Hooper SL, Marder E. Modulation of the lobster pyloric rhythm by the peptide proctolin. *J Neurosci* 7: 2097–2112, 1987.

Khorkova O, Golowasch J. Neuromodulators, not activity, control coordinated expression of ionic currents. *J Neurosci* 27: 8709–8718, 2007.

King J, Zheng Y, Liu P, Darlington CL, Smith PF. NMDA and AMPA receptor subunit protein expression in the rat vestibular nucleus following unilateral labyrinthectomy. *Neuroreport* 13: 1541–1545, 2002.

Lindsay L, Liu P, Gliddon C, Zheng Y, Smith PF, Darlington CL. Cytosolic glucocorticoid receptor expression in the rat vestibular nucleus and hippocampus following unilateral vestibular deafferentation. *Exp Brain Res* 162: 309–314, 2005.

Luther JA, Robie AA, Yarotsky J, Reina C, Marder E, Golowasch J. Episodic bouts of activity accompany recovery of rhythmic output by a neuromodulator- and activity-deprived adult neural network. *J Neurophysiol* 90: 2720–2730, 2003.

Marder E, Tang LS. Coordinating different homeostatic processes. *Neuron* 66: 161–163, 2010.

Mizrahi A, Dickinson PS, Kloppenburg P, Fenelon V, Baro DJ, Harris-Warrick RM, Meyrand P, Simmers J. Long-term maintenance of channel distribution in a central pattern generator neuron by neuromodulatory inputs revealed by decentralization in organ culture. *J Neurosci* 21: 7331–7339, 2001.

Moulins M, Cournil I. All-or-none control of the bursting properties of the pacemaker neurons of the lobster pyloric pattern generator. *J Neurobiol* 13: 447–458, 1982.

Murray KC, Nakae A, Stephens MJ, Rank M, D'Amico J, Harvey PJ, Li X, Harris RL, Ballou EW, Anelli R, Heckman CJ, Mashimo T, Vavrek R, Sanelli L, Gorassini MA, Bennett DJ, Fouad K. Recovery of motoneuron and locomotor function after spinal cord injury depends on constitutive activity in 5-HT2C receptors. *Nat Med* 16: 694–700, 2010.

Nagy F, Dickinson PS, Moulins M. Rhythmical synaptic control of axonal conduction in a lobster motor neuron. *J Neurophysiol* 45: 1109–1124, 1981.

Rossignol S, Bouyer L, Langlet C, Barthelemy D, Chau C, Giroux N, Brustein E, Marcoux J, Leblond H, Reader TA. Determinants of locomotor recovery after spinal injury in the cat. *Prog Brain Res* 143: 163–172, 2004a.

Rossignol S, Brustein E, Bouyer L, Barthelemy D, Langlet C, Leblond H. Adaptive changes of locomotion after central and peripheral lesions. *Can J Physiol Pharmacol* 82: 617–627, 2004b.

Selverston AI. Invertebrate central pattern generator circuits. *Philos Trans R Soc Lond B Biol Sci* 365: 2329–2345, 2010.

Smarandache CR, Stein W. Sensory-induced modification of two motor patterns in the crab, *Cancer pagurus*. *J Exp Biol* 210: 2912–2922, 2007.

Spitzer N, Cymbalyuk G, Zhang H, Edwards DH, Baro DJ. Serotonin transduction cascades mediate variable changes in pyloric network cycle frequency in response to the same modulatory challenge. *J Neurophysiol* 99: 2844–2863, 2008.

Stein W. Modulation of stomatogastric rhythms. *J Comp Physiol A Neuroethol Sens Neural Behav Physiol* 195: 989–1009, 2009.

Swensen AM, Marder E. Multiple peptides converge to activate the same voltage-dependent current in a central pattern-generating circuit. *J Neurosci* 20: 6752–6759, 2000.

Swensen AM, Marder E. Modulators with convergent cellular actions elicit distinct circuit outputs. *J Neurosci* 21: 4050–4058, 2001.

Temporal S, Desai M, Khorkova O, Varghese G, Dai A, Schulz DJ, Golowasch J. Neuromodulation independently determines correlated channel expression and conductance levels in motor neurons of the stomatogastric ganglion. *J Neurophysiol* 107: 718–727, 2012.

Thoby-Brisson M, Simmers J. Neuromodulatory inputs maintain expression of a lobster motor pattern-generating network in a modulation-dependent state: evidence from long-term decentralization in vitro. *J Neurosci* 18: 2212–2225, 1998.

Thoby-Brisson M, Simmers J. Long-term neuromodulatory regulation of a motor pattern-generating network: maintenance of synaptic efficacy and oscillatory properties. *J Neurophysiol* 88: 2942–2953, 2002.

Tillakaratne NJ, Guu JJ, de Leon RD, Bigbee AJ, London NJ, Zhong H, Ziegler MD, Joynes RL, Roy RR, Edgerton VR. Functional recovery of stepping in rats after a complete neonatal spinal cord transection is not due to regrowth across the lesion site. *Neuroscience* 166: 23–33, 2010.

Turrigiano GG. The self-tuning neuron: synaptic scaling of excitatory synapses. *Cell* 135: 422–435, 2008.